DESIGN AND PROTOTYPE OF A PHASED-ARRAY ANTENNA FOR NANOSATELLITE RADAR AND COMMUNICATION APPLICATIONS

SIDDHARTH DAVE

A THESIS SUBMITTED TO THE FACULTY OF GRADUATE STUDIES
IN PARTIAL FULFILLMENT OF THE REQUIREMENTS FOR THE DEGREE OF
MASTER OF SCIENCE

GRADUATE PROGRAM IN EARTH AND SPACE SCIENCE ENGINEERING
YORK UNIVERSITY
TORONTO, ONTARIO

JULY 2018

ABSTRACT

Reconfigurable software defined radios are capable of altering radio frequency parameters of a transceiver to add functionality and improve performance. Initially static by design, reconfigurable radios have become common on nanosatellites, assisting in reduction of launch costs and addition of functionality. Antenna designs have also become reconfigurable, by being able to change frequency range, polarization and many other characteristics. Some antenna designs also perform lobe (beam) steering; however, they are not commercially available for nanosatellites. Some of the added benefits of beam steering are debris detection and satellite-to-satellite communication. Therefore, this research combines antenna frequency reconfigurability and beam steering using an array to design an antenna that can be mounted on a nanosatellite.

Several antenna types are tested for frequency reconfigurability and then upgraded to a 2-dimensional array for beam steering. The design, fabrication process and testing of the phased-array antenna (PAA) is demonstrated. Frequency reconfigurability and beam steering abilities to receive signals from existing radiation sources is assessed. Testing of the custom PAA revealed that interference coupling between antennas in an array disrupt the frequency and gain response. Minor modifications are specified, which can improve the performance of the PAA.

This thesis demonstrates the design of a single element frequency reconfigurable micro-strip antenna that is operational in both S- and L-bands, between 1.4 to 2.3 GHz. This thesis also demonstrates the feasibility of mounting an 18 cm by 18 cm, 16 element, 2 dimensional, and frequency reconfigurable PAA on-board a nanosatellite, operational between 1.5 to 2.3 GHz.

ACKNOWLEDGEMENT

I would like to express my sincere gratitude towards my supervisors, Professor Regina Lee and Professor Sunil Bisnath, for providing me the opportunity to be a member of their research team and to learn under their guidance. I would also like to thank them for their continuous support and always keeping my best interests in mind.

I also would like to thank my parents and my extended family for believing in me and motivating me to accomplish my goals. Without their support, my work would not have been possible.

I extend my sincerest gratitude to my colleagues from the GNSS Lab, especially Surabhi, for helping me improve my academic skills. I wish them the best of luck in their endeavors.

I would like to give a special thanks to Jr Colmenar from Omega Circuits for his commitment to deliver fabricated antenna designs, often on short notices.

Last but not the least, my warmest regards to my little kitten, Mittu, who stayed up with me many nights keeping me company.

TABLE OF CONTENTS

LIST OF FIGURES

LIST OF TABLES

LIST OF ACRONYMS

AC	Alternating Current
ACS	Attitude Control System
ADC	Analog to Digital Converter
AUT	Antenna Under Test
DAC	Digital to Analog Converter
dB	Decibels
DC	Direct Current
EM	Electromagnetic waves
FPGA	Field Programmable Gate Array
GPS	Global Positioning System
HFSS	High Frequency Simulation Software
IC	Integrated Circuits
IF	Intermediate Frequency
LEO	Low Earth Orbit
LHCP	Left Hand Circular Polarization
LP	Linear Polarization
MEMS	Micro-electromechanical Systems
PAA	Phased Array Antenna
PCB	Printed Circuit Board
REF	Reference Antenna
RF	Radio Frequency
RHCP	Right Hand Circular Polarization
RSO	Resident Space Objects
SBSS	Space based Space Surveillance
SDR	Software-defined Radio
SLR	Satellite Laser Ranging
SMA	Sub-miniature version A connector
SNR	Signal to Noise Ratio
SSN	Space Surveillance Network
UHF	Ultra High Frequencies
VHF	Very High Frequency
VNA	Vector Network Analyzer

LIST OF SYMBOLS

f_c	Centre Frequency
ε_r	Relative Dielectric Permittivity
c	Speed of Light
k	Wave Factor
λ	Wavelength
G	Conductivity
R(x)	Impedance Function
Z	Impedance
V	Voltage
I	Current
L	Length of Micro-strip
W	Width of Micro-strip

CHAPTER 1: INTRODUCTION

Nanosatellite development has been accelerated in the last decade partly due to technological advances in the computer and electronics sector (Hertzfeld, 2011). Reduced manufacturing and launch costs have empowered interested investors and collaborators to join the growing interest in space technologies. Satellite missions with static payloads have evolved into reconfigurable platforms, where satellite performance and usage can be modified. Additionally, with the reduction in size, mass and cost of these satellite-mounted components, the overall launch costs have also decreased.

1.1. Radio design and Reconfigurability

Satellites communicate with the use of a radio transceiver, which consists of an antenna, a front-end and a back-end. The antenna has two primary tasks: to transmit radio frequency (RF) signals that originate from the satellite and to receive signals generated from other antennas. The antenna is an analog component that interfaces the electromagnetic field with other circuit components. As a transmitter, the antenna requires an analog signal input and outputs the signal into the electromagnetic field. As a receiver, the antenna outputs an analog signal based on the electromagnetic field input. The signal obtained by the antenna is forwarded onto a sequence of filters and power amplifiers. Figure 1.1 shows a front-end block diagram with ‘RF in’ marked where the antenna is connected. The signal obtained by the antenna is weak in strength and carries with it some noise, which the antenna cannot filter out on its own. The first sets of filters on the front-end are designed to weaken signals outside a predetermined bandwidth. The bandwidth is a frequency range which covers the signal of interest. Once the unwanted RF signals are weakened, the Low Noise Amplifier (LNA) increases the overall signal strength. The

placement order of the amplifier and filter is application specific, but many designs repeat these stages to further improve the signal quality. The signal quality is measured as signal-to-noise ratio (SNR) and it compares the strength of a signal to the noise that is captured in decibels. When receiving signals, the SNR of the front-end output signal is higher than the SNR of the antenna because of the filtering and amplification stages.

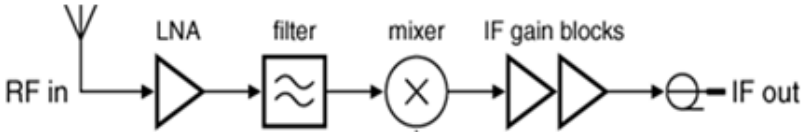

Figure 1.1: Radio front-end receiver and intermediate frequency (Electronic Products, 2013)

As RF signals reach higher frequencies, it becomes difficult for a processing element such as a Field Programmable Gate Array (FPGA) or a microprocessor to process the signal due to limitations of the analog to digital converter (ADC) and digital clock speed limitations on a processing element (Abidi, 2006). Thus, RF signals are down-converted using a mixer to a lower frequency known as the intermediate frequency (IF). A mixer, as the name suggests, mixes two input signals and produces an output signal that is a combination of two new signals produced from the sum and difference of the original input signals. For example, if one input is oscillating at 2100 MHz and a second input signal is oscillating at 600 MHz, the output of the mixer will be the sum and difference, respectively, of the values of the two input signals repeated at 2700 MHz and 1500 MHz. However, mixers generate several other signal harmonics at many other frequencies other than the sum and difference outputs. Therefore, to remove these newly generated harmonics, the mixer is followed by another set of IF filters and amplifiers, not unlike their RF counterparts.

The IF output signal is then digitized by an analog to digital converter (ADC) in a process known as sampling, and this marks the beginning of the back-end of a radio transceiver. The back-end is the main processing unit where the information transmitted over the RF signal can be interpreted as data and used for application specific needs. The now digitized signal, converted to binary 1s and 0s, makes it possible for a back-end system, usually an FPGA or microprocessor, to analyze the information the way that a computer does. For a transmission, the information or data to be transmitted from the antenna is first organized into network protocol specific packets and passed onto the digital to analog converter (DAC). The DAC uses a locally generated signal to produce an IF signal with the data from the back-end, followed by an up-converter (mixer), converting the signal to a higher frequency. After a sequence of filters and high-power amplifiers, similar to the receiver, the signal is then transmitted by the antenna. Nearly all transceivers follow the above design; however, each can be customized as per the application (Faraone, 2012).

Most of the hardware components mentioned above, such as amplifiers, filters and mixers are application specific and static in nature. Once these components are soldered onto a printed circuit board (PCB), they perform only in the frequency range they are designed for and any application or implementation changes require a design modification. However, the back-end does not have such issues, because software updates can easily be programmed onto the FPGA without making any physical modifications. Motivated by the reconfigurability of software in the back-end, new approaches to replacing simple stages of the front-end using the software defined radio (SDR) approach emerged (Jondral, 2005) and eventually led to the development of hand-held cellular devices with software reconfigurable radios. Not only did SDR provide design flexibility, it improved design efficiency and reduced the size and weight of the bulky front-end (Abidi, 2006).

In the SDR approach, complex and bulky RF components have been replaced with streamlined software and computational hardware components, which require less space, consume less power, and are lighter (Faraone, 2012). Front-end tasks such as signal filtering, which is a static operation on the hardware filter, a PCB component, is replaced with reconfigurable software, adding flexibility to the transceiver design. This flexibility is controlled by the back-end, which acts as the central control unit for the radio. Other tasks performed by components such as the mixer, amplifier, signal modulator and demodulators are duplicated by the SDR, blurring the line between back-end and front-end. However, ADC limitations for sampling signals at and above Ultra High Frequencies (UHF: 300-3000 MHz) require a hardware component-based front-end before the signal is digitized for an SDR (Puvaneswari, 2004). Despite the benefits of the SDR, certain operations still require an analog touch.

Since the RF communication medium remains unchanged, the design flexibility offered by the SDR can be limited by the physical hardware components, one of which is the antenna. Considering the SDR benefits, antenna design requirements have also changed. Traditionally, static antenna designs have a fixed frequency response in order to maximize the signal-to-noise (SNR) for a specific application given a static operational frequency range. On a hardware front-end, where the design is static, it is beneficial to have a narrow bandwidth antenna, as it simplifies the filtering on the static front-end. However, when dealing with SDRs, antennas with wider bandwidths are preferred (Faraone, 2012), because the operational frequency range varies. With a static antenna, if the SDR operates outside the antenna's operational frequency range, the SNR will suffer because the antenna is not optimized for this frequency. However, the choice of using a wide bandwidth antenna for a SDR causes the noise surrounding the signal to be interpreted at the same SNR as the signal of interest, requiring a better front-end. The additional

captured signal requires a better noise filter on the SDR, and if the frequency of the signal of interest is too high for the ADC to digitize, there will be additional noise added in the front-end due to mixer harmonics, which now must deal with a much wider band of input signal (Faraone, 2012). By changing the geometry of antenna layout, the frequency response of an antenna can be modified to better suit the application. The variable frequency design complication has motivated antenna designers to experiment with the physical layout and geometry of static antennas for better use with SDRs as will be discussed in Chapter 2. Non-static antennas, or reconfigurable antennas, also offer an alternative to static antennas for use with SDRs. Furthermore, antenna reconfigurability is not limited to the frequency domain as other antenna parameters such as polarization, radiation pattern and bandwidth add to the potential flexibility that antennas can offer to the SDR design.

Reconfigurable antennas and SDRs offer flexibility to a satellite's operational capabilities. Additionally, reconfigurable radios can replace the need for many static hardware components, and assist in reduction of equipment size, weight and cost for a launch. Although, it is not yet possible to have a software defined front-end capable of bandwidth hundreds of MHz wide (Puvaneswari, 2004). However, with the assistance of a reconfigurable antenna, different front-ends, which cover a wider frequency range, can utilize the same antenna. The reconfigurable nature of the radios can especially be beneficial to smaller satellites.

1.2. Cubesat specifications

In recent years, nanosatellite launches have become more frequent compared to the 1990s, when they became of interest in the low budget space community (Buchen, 2014). A CubeSat (a type of nanosatellite), is as named, a $10\times10\times10$ cm^3 satellite with a mass of up to 1.33 kg as shown in Figure 1.2. These nanosatellites are designed for small payloads and operate in the Very High

Frequency (VHF)/Ultra High Frequency (UHF) bands, which ranges from 30 to 3000 MHz, for ground communications. CubeSats also vary in sizes from 1U (which is 10×10×10 cm^3) to 2U and 3U. A larger configuration allows for more payloads, but more importantly, it provides more power. There are many ways to power a CubeSat, of which the most common is by solar panels attached on the outside of multiple side walls, which can generate 2 to 20 Watts depending on the size of the solar panels and orbit of the satellite (Heidt, 2000). The amount of power generated is enough to mount an on-board FPGA and a front-end with an antenna capable of transmitting to the ground.

Figure 1.2: CubeSat frames of varying sizes, from left to right 1U, 2U, 3U and 4U (Victor, 2015)

Nanosatellites carry a varying range of payloads and are commonly used as a means for technology demonstration. Past missions such as the Cygnus Mass Simulator to test cell phone based avionics in 2013 (Orbital Sciences, 2013), the Flock-1 constellation for Earth imaging in 2014 (Werner, 2014), and the Indian Space Research Organization's record launch of 104 satellites on a single rocket in 2017, of which 101 were CubeSats (Rueters, 2017), are just a few examples of the increasing popularity of nanosatellites due to launch cost reductions. Despite the

varying objectives of past CubeSat missions, the design standard relies on a dependable radio communication link to the ground.

Satellite antenna placement, although customized for each mission, is commonly done to reduce RF signal scattering effects. Antenna designs can vary in size, weight and mounting configuration, and typically one antenna is installed. For example, the exterior of a 6-sided CubeSat has one side reserved for a micro-strip antenna (Drysdale, 2014). Depending on the radiation pattern of the antenna and the mission requirements, the radio can transmit and receive signals without re-orienting the antenna or re-orientation is performed before the radio can transmit or receive. Therefore, these requirements place significant size and weight constraints on the antenna.

1.3. Satellite radio communications

As interpreted from past missions, nanosatellites are generally secondary missions to larger satellites, which effectively reduce launch costs. Many of these missions take place with the nanosatellite in a low earth orbit (LEO) (Bouwmeester, 2010). The LEO is defined as a circular orbit with an approximate altitude of 1000 km or less with an orbital period ranging from 85 to 120 minutes (CSA, 2003). As a satellite orbits the Earth, it performs important tasks such as recharging the batteries, data dumps (satellite to ground transmission), and other payload or mission specific tasks. Since the ground stations are at fixed locations and the satellite orbit is approximately 90 minutes, the time required to perform a data dump is short. Depending on the amount of the data to be transmitted, a communication bottleneck is possible. For example, if the amount of data collected during one orbit exceeds the amount of data that can be transmitted to the ground in one pass. Although data transfer speeds have increased greatly, so has the amount of data being transmitted.

A proposed constellation idea from the Defence Research and Development Canada suggests an inter-satellite link, where smaller satellites can perform a data dump at any point during their orbit (Gavigan, 2013). The data from a smaller satellite, which is intended for a ground station, is first transmitted to a communications-specific satellite within the constellation. Once the larger communications satellite is above a ground station, it can use a high-frequency transmitter to perform a data dump at a much faster rate. The proposed method has two major advantages for the nanosatellite and the satellite constellation: the satellite can perform data dumps more frequently during its orbit, and the satellite constellation can help reduce latency of the data reaching from the nanosatellite to the ground station. However, the antenna is generally mounted on one side of the satellite and needs satellite attitude change to physically point the antenna towards the target. Directing the antenna towards the target is not an issue when the ground station is a fixed location on the surface of the Earth, but communicating with another satellite may require the satellite to re-orient itself. Satellite attitude change requires resources, which are often limited, potentially reducing the lifetime of a satellite. To avoid satellite attitude change, antenna designs have a much wider main lobe. The main lobe of an antenna, as shown in Figure 1.3, is the sensitivity of the antenna to detect and receive RF signals in a particular direction and is measured in dB (decibel). The half-power points are marked where the antenna sensitivity is half or 3 dB lower than the peak at the main lobe. Antenna directional sensitivity, especially for a narrow main lobe, places additional constraints on the attitude control system (ACS) of a nanosatellite. The complication of orienting the main lobe is further amplified when the target is another satellite in orbit. A wider main lobe also has the disadvantage of receiving unwanted signals, which further complicates the front-end design as discussed earlier.

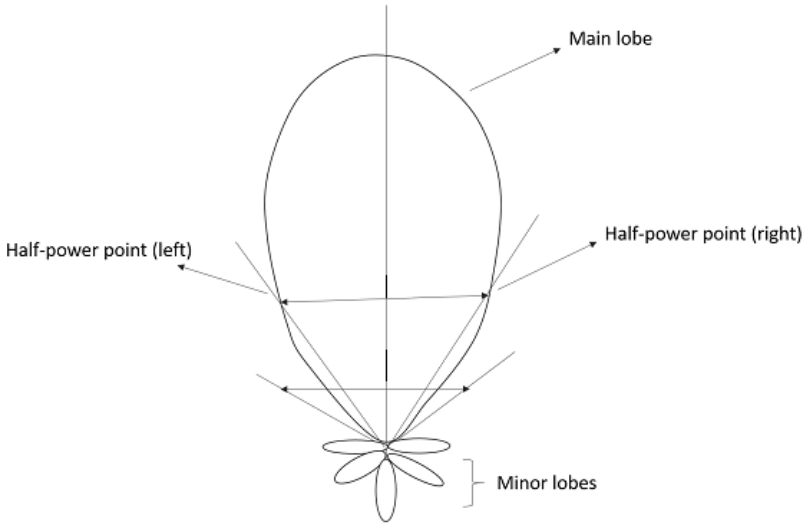

Figure 1.3: Antenna lobes and half-power point, (Tutorials Point, 2018)

Many of the antenna requirements for satellite-to-satellite communications are shared with single point radar. Single point radar is a method of determining the relative position and velocity of an object using radio waves from one point of reference. In a satellite-to-satellite link, both satellites act as single point radio element, with their respective main lobes targeted towards each other. The main lobe on a traditional micro-strip antenna is fixed, and therefore the satellite is required to manoeuvre. Much like radar on the Earth, radar in space could also track objects around the satellite. The ability to steer signals in all directions from a satellite, like radar, is also beneficial in tracking other satellites and debris.

1.4. Space debris detection

Debris or resident space objects (RSOs) are considered a major threat to the expanding space industry. As launch costs decrease, more and more organizations contribute satellites to the vast, yet limited space in LEO. As to the number of satellites in orbit increases, the probability of a collision between the RSOs also increases. Figure 1.4 is a visual representation by the European Space Agency (ESA) of the crowded orbits of the Earth. Because of expanding space programs,

many orbits house inactive and unmonitored satellites, which have the potential to collide. In February of 2009, a Russian satellite (Cosmos-2251) and an American satellite (Iridium 33) collided at a relative speed of 11.7 km/s in LEO (Malik, 2017). The collision destroyed both satellites and released thousands of pieces of debris, some larger than 10 cm. Satellite-on-satellite collisions, despite being rare, can have enormous potential impact due to the debris released (Craig, 2015). Space debris from such collisions varies in size and potential damage ranging from small dust particles up to large satellite fragments. While in orbit, the debris can damage other satellites, thus posing a constant risk.

Figure 1.4: Visualization of RSOs by the European Space Agency (ESA, 2013)

With the increasing number of satellites, collision mitigation has become a topic of interest in the scientific community. Ground-based facilities have been designed, such as the Satellite Laser Ranging (SLR) station in Germany (Buske, 2013), to contribute in the effort to track RSOs. However, these ground stations can prove to be expensive and have several performance limitations.

Ground-based tracking of RSOs can primarily be broken down into two categories: active and passive tracking, both of which can be further divided using optics or radar. There are other ways of tracking RSOs, however optical- and radar-based instrumentation have been the most popular. Active tracking refers to a method where the initial input is provided by the tracking system, such as a laser source or transmitting antenna, and the reflected response is measured to determine positional information of the target. For example, SLR is an active system that transmits short pulses of light and measures the reflected response. Passive tracking refers to a method where the variations in a pre-existing or predictable system are used to determine positional information of the target. For example, ESA operates an Optical Ground Station (OGS) in Spain, which uses a telescope to detect and track RSOs (ESA, 2013). The OGS is passive because it does not provide any input response; rather, it relies on the sunlight to reflect off of the RSO.

As mentioned earlier, ground-based tracking can be expensive and carries with it several limitations. Optical instruments, such as lasers, reflectors and telescopes, depend on a clear line of sight between the tracking instrument and the RSO. effects of weather and daylight pollution, optical tracking facilities are located far from cities and at a higher altitude, part of why they can be expensive to construct. Despite being located away from sources of light pollution, OGS from ESA can only track objects at night provided the orbit of the RSO is within the Daylight pollution and scattering from the atmosphere are also an additional cause for complications. To minimize the line of sight of the ground station. Expensive infrastructure, operational limitations and lack of flexibility have limited the usage of ground-based optical tracking of uncatalogued RSOs. However, the ground-based optical tracking stations excel in their ability to track known RSOs. The SLR ground stations are specially designed as a laser ranging instrument for satellites

that carry a customized reflector, acting as a tracking service for satellite operators and contributing to the International Earth Rotation and Reference Systems Service (IERS, 2013) catalogue of known RSOs.

Unlike optics-based facilities, radar stations are less affected by weather due to the propagation characteristics of electromagnetic (EM) waves. The atmospheric scattering of EM waves is not only minimal (compared to light), but also well-modelled, which helps in the mitigation of signal errors. However, there are two major limitations to ground-based radar tracking of RSOs: free-space propagation loss and radar design complexity. Free-space propagation loss is the attenuation of signal strength in a medium over a distance, as described by Equation 1. “A” is the attenuation measured in decibels (dB), “d” is the distance in metres and “λ” is the wavelength of the signal in metres.

$$A=\left(\frac{4\pi d}{\lambda}\right)^{2} \tag{1}$$

For example, the Global Positioning System (GPS) L1 carrier signal, at 1575.42 MHz or a wavelength of 0.19 m, travels approximately 20,200 km attenuating the signal strength by 180.5 dB (Gerald, 2014). Since visible light is also an EM wave, it is affected by the same attenuation factor. However, unlike the EM waves used in radar-based systems, light- or optics-based systems have the advantage of a powerful transmitter. The Sun acts as a powerful transmitter of not only visible light, but many other frequencies that can be utilized by optical instruments. For radar instrumentation, the initial signal must be provided by the system. For example, the AN/FPS-117 long-range radar system designed by Lockheed Martin (2013), as depicted in Figure 1.5, is an active radar installation intended to detect and track flying objects within a 470 km range. The system consists of a long-range L-band radar used to track objects in the

atmosphere and LEO by transmitting a high-power RF signal and then analyzing the reflected response. Using 175-215 MHz at 1.2 MW as peak power output, it was designed for the US Navy/Air Force to track missiles at high altitudes. However, the main factors limiting the range of an active radar design are the transmitting power and the receiver's sensitivity. If the transmitting signal strength is not large enough, the attenuation due to free space propagation loss and absorption by the target would make the receiver unable to detect the reflected signal. The AN/FPS-117 can demand up to 24.6 kW of power, which requires a power management unit and increases the cost and size of the system. The power requirement induced range complication is one of the performance limitations of radar designs, especially for space applications.

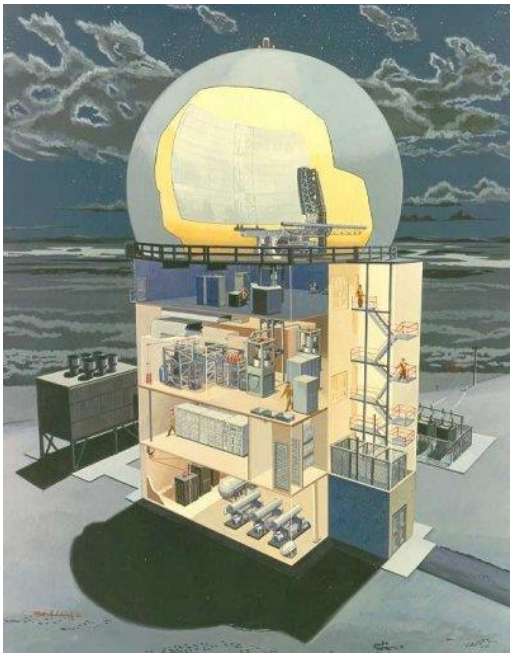

Figure 1.5: AN/FPS-117 radar design model (Lockheed Martin, 2013)

The second limiting factor of a ground-based radar system is design complexity. To track or detect a target, the system has to be able to interpret a few parameters: distance from the target,

velocity of the target, and size of the target. One antenna as a receiver is incapable of interpreting all this information, as there is no directional or range differentiation. A single radiating antenna is incapable of distinguishing the distance to the source of a signal (when used only as radar), therefore an array of antennas is required to track an object. Antenna arrays, as will be discussed in the next section, require a complex feed network and front-end design that can interpret the phase of each element. The complexity in the design of a front-end for a phased array antenna, especially with high power systems like the AN/FPS-117, further drives up cost.

Expensive infrastructure design and installation, performance limitations and design complexity are few of the reasons ground-based RSO tracking is not an adequate response to the increasing threat of space debris (Bauman, 2013). Satellite-based debris tracking, as will be discussed in Chapter 2, has similar antenna requirements as satellite-satellite communications (with regards to signal steering) giving one radio design the ability to perform multiple tasks.

1.5. Phased-array antenna

Signal steering is the ability to change the direction of the main lobe of an antenna. Signal steering can be achieved by placing the antenna on a rotating mount, or, in case of a satellite, rotating the satellite. Physical change in the antenna's orientation can be avoided with an electronically-steered antenna, such as a phased-array antenna (PAA). A PAA is a structured array of radiating elements (antennas) that uses phase differences across each/multiple antenna(s) to direct radio waves in the desired direction (Hansen, 2009), as illustrated in Figure 1.6. The red and blue lines represent crests and troughs of the electromagnetic signals propagating outwards from the antenna, creating ripples that add to or annihilate each other, causing a directional component. PAA systems are mainly used in military applications for their high precision and

the absence of moving parts, which is why they are comparatively just as large as conventional radars.

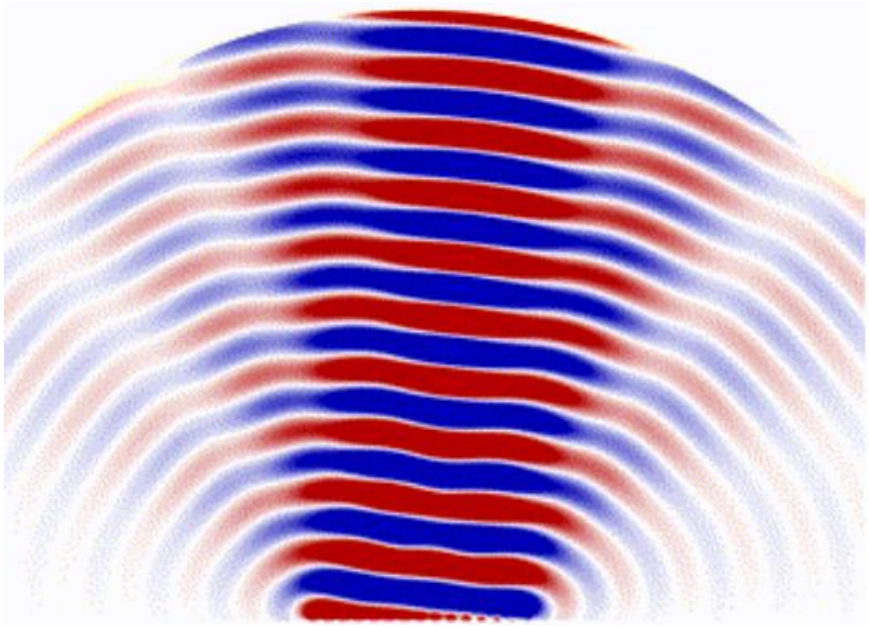

Figure 1.6: Phased-array steering (Wikimedia, 2016)

Additionally, traditional antennas radiate signals in all directions evenly, but a PAA system can choose the direction to send and receive from, therefore each radiating element may use only a fraction of the required power to focus energy on a specific target, reducing the need for large amplifiers in their design. But the key advantage of this design is to filter out signals originating in specific regions by adjusting the phase of each antenna's output, allowing all necessary calculations for directional stability to be performed by the onboard computer (Hansen, 2009). Although the PAA has many advantages for tracking objects, it is complicated to design and therefore is rarely used on commercial products.

Many PAA design complications arise with the need to separate the RF signals associated with each antenna element. Figure 1.7 illustrates how the direction of the incident wave is a function

of the time delay between signals at each measured node, which are points along the vertical axis. Each node represents an individual antenna, as part of a linear array that receives a slightly delayed signal due to the physical distance between them. The time-delayed signal, or phase-shifted signal, needs to be processed real-time to compute the direction of the incident wave or the main lobe of the PAA.

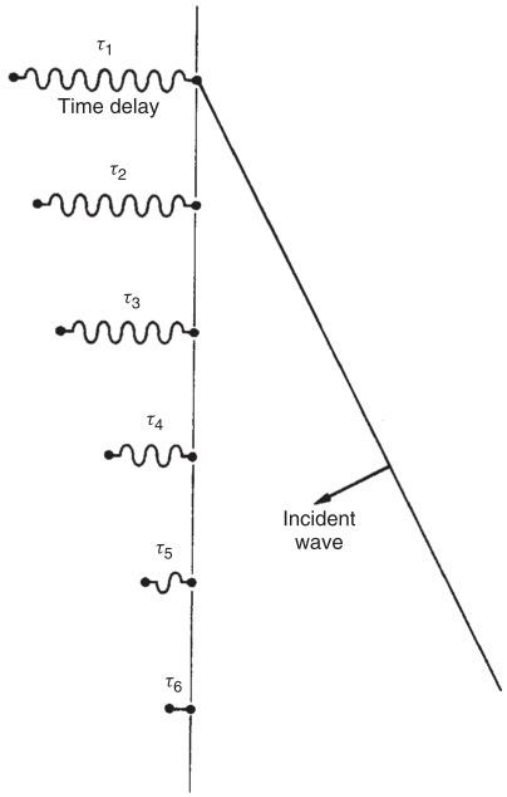

Figure 1.7: Linear array with time delay (Milligan, 2005)

As a receiver, the front-end of a PAA must separately determine the phase-shift of the EM waves measured at each antenna. The phase-shift values can be determined before digitization by the ADC, which would require more hardware components or more computation for a SDR, and increasing power usage. The phase-shift can be determined post-digitization, which would require every antenna signal to be digitized separately, adding to power usage and design costs.

As a transmitter, the front-end of a PAA must separately generate the phase-shifted signals that are to be provided to each antenna. The phase-shift values would be provided by the back-end and additional circuitry or SDR software would organize the signals to the respective antennas. Increasing the number of antennas in a PAA improves the accuracy of the directional control for the incident wave (Hansen, 2009), however the design complexity and power usage also increases. As the signals are separated in the front-end, each signal requires its very own sequence of filters, amplifiers and mixers, reducing the overall efficiency. Design complexity, power consumption and cost are part of the reasons why PAA designs are not common on commercial satellites.

The characteristics of a PAA are beneficial to the concerns mentioned in the previous sections: the signal steering capability is a bonus to the reconfigurable design aspect of a SDR; the PAA's steering is also advantageous for satellite-to-satellite communications; space-based debris tracking will also benefit from the flexible nature of a PAA; and if mounted on a nanosatellite/CubeSat, it can be a positive technology demonstration for the commercial sector. In addition to signal steering, reconfigurability in the frequency spectrum promotes a radio design that can be moulded to a wide range of requirements. As an implementation example, imagine a radio design consisting of a PAA, a front-end, a back-end that can receive GPS signals at 1575.42 MHz, communicate with another satellite at 2.4 GHz, and track space debris while being mounted on a nanosatellite. The effects of adding functionality and flexibility to an existing component on nanosatellites can be: more space technology demonstrations, reduced launch costs, increase in payload capacity, and contribution to RSO tracking.

1.6. Research objectives

A nanosatellite mountable and reconfigurable PAA design offers many advantages to the issues listed in the previous sections such as signal steering, high gain and adaptability for different applications. Frequency reconfigurability adds operational flexibility to SDRs, receiver direction control improves front-end performance and enables the ability to track, and a smaller design helps keep satellite costs down. The research objective of this thesis is to design a frequency reconfigurable phased array antenna for use as a radar receiver and a data communications transceiver in S-band and L-band. This research attempts to demonstrate the compatibility of frequency reconfigurability and signal steering in an antenna design that is nanosatellite mountable, which has not been attempted before.

The antenna simulations and designs will be examined based on the IEEE Standard Test Procedures for Antennas, by applying the gain comparison methodology to produce S11 (signal reflection) and frequency response plots which demonstrate the antenna's frequency reconfigurability. Individual antenna designs are first simulated as a single micro-strip antenna with varying antenna design parameters, like input feed type, micro-strip's length and width etc., and then upgraded for frequency reconfigurability. After simulation results are studied, a proposed design for an antenna array is simulated. Single micro-strip antenna, single micro-strip frequency reconfigurable antenna and the frequency reconfigurable antenna array are then fabricated and tested to acquire antenna characteristics as simulations for comparison.

1.7. Thesis outline

This thesis is divided into 6 chapters. Chapter 1 has introduced the challenge of having a PAA on a nanosatellite. Chapter 2 gives a brief background of antenna designs and applications that have

been incorporated or were suggested previously. Chapter 3 describes the design process starting with the fundamental concepts of micro-strip antenna designs and the detailed PAA design. Chapter 4 explains the test procedures, followed by Chapter 5, which contains the test results. Chapter 6 concludes with the findings of the test results, a short summary and recommendations for future work.

CHAPTER 2: DEBRIS TRACKING APPROACH AND RECONFIGURABLE ANTENNA DESIGNS

This chapter will describe the different methodologies of tracking RSOs. By studying the current technologies in debris tracking, this chapter attempts to find gaps in the existing RSO tracking system that can be filled by a satellite-based radar detector. The gaps may exist due to technological design limitations, performance limitations, and or system cost. After understanding the requirements expected of an antenna design for a space-based debris tracking, antenna reconfigurability designs are described to understand which methodology would be most useful for an RSO tracking application.

2.1. Debris tracking

RSO congestion, especially in LEO, is of growing concern in the scientific community, as it threatens existing and future launches. RSO tracking systems, such as Space Surveillance Network (SSN), catalogue over 20,000 objects (Douglas, 2010) in LEO using a combination of radar and optical sensors (Haines, 2011). The SSN maintains debris tracking facilities all over the world. However, there are identifiable gaps in the SSN: as per United States Air Force (USAF) requirements, Gaposchkin (2000) highlights that the SSN tracking gap times between tracks is longer than needed; and additionally, not all regions of LEO are monitored regularly. The shortcomings of SSN may be because it primarily relies on ground-based optical systems. Gaposchkin (2000) proposes a satellite based optical sensor to fill the SSN gaps.

Tracking debris systems can be categorized in two different ways; active and passive tracking. As mentioned in the previous chapter, the two most common methods of tracking debris are using radar and optical instruments.

2.1.1. Optics-based satellite RSO tracking

Space surveillance is the process of generating and updating a catalogue of potentially Earth-bound objects but can be extended to the catalogue of objects in orbit as well (Douglas, 2010). Passive optical systems have performance limitations, like daylight pollution and weather. To overcome this hurdle, designers have changed their focus to satellites that possess the capability of tracking and cataloguing objects in orbit. Similar to how the Hubble space telescope operates, the Space Based Space Surveillance (SBSS) by Boeing and the USAF (as proposed by Gaposchkin in 2000) is a satellite-based optical telescope designed to track RSOs in and falling out of orbit. Launched in 2010, the Space Based Space Surveillance satellite is one of many satellites in a planned constellation supporting ground infrastructure intended to track objects in LEO and Geostationary Earth Orbit (GEO) regions.

Similar to passive optical trackers, active systems use a telescope to capture reflected light from objects of interest, with an exception that the reflected light is generated by the system itself. In the case of Satellite Laser Ranging (SLR), a powerful laser transmits pulses of light, e.g., 532 nanometres wide at a rate of 10 nanoseconds and a photon detector is able to capture the reflected light and determine the range of the RSO (Buske, 2013).

SLR is a ground based optical/laser system that relies on a pre-existing catalogue and orbit trajectory of a satellite to aim a laser in order to determine the altitude of the RSO: therefore, it is unable to track RSOs by itself. SLR is beneficial in RSO tracking field due to its high accuracy

in determining the altitude of the object compared to other optical methods, making it a great addition to an existing telescope. This system implements the combination of two ranging methods, telescope to detect debris and a laser for accurate range calculation. The telescope continuously scans the night sky for objects moving with reference to the stars. Once an object is detected, the laser is used to obtain the object's orbital characteristics and emits a pulse of light, which is reflected back to determine the altitude of the debris with relatively high accuracy (Buske, 2013). By understanding how RSO trackers like the SLR work, nanosatellites can be designed to complement existing systems. By providing rough location estimates of several RSOs within its vicinity, a nanosatellite can provide the SLR with enough information to track and collect more data on the RSO.

2.1.2. Radar-based satellite RSO tracking

Using a similar design as the active optical tracker, radio signals are used to track objects in orbit. By emitting powerful RF signals and measuring the reflected response, multiple objects are catalogued at once. There are several advantages to radar-based systems compared to optical-based systems: RF signals (at specific frequencies) can penetrate varying weather conditions with little signal loss or refraction, they are able to operate at any time of the day even from the surface of the Earth, and they are able to track multiple objects at once and have the ability to determine range with relatively high accuracy.

Tracking multiple objects at distance using radar has been used since the 1940s and over the years, advancements in RF development has led to large missile defence radar installations. Since radar stations already tracked objects in the Earth's atmosphere, such systems were extended to reach LEO. However, RF signals lose their energy density much faster than light.

The weaker energy density implies that the reflected signals from distant and small objects would be weak in strength and undecipherable in case of low signal-to-noise ratio (SNR).

Adapting from this loss of signal strength, a proposal was made to mount an active radar design on the International Space Station (ISS) in 1993. In the early 90s, space debris was considered a threat to the Freedom Station (now the ISS), and several proposals were put forth for an onboard system to detect debris and perform emergency manoeuvres. One of the proposed plans was to design a large dome antenna to track 1 cm particles up to a range of 100 km. The proposed research was to mount the large antenna on the exterior of the ISS as a transceiver. The transmitted signals would reflect off the debris and the signals received back to the ISS would be analyzed to determine relative velocity and distance (Arndt, 1993). This design was never mounted on the ISS due to the 10 kW power requirements and the 16 m^2 antenna dish which would add to the launch cost.

Due to power and weight constraints, radar installations have been limited to the ground. The power constraints are a result of the energy required to transmit a signal strong enough to reflect off a RSO several hundred kilometres away and return to the receiver. However, a passive radar receiver could meet the power and weight budget for a smaller satellite provided there was a signal being transmitted at a known frequency (Haines, 2011).

Lockheed Martin's Space Fence could be used for this purpose. The Space Fence is a series of large mobile radar platforms spread over multiple continents and thousands of kilometres (Haines, 2011). The large S-band antennas constantly transmit signals at 766 kW from Earth into space, where the debris reflects the signals back towards Earth which are then detected by several receiver S-band stations also located over a vast area. The receivers and transmitters are

interconnected, allowing them to determine the position and velocity of objects being tracked. The design was due for setup in 2017 for operation by 2019 (Gruss, 2014) where it would replace aging systems by placing more than 400 deployable radar stations (mobile) to catalogue and continuously monitor LEO. It would also be compatible with the SSN (Space Surveillance Network) mentioned earlier, appending to the large catalogue list of RSOs in LEO.

The US Air Force Research Lab and NASA conducted a study to outline the future of space debris tracking and concluded that optics, ladar (laser radar) and radar are not sufficient on their own to track all types of debris from all platforms, space- or ground-based. Future systems that would add onto the SSN would have to be a combination of both ground- and space-based systems (Campbell, 2000).

The signal steering capabilities of ground-based radar do not require a re-design of the single element antenna. The complications of signal steering are mainly dependent on the front- and back-end designs. Antenna array layout and beam steering are largely independent of the single element antenna. The geometry of a single micro-strip, provided it is symmetrical and duplicated, will have little effect on the beam steering once the phase centre has been calibrated for. The phase centre offset for an antenna array is caused due to minor symmetrical and design imperfections of the individual elements. The offset is calibrated for by the front-end. Therefore, individual micro-strip antennas in an array can be made reconfigurable, while maintaining beam steering capabilities. Thus, the proposed concept of a satellite mountable phased-array antenna, that can perform signal steering, has the ability to passively track space debris. Phased-array antennas, as implemented on the AN/FPS-117, possess the ability to utilize signal steering as a means of determining characteristics such as velocity, relative position and electromagnetic property of the object being tracked, which are similar to the requirements for tracking space

debris. The novelty of this research is not only to design a phased-array antenna as a radar on a nanosatellite, but to also improve on the static nature of antennas by combining signal steering and frequency reconfigurability.

2.2. Antenna reconfigurability

The concept of the micro-strip antenna dates to the 1970s, when initial publications and several designs had been proposed (Peixeirco, 2011). However, the concept of a reconfigurable micro-strip antenna is relatively new, as publications date back to the mid to late 2000s (Guo, 2010). The reconfigurable aspect of a micro-strip antenna depends on the substrate (a layer of material which the antenna rests on), geometry of the antenna and the input type, all of which adjust various antenna characteristics. Characteristic modifications such as frequency, radiation pattern and polarization are specific to the application, and are managed by changing the flow of current that allows signals to radiate. This ability to reconfigure is useful on smaller nanosatellite platforms, both for saving space/mass and for adding functionality at a lower cost.

An example of a frequency reconfigurable antenna, designed by Azarmanesh (2012), is illustrated in Figure 2.5. The antenna is an ultra-wideband (wide frequency range) fixed circular micro-strip on the top layer of a PCB, under which is the substrate followed by the ground plane. A typical ground plane is a fully-covered conductive copper layer under the substrate. However, Azarmanesh's design incorporates a ground plane with a slit shown in Figure 2.5 as the yellow trace and the vertical arms. Using a capacitor and a p-n switch-diode (electronically controlled switch and low pass filter) in a series connection, Azarmanesh created an RF switch for low frequencies. By applying 0.7 V to this switch-diode between two micro-strips, the length of the filter element (ground plane cut-out/slot) placed on the ground plane changes as seen in Figure 2.5. The change in length of the slot affects the frequencies that are resonated on the designed

antenna: like a filter. By adding four total switches at different lengths, the frequency response can now be changed electronically. The four configurations show different slot lengths on the ground plane and how they act as a filter to affect antenna characteristics. The centre frequency of the antenna shifts with each configuration: configuration 1 was centred at 5.5 GHz, configuration 2 at 3.7 GHz, configuration 3 at 2.5 GHz, and configuration 4 at 2.5 and 5.6 GHz.

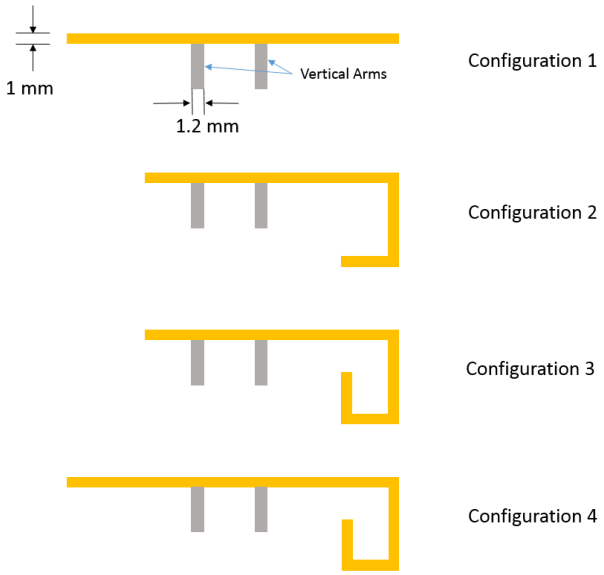

Figure 2.5: Substrate embedded RF switch by Azarmanesh (2012)

Azarmanesh's frequency reconfigurable micro-strip design incorporates two components: an ultra-wideband micro-strip antenna and a micro-strip filter. Azarmanesh's design benefits from ground plane modification by negating the need to optimize switch trace thickness, as the trace width can affect the frequency response as well. RF traces on PCBs are susceptible to noise and therefore require special attention during layout; however, by modifying the ground plane geometry, Azarmanesh reduces the effect of noise on the frequency response.

Similarly, Singh (2014) designed a Steering Wheel Shaped Frequency Reconfigurable Antenna, shown in Figure 2.6, to act as a fast switching antenna. The design illustrates a circular patch in the middle with an outer casing like a steering wheel connected to the circle through Micro-Electromechanical System (MEMS) switch at four ends. The switch is controlled by DC voltage that can be applied electronically, which makes the antenna capable of operating at seven frequencies between the ranges of 6.25 to 8.25 GHz. By turning the switches on or off, the geometry of the patch antenna changes, affecting the frequency response and the radiation pattern. The effect on the radiation pattern changes the half power beamwidth and the direction of the main beam as illustrated in Figure 2.7.

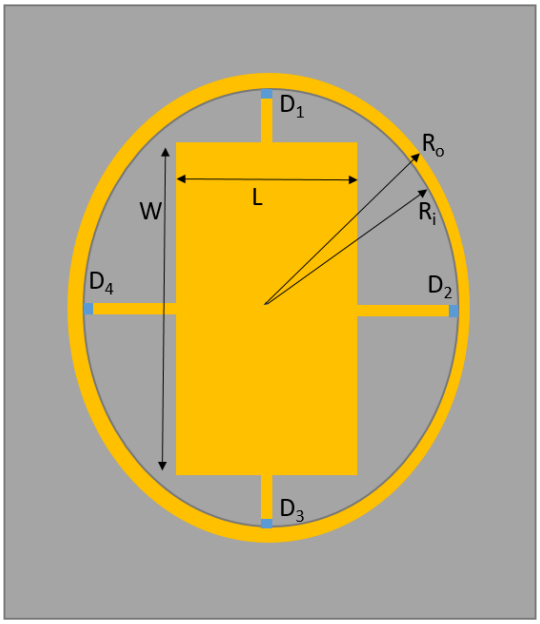

Figure 2.6: Circular patch with configurable input using MEMS. (Singh, 2014)

Figure 2.7 illustrates the change in radiation pattern of Singh's micro-strip due to a specific switch configuration. Compared to an antenna array, the radiation pattern change is limited to the 12 different combinations of switch configurations, whereas the array is limited only by the

front-end's phase accuracy. Although the beam steering capability of Singh's design is limited to a fixed number of directions/orientations, the wider main lobe negates the need for highly accurate directional control.

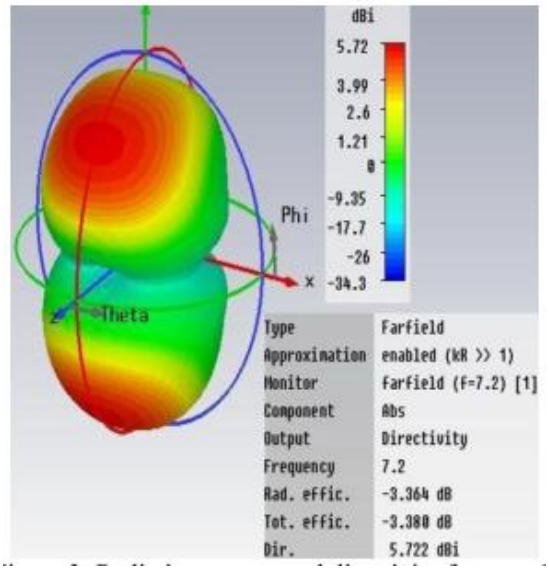

Figure 2.7: Main lobe direction change. (Singh, 2014)

Mohammad (2010) proposed a reconfigurable antenna with extended U-Slot used as a switchable polarization for wireless applications (Figure 2.8). The extended U-Slot represents a cut-out or a slot shaped like the letter U inside a micro-strip, which can be extended using switches. The switch is also a diode-switch, which can be controlled electronically by applying DC voltage. The antenna is capable of switching between linear polarization (LP), left hand circular polarization (LHCP) and right hand circular polarization (RHCP). The design of the slot or cut-out around the input coaxial-feed has three switches that connect and disconnect the gap created by the rectangular slot. For antenna 1, when the switch is connected, the current will flow out through the connecting medium and if there is symmetry in the design, the antenna will be linearly polarized. When the switch is disconnected, the capacitor acts as a filter for low

frequency signals. For antenna 2, when the left switch is connected, the antenna acts as LHCP, and when the right switch is connected, the antenna acts as RHCP.

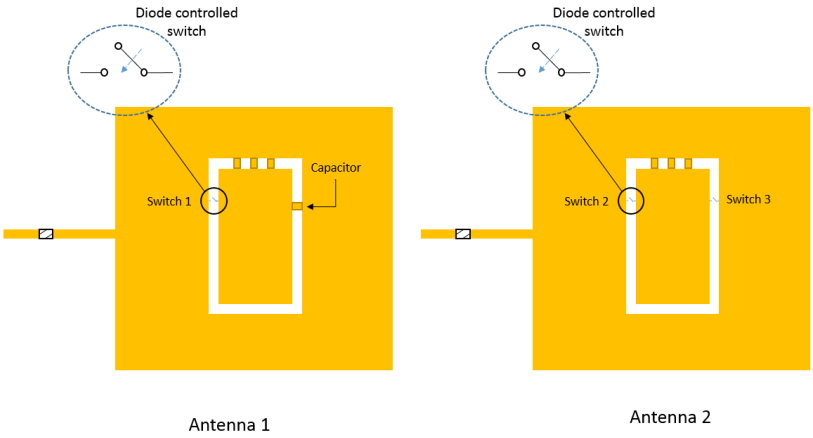

Figure 2.8: Polarization switching reconfigurable patch designs. Mohammad (2010)

Although Mohammad designed the antennas in Figure 2.8 for polarization reconfigurability, the switch configurations also modified the frequency response ranging from 5.7 to 6.3 GHz. It is important to note that geometrical changes to a micro-strip affect the frequency response and will be discussed further in the next chapter.

While there have been significant advances in micro-strip antenna reconfigurability, few proposals progress to testing them as an array. As seen above, single micro-strip reconfigurability is achieved via the modification of the signal input to the radiating micro-strip, either by filtering the signal or changing the geometry of the micro-strip. On such a reconfigurable single micro-strip antenna, the feed network is straightforward to route. As illustrated above, the inputs to a reconfigurable single micro-strip antenna are the RF input (for the signal), and the DC power and ground pins. However, when dealing with an array of reconfigurable antennas, the routing becomes difficult and has a detrimental effect on the

performance of the antenna. This detrimental effect can be in part due to interference between the input trace lines and the radiating micro-strip. However, there are many more ways to provide an input signal to a micro-strip and these will be discussed in the next chapter. To understand the effects of an input feed network, several feed networks will be studied in simulation to determine which input methodology is suitable not only for frequency reconfigurability, but also for a phased-array. The chosen geometrical layout, the input feed network, and other antenna characteristics are to be determined based on their compatibility with scaling into an array. Once the gain characteristics of the antenna array are tested, its compatibility as a passive radar debris tracker on a nanosatellite can also be determined.

CHAPTER 3: ANTENNA THEORY AND DESIGN

This chapter will discuss antenna theory and design using simulations. Several antenna characteristics will be analyzed to determine their effects on performance as a single antenna, as a reconfigurable antenna, and as an antenna array. Antenna characteristics will be modified based on their simulation results and how they apply towards the objective of this thesis. Characteristics such as: input feed network, substrate material, reconfigurability, polarization, and radiation pattern control will be simulated and analyzed in detail using scientific principles.

3.1 Patch antenna geometry

Patch or micro-strip antennas have been proposed since the 1970s, but initially suffered with low bandwidth and inefficiency due to poor choice of substrate material and not enough space for the components that followed an antenna (Pozar, 1996). As technology progressed, scientists could improve upon these shortcomings making the micro-strip one of the most revolutionary antenna designs. The simplicity of a micro-strip antenna and its functionality allows for complicated designs such as the Phased-Array Antenna (PAA) to be fabricated on one PCB with ease. The different size, shape and placement configurations allow for various application-specific designs, in many cases without additional hardware requirements (Hansen, 2009).

In essence, a micro-strip antenna works on the principle of flowing electricity that induces changes in the electro-magnetic (EM) field (Khan, 2012). Figure 3.1 shows the basic shape and design of an inset-feed micro-strip antenna. The micro-strip itself is usually made of highly conductive material, like copper, which represents the top layer over a dielectric substrate, and the substrate is sandwiched between the top layer and the bottom layer (usually ground). In order to drive power into this antenna, an input transmission line is attached to one side.

Characteristics of a micro-strip antenna, such as centre frequency and bandwidth, are primarily dependent on the length and width. Other characteristics of a micro-strip antenna, such as input impedance and signal reflection (a measurement of coupling between the transmission line and the micro-strip as a function of frequency) are primarily dependent on the input feed type and geometrical layout. The overall frequency response of a micro-strip antenna is a combination of the two characteristics mentioned above. Substrate thickness and material composition (or the dielectric constant) are also key parameters that affect the frequency response (especially bandwidth) of the antenna (Hansen, 2009).

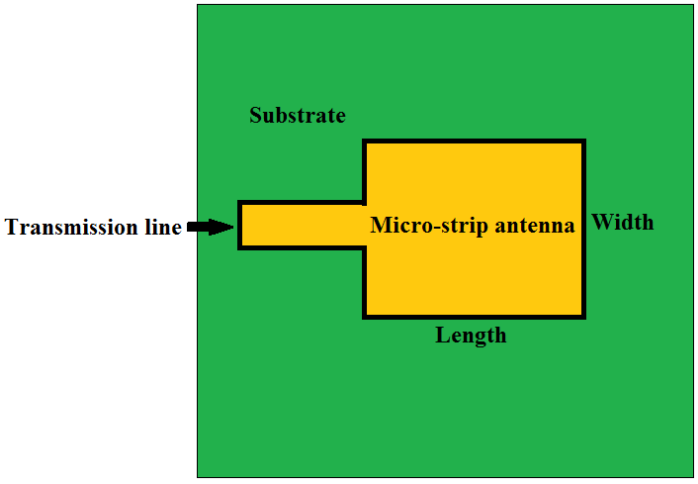

Figure 3.1: Inset-feed micro-strip antenna (Milligan, 2005)

A micro-strip antenna is an open source circuit, as there is no exit for the current flowing in the micro-strip from the transmission line. Instead of current outflow, a reflection of the inflowing current from the transmission line rebounds from the opposite side. Some of the reflected current returns back through the transmission line, which can be measured as the signal reflection response or better known as the S11 response (Milligan, 2005).

With a direct current (DC) input, the entire transmission line and micro-strip antenna are fixed at the same voltage and current. However with an alternating current (AC) input, the voltage and current varies across the micro-strip. Figure 3.2 illustrates the varying current from the transmission line to the micro-strip's edge. Depending on the frequency the current alternates at, there is a stabilization point where exactly half the wavelength of the input current is equal to the length of the micro-strip. An illustration of half wavelength resting is depicted in Figure 3.2, where the connection between the transmission line and micro-strip is at 0 amperes and the peak current is halfway between the two sides of the micro-strip antenna.

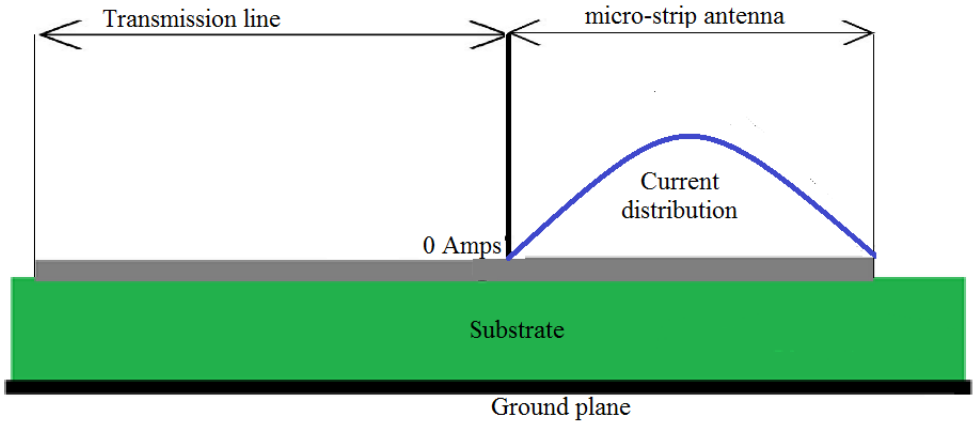

Figure 3.2: Current distribution on a micro-strip antenna (Milligan, 2005)

Similarly, Figure 3.3 defines the voltage strength across the patch, which highlights a key property of an open-ended circuit: the AC voltage and current are orthogonally out of phase (Hansen, 2009). In an open ended micro-strip antenna design, the voltage peaks at either edge of the micro-strip and is zero at the centre. When comparing the voltage and current distribution, the two signal characteristics are out of phase by 90 degrees.

In order to optimize the performance of a micro-strip antenna at a selected centre frequency, orthogonal pairing of the current and voltage is required. While transmitting or receiving, any wavelength multiples that can fit in the length of a micro-strip antenna will have better performance when compared to other signals with wavelengths that cannot fit within the length. As shown in Figures 3.2 and 3.3, only one half of a wavelength of the current and voltage plots is reflected onto the antenna, meaning that a signal with the wavelength in integer multiples of the micro-strip's length will have optimized performance. However, the optimized performance is not always differentiable on the antenna's frequency response plot, because the overall frequency response is a combination of the micro-strip's frequency response and the S11 of the input feed.

Figure 3.3 also highlights the source of the electro-magnetic radiation. As the AC voltage fluctuates, one side of the micro-strip is positively charged, where the electro-magnetic field strength flows from the micro-strip into the substrate towards the ground plane, and the other side is negatively charged, where the electro-magnetic field strength flows from the ground plane into the substrate from towards the micro-strip. The electro-magnetic field not only flows straight through the substrate, but also curves out in what are known as fringing fields (Milligan, 2005). Since the positive and negative voltages are equal on both sides, the Y-axis component fields from the positive side cancel out the Y-axis component fields on the negative side due to opposing directions. The X-axis component of the collective electro-magnetic field flows towards the right for both the positive and negative ends of the micro-strip (for the scenario presented in Figure 3.3). When the voltage fluctuates and switches polarity (due to it being AC), the collective electro-magnetic field strength has a left X-component. The constant switching of the electro-magnetic field strength direction creates RF waves that propagate orthogonally along

the Y-axis. Since the ground plane acts as a reflector to RF waves (as they are also electro-magnetic in nature), a majority of the power supplied flows upwards.

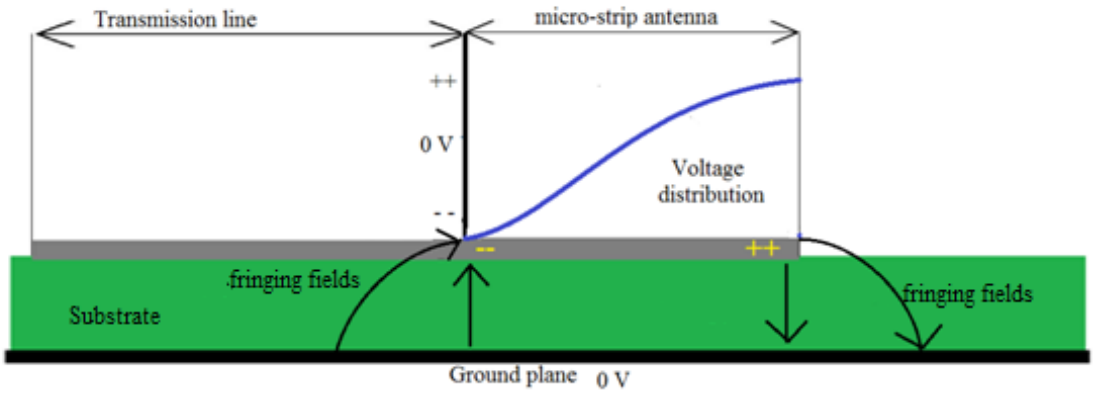

Figure 3.3: Voltage distribution on micro-strip antenna (Milligan, 2005)

In order to demonstrate how the propagation properties of a micro-strip depend upon its geometry, a control design is established to compare the changes. Antenna designs in this thesis will range in the L and S bands (L-band: 1-2 GHz and S-band: 2-4 GHz), because nanosatellites use 3 to 3000 MHz for ground communications.

Assuming a sample centre frequency of 2.1 GHz, Equation 1 is used to derive the length of the micro-strip antenna, given the use of Rogers RT Duroid 5880, which is widely used for antenna dielectric substrate (Ali, 2011) with a dielectric constant of 2.33.

$$f_c = \frac{c}{2L\sqrt{\varepsilon_r}} \qquad \text{(Milligan, 2005)} \qquad (2)$$

$$w = \frac{c}{2f_c}\sqrt{\frac{2}{\varepsilon_r+1}} \qquad \text{(Milligan, 2005)} \qquad (3)$$

In Equations 2 and 3, f_c is the centre frequency at 2.1 GHz, c is the speed of light at $3x10^8$m/s, ε_r is the relative dielectric constant of the substrate at 2.33, the length L which is calculated to be 46.7 mm, and the width w which is calculated to be 55.3 mm. The next step is to determine how deep the transmission line will be inset into the micro-strip:

$$R(d)= R(0)\cos^2\left(\frac{\pi d}{L}\right) \quad \text{(Milligan, 2005)} \quad (4)$$

$$R(d)= \frac{1}{2G} \quad \text{(Milligan, 2005)} \quad (5)$$

$$G= \frac{\cos(wk) + kW + \sin(wk) + \frac{\sin(wk)}{wk} - 2}{120\pi^2} \quad \text{(Milligan, 2005)} \quad (6)$$

$$k= \frac{2\pi}{\lambda} \quad \text{(Milligan, 2005)} \quad (7)$$

$$d= \frac{L}{\pi}\cos^{-1}\sqrt{\frac{R(d)}{R(0)}} \quad \text{(Milligan, 2005)} \quad (8)$$

In equations 4-8, d is the depth of the input feed line in Figure 3.4, R(x) is a function to represent impedance, G is the conductivity at the input transmission feed, k is the wave factor, and λ is the wavelength at the centre frequency. The value of the inset length is determined to be 11 mm.

The antenna designed in Figure 3.4 is based on theoretical calculations only, and therefore would not yield the exact response required. The software tool used to simulate the antenna is called ANSYS or specifically High Frequency Simulation Software (HFSS). ANSYS is a widely accepted industrial high-frequency simulation software and is popular for antenna design and simulations. A majority of the antenna designs discussed in section 2.2 were performed on

ANSYS by their respective authors. HFSS attempts to model a realistic situation as closely as possible; however, the equations used above do not consider several error sources. Some error sources are: effects of air as a substrate, temperature fluctuation effects, fabrication errors, and surrounding RF noise that can alter the performance of an antenna. In software simulation, modelling is not always possible for all real-world scenarios, for example imperfect fabrication. The theoretical calculations, made using the above-mentioned equations, operate as a guideline for understanding which parameter changes what characteristic of the antenna. Simulations based on theoretically calculated values almost never provide the desired output. However, using the equations, antenna parameters can be changed to obtain a desired output.

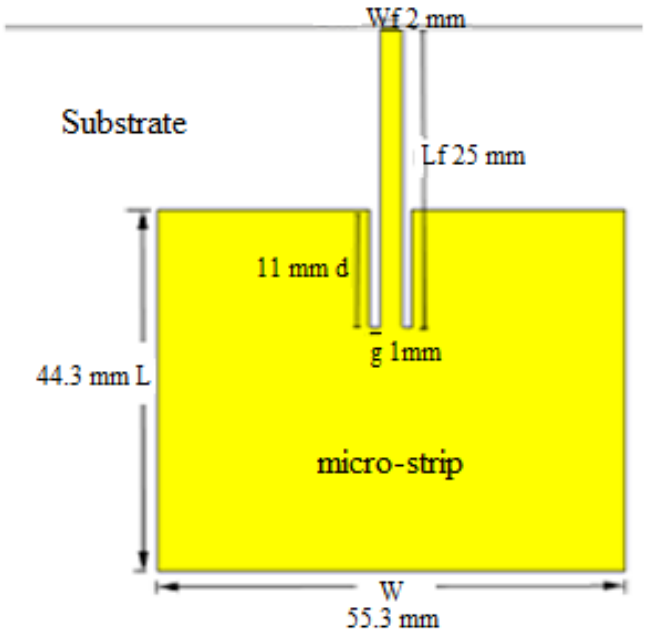

Figure 3.4: Calculated values of the micro-strip antenna (Milligan, 2005)

3.2 Input feed

There are three primary ways of designing a feed system for a micro-strip antenna; inset-feed, aperture-feed and coaxial-feed (Milligan, 2005). A micro-strip antenna feed network affects the

S11 or signal reflection loss characteristic (Peixeiro, 2011). Therefore, analysis of the three feed networks is described and simulated in this work.

3.2.1 Inset-feed

To receive and reference signals through the transmission line, impedance matching is necessary. Impedance mismatched antennas reflect power back against the input transmission line and generate standing waves that degrade the performance of an antenna. Voltage standing-wave ratio (VSWR) is used to describe the efficiency of power transfer between the load and the antenna, which is directly affected by impedance matching (Milligan, 2005). Impedances for antennas are commonly standardized at 50 ohms. Impedance (Z) in a micro-strip antenna is characterized by Equation 9.

$$Z = \frac{V}{I} \qquad \text{(O'Sullivan, 1980)} \qquad (9)$$

Comparing the voltage and current distribution over the micro-strip, the input impedance at the connection between the micro-strip and the transmission feed would be a large value because the current is close to zero and the absolute voltage is high. However, at the centre of the micro-strip, the input impedance would be nearly zero, since the current is high and the voltage is low. Therefore, in order to match impedance at approximately 50 ohms, the transmission feed would be inset towards the centre of the micro-strip. By insetting the transmission feed, the voltage and current parameters balance to provide an input impedance of approximately 50 ohms at a given frequency.

The signal reflection loss or the S11 response of an inset feed design, as shown in Figure 3.5, is shown in Figure 3.6. The S11 response of an antenna is measured using a network analyzer. A

network analyzer transmits signals of varying frequencies to the antenna (via a physical connection) and measures the response through the same connection/port. The antenna connected to port 1 (of a network analyzer) would both transmit and receive through the same port, hence the name S11. The S11 response measures the coupling between the input feed network and the micro-strip antenna. The lower the strength of the reflected signals the better the performance at that frequency.

Figure 3.6 is the S11 plot for the antenna designed in Figure 3.4. The design requirement had a centre frequency at 2.1 GHz; however, the S11 plot illustrates the acquired centre frequency was at 2.8 GHz. In Figure 3.6, the sharp dip at 2.8 GHz illustrates that -24.5 dB of the signal sent to the antenna reflected back. The plot confirms that the designed antenna performs best at 2.8 GHz. As mentioned before, theoretical calculations made based on the equations do not necessarily model the real world. Additionally, many assumptions are made, which may not exist in the simulated design shown in Figure 3.5. For example, the formula assumes the ground plane is of infinite length; however, the ground plane is not infinite in simulation or the real world. Other factors such as substrate thickness, transmission feed radiation, impedance mismatch/inaccuracy, and limitations of the real-world simulations of the software also add to the simulation errors.

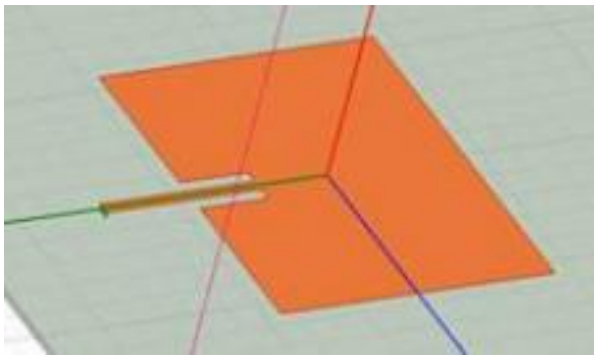

Figure 3.5: Inset-feed micro-strip S-band antenna

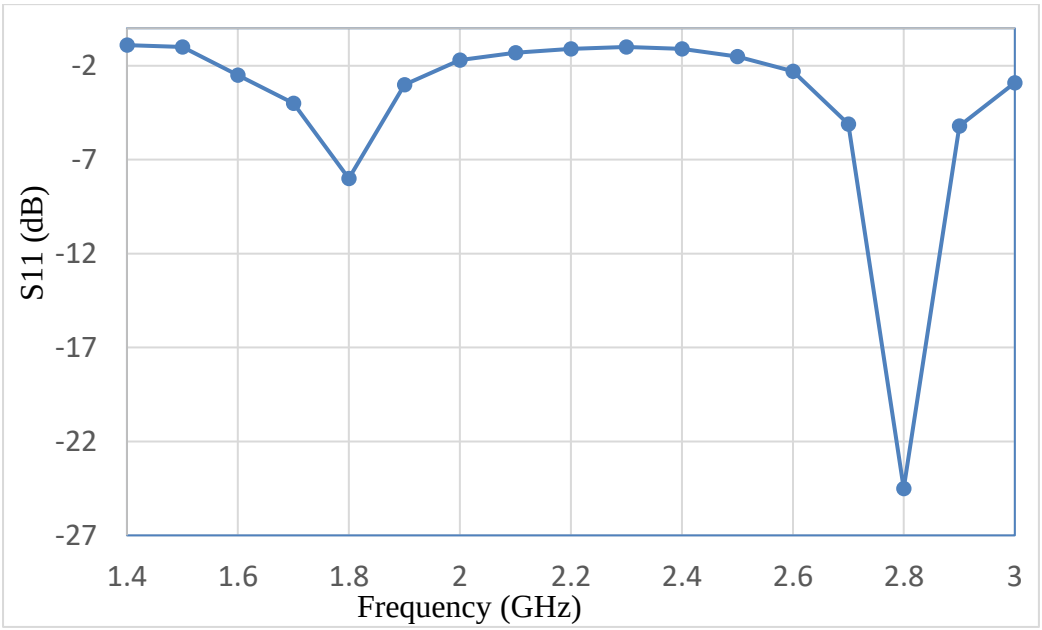

Figure 3.6: S11 response of an inset-feed micro-strip antenna

In order to overcome design drawbacks, and achieve the desired output, antenna designers vary individual parameters to study the change. Equation 2 illustrates an indirectly proportional relationship between the length of the antenna and the centre frequency. Therefore, since the simulation result yielded 2.8 GHz, the length of the antenna should be increased in order to reduce the centre frequency.

Inset feed antennas are easier to design and modify than an aperture or coaxial feed antenna. The length and width mainly control the centre frequency, the transmission line thickness and length offer bandwidth control, but most importantly, the inset value (how far in the transmission line is inset) controls the input impedance (Milligan, 2005).

3.2.2 Aperture-coupled

An aperture-coupled antenna design has a top layer micro-strip, substrate and ground plane similar to the inset-feed design, however, the transmission line is below a second layer of substrate material underneath the ground plane. The design of aperture-coupling, as shown in Figure 3.7, works on the principle of having an opening (a slot or aperture) in the ground plane between the top and bottom substrate layers. The transmission feed then couples with the micro-strip patch, which then behaves like being inset-feed in the centre of the patch (Carver, 1981).

The coupling occurs because the aperture cut in the ground plane is positioned close to the centre of the antenna, which insets the input signal closer to the centre of the patch. The S11 response in Figure 3.8 of a similarly designed aperture-coupled antenna appears to have a wide bandwidth and a slightly weaker response when compared to inset-feed. This coupling is more suitable for applications where the range of operation is variable and therefore a good coverage of a large portion of the frequency spectrum is necessary (Arora, 2015). Designs for narrowband implementations of aperture-coupled micro-strip antennas require strict control over the antenna board thickness, as board thickness can affect the frequency response of the coupling, making it imperfect for reconfigurable designs. Aperture-coupled antennas will be discussed further in Chapter 4.

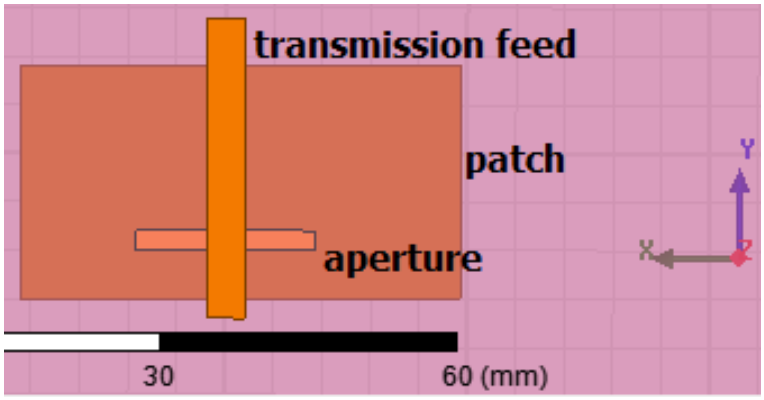

Figure 3.7: Aperture-coupled micro-strip antenna

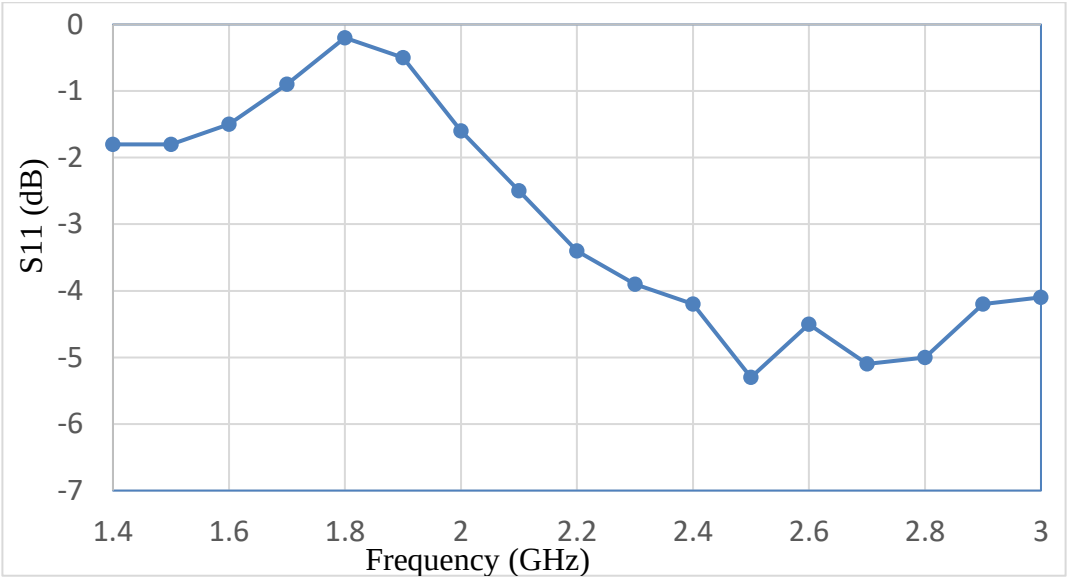

Figure 3.8: S11 response of an aperture-coupled micro-strip antenna

Aperture-coupled antennas can benefit not only from changing micro-strip geometry, but also the geometry of the aperture itself. Aperture shapes can be modified to achieve larger bandwidths and increase coupling between the transmission line and the micro-strip, improving efficiency (Milligan, 2005). However, since the transmission line is exposed on the opposite side of the micro-strip, it is susceptible to noise: aperture-coupled antennas can have low front-to-back ratio.

Front-to-back ratio is the proportionality of gain towards the front, where the micro-strip is, compared to the gain at the back, the bottom/opposite side of the PCB.

3.2.3 Coaxial-feed

Feeding micro-strip antennas via a coax pin requires the input transmission line to come from beneath the ground plane, and travel through the substrate layer before being soldered to a micro-strip from underneath (Milligan, 2005). In Figure 3.9, the circles presented at the bottom right corner represent this coaxial connection from underneath the board.

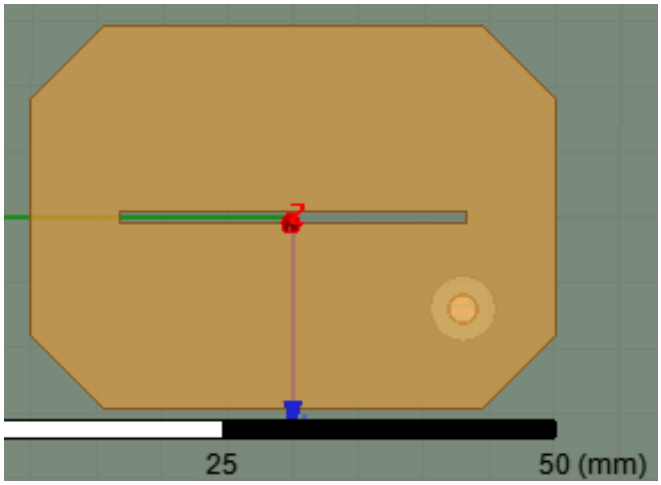

Figure 3.9: Coaxial-feed micro-strip antenna

The advantage of such a feed network is the ability to place the input signal (the coax pin) anywhere on the micro-strip antenna. The freedom to position the signal source simplifies a major parameter when considering feed networks: input impedance matching. As mentioned earlier, most antennas are standardized at 50 ohms, which allows for a 5 V signal from one antenna to appear as a 5 V signal at another antenna, despite the loss in signal strength. In order to match the input impedance at 50 ohms, antennas can be inset-fed, the aperture slot and size can vary, and in the case of a coaxial-feed design, the input transmission line can be placed

anywhere on the micro-strip. Additionally, this freedom provides engineers to design complex geometrical micro-strip antennas with varying characteristics; of which one notable characteristic is the circular polarization of signals. Polarization will be described in detail later in Chapter 3.

The S11 response of the coaxial-fed antenna, shown in Figure 3.10, highlights a narrow bandwidth response. It is important to note that the geometric changes on the patch do not affect S11 response, as it is the measure of the signal that is reflected back from the input feed to the source. Therefore, the input impedance of the antenna is determined by the thickness of the input pin. However, in order to match the impedance of the antenna to 50 ohms, the input pin is setup away from the centre of the length on the micro-strip (Milligan, 2005).

Despite the benefits of a coaxial-feed antenna, the design complexity of providing a signal to the micro-strip via a pin through the ground plane and substrate can make it unappealing for array designs. The placement of the feed network, for a coax-pin input, conflicts with the ground plane, and many designs embed the feed network as a sub-layer inside the substrate. The sub-layer feed network can result in design complications, as the signal flows to the micro-strip through vias. A via is a hollow tube, or a small cylindrical hole dug into the substrate, covered with conductive material to provide a connection between layers of a PCB. Conductive material between the micro-strip on the top layer and ground on the bottom layer can have adverse effects on the electromagnetic field, and can disrupt the antennas propagation characteristics. Coaxial-feed antennas are popular with thicker boards, since the length of the coaxial pin that connects to the micro-strip has little effect on the input impedance of the antenna (Milligan, 2005)

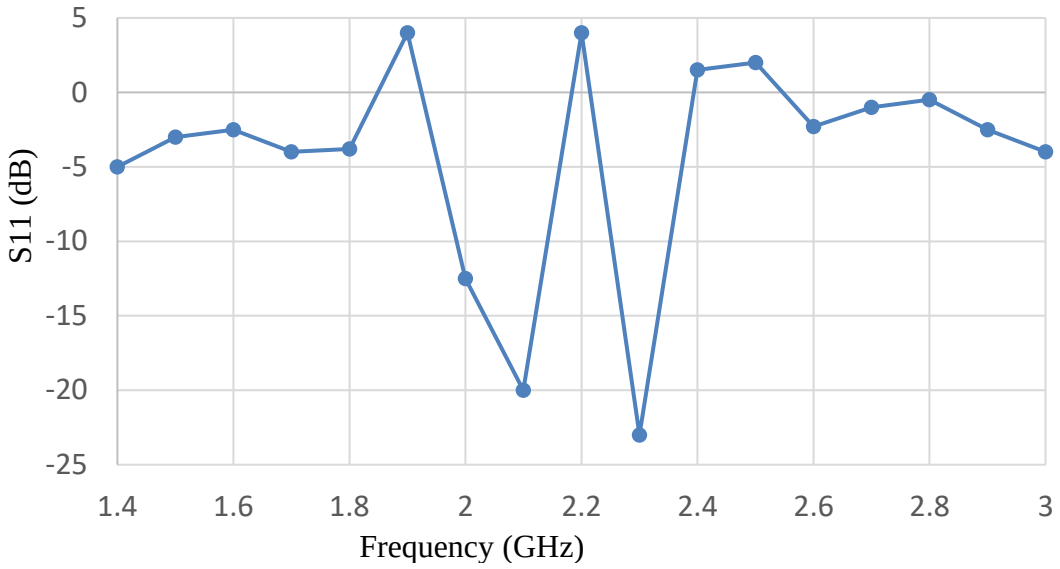

Figure 3.10: S11 response of a coaxial-feed micro-strip antenna

3.3 Substrate material

The substrate material beneath the micro-strip affects the way signals permeate and penetrate through it. Notably, the relative permittivity and permeability of a material determine their performance when considering electro-magnetic fields. Among the input feed networks, the aperture coupled design depends on the substrate material's permittivity for a coupling to take place and thus this feed design will be used to study some substrate materials. It is important to note that not all micro-strip antenna designs react the same way to substrate changes; however, some of the most popular substrates for antennas are Rogers Corporation's (a substrate and materials manufacturer) RT/duroid laminates (Ali, 2011).

As explained in Hosain (2015), the dielectric constant of the substrate material in use has a range of impact on the performance of micro-strip antennas. Hosain (2015) describes using Equation 3 how an increase in the dielectric constant causes a decrease in resonant frequency as they are indirectly proportional. In this research, the objective to minimize antenna size requires the

antenna width to be as small as possible, which in turn requires the substrate dielectric constant to be large. Additionally, most PCB-based coaxial connectors have a specific thickness limitation of 0.8 mm. Hosain (2015) explains that an increase in substrate thickness causes a decrease in the resonant frequency of the antenna. In order to balance out antenna design parameters and substrate choice, a few antenna parameters need to be predetermined. Substrate thickness is fixed at 0.8 mm, the centre frequency is fixed at 2.4 GHz and 1.6 GHz. In order to place the antennas in an array configuration within a 20 cm squared surface, the spacing between micro-strips is required to be approximately a quarter wavelength. The quarter wavelength at 2.4 GHz is approximately 30 mm, which allows 4 elements to be placed linearly, occupying 120 mm of space. The remaining 80 mm is divided amongst the width of the antenna; therefore, the maximum width of the micro-strip antenna can be 20 mm. Knowing the values of length/width, frequency and the speed of light, the dielectric constant of the substrate required can be determined using Equation 2 to be 1.8. Therefore, it is important to use a substrate with a low dielectric constant to remain within the defined size of the antenna array. For this reason, Rogers RO3210 and RO 6002/duroid are chosen because their low dielectric constants.

The FR4 epoxy is a suitable PCB insulator to separate the circuit components from the ground plane underneath, but this degrades antenna coupling and shortens the signal bandwidth (Milligan, 2005). Figure 3.11 shows the Frequency response of an inset- , coaxial- , and aperture-feed micro-strip antenna with FR4 epoxy, Rogers RO3210 and Rogers RO 6002/duroid, respectively. Rogers RO3210, the substrate used in the aperture-feed design, provides a wider range of frequency coverage as compared to FR4 epoxy with a noticeable drop in the antenna gain. As mentioned earlier, tuning is an important aspect of improving antenna performance after the initial theoretical design. However, for the purposes of demonstrating the frequency response

of different substrates on same antenna, there are no differences between the antenna designs, except the substrate. Figure 3.11 with the inset-feed FR4 epoxy substrate has a peak gain of 7 dB at 2.4 GHz and a narrow bandwidth, whereas the Rogers RO3210 substrate has a peak gain of 1.5 dB at 2 GHz and a wider bandwidth. A third substrate, Rogers RO 6002/duroid, has a peak gain of -1 dB at 2.3 GHz with very wide bandwidth. The nature of Rogers RO 6002/duroid illustrates multiple narrow bands, over a wide range of frequencies with a sequential and repetitive filtration - a concept similar to that of how frequency reconfigurable implementations function.

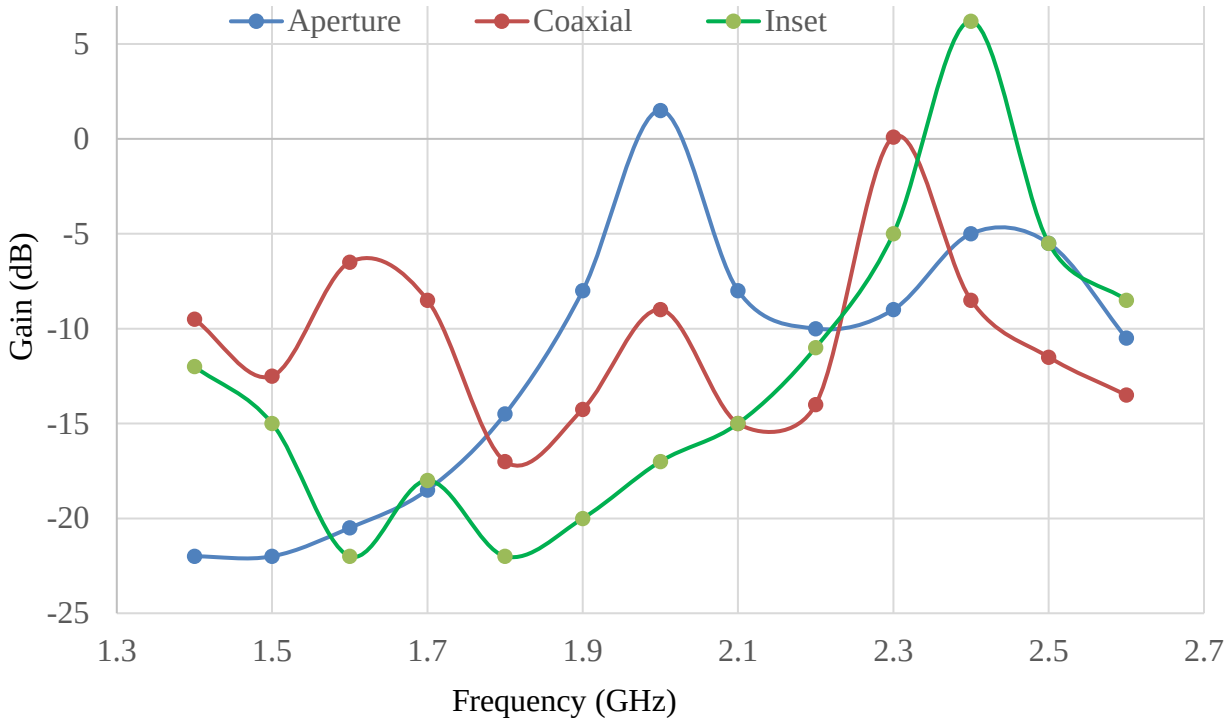

Figure 3.11: Frequency response of an inset- , coaxial- , and aperture-feed micro-strip antenna with FR4 epoxy, Rogers RO3210 and Rogers RO 6002/duroid, respectively

The dielectric constant of a substrate is the major parameter to consider when making a decision. Dielectric constant can affect bandwidth, gain, antenna efficiency, S11 and input impedance (Khan, 2012). The RT/duroid series of antenna substrates are known for their high frequency response and low dielectric constant, which increases bandwidth as seen in Figure 3.11 for the aperture-coupled antenna at a centre frequency of 2 GHz.

3.4 Secondary patch

As stated in the objectives, the micro-strip antenna designed is oriented towards frequency reconfigurability. As explained in the beginning of this chapter, the radiating length of the antenna directly affects the centre frequency. Therefore, to modify the length of a micro-strip, a switch based system is demonstrated in Figure 3.12. The many different connecting components between the main patch and the secondary patch are soldering pads for RF switches packaged as integrated circuits (ICs). These ICs are activated via a 2.7–3 V DC supply that allows current flow from the main patch to leak onto the secondary patch. The current flow suffers from phase-lag and loss of signal strength due to a non-straight path from one end of the switch to another (Kovitz, 2014). Switch designs, such as the ones based on micro-electromechanical systems (MEMS), can mitigate phase-lag and loss of gain factors providing a close to ideal scenario as represented in Figure 3.13 (Tang, 1999).

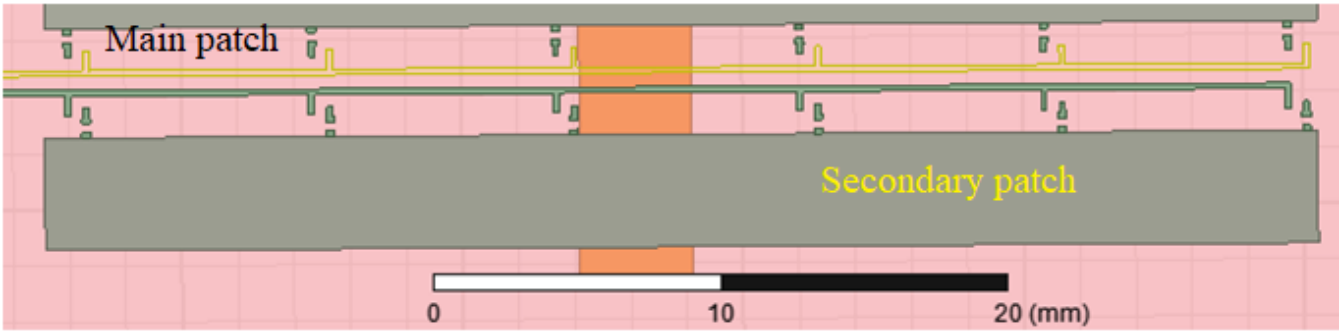

Figure 3.12: IC pad connections between the main and secondary patch

The switch configuration enables the antenna to change its centre frequency to cover multiple narrow bands over a large bandwidth at will. This design allows the front- and back-end to determine what functionality it chooses for the antenna based on the mission at hand. Switch-based reconfigurability is not limited to frequency shifts, but it is also used to change other antenna parameters, such as polarization and radiation pattern as shown in Chapter 2.

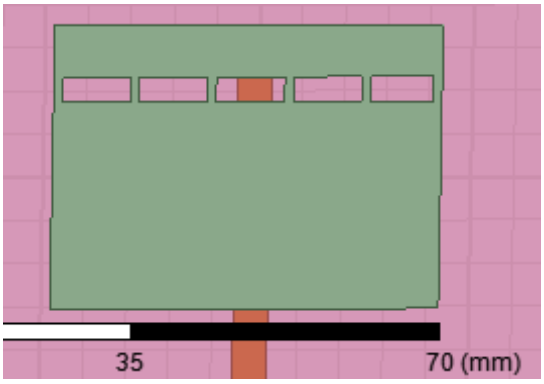

Figure 3.13: Ideally connected switches merging the main and secondary patch

The frequency response plot in Figure 3.14 based on the aperture-feed design in Figure 3.12, illustrates a well simulated model of a micro-strip antenna capable of performing a high frequency shift between the 4.1 dB peak at 1.6 GHz and a 0.8 dB peak at 2.3 GHz with potentially higher peaks in the upper S-band region. In this example, the frequency switch

enables the same antenna to be used for mid-to high-S-band communications and mid-L-band signals like GPS L1.

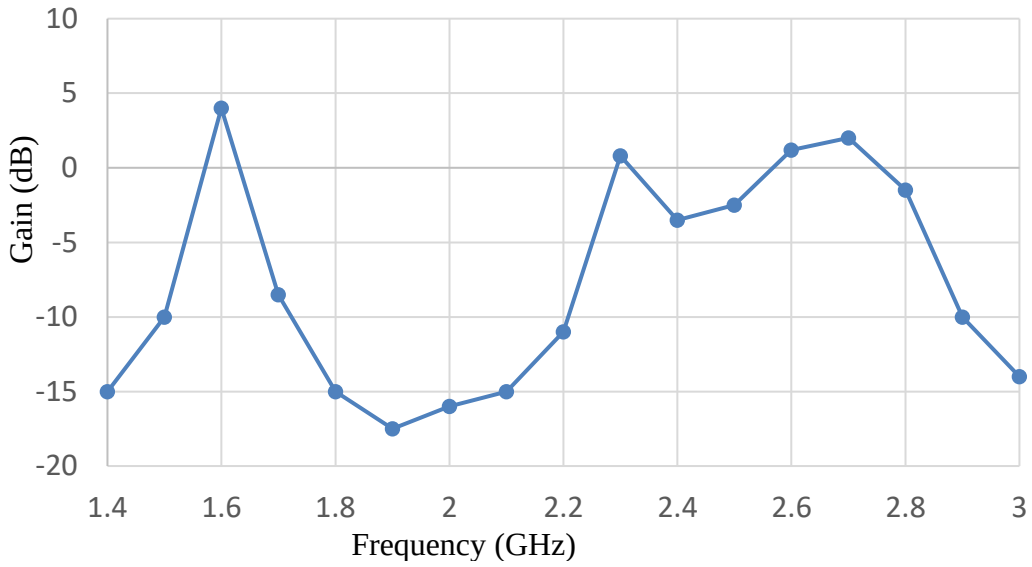

Figure 3.14: Frequency response of the aperture-feed design in Figure 3.12

3.5 Polarization

Circular polarization is the effect of linear polarization in both directions of the patch (width and length). Circular polarization is popular in space applications due to its ability to pick up signals even when they are not directly perpendicular to the antenna. In order to obtain circular polarization from a micro-strip antenna, the antenna must radiate along the width and length with a phase delay of 90˚ (Milligan, 2005). Figure 3.15 explains how linear polarization occurs when signals on a micro-strip only radiate lengthwise, and how circular polarization occurs when signals on the antenna radiate both lengthwise and widthwise with an orthogonal phase delay. The orthogonal phase delay ensures the peak of one signal never meets the peak of another; in fact, the signal strength peaks always coincide in an opposite manner, because the signals are identical.

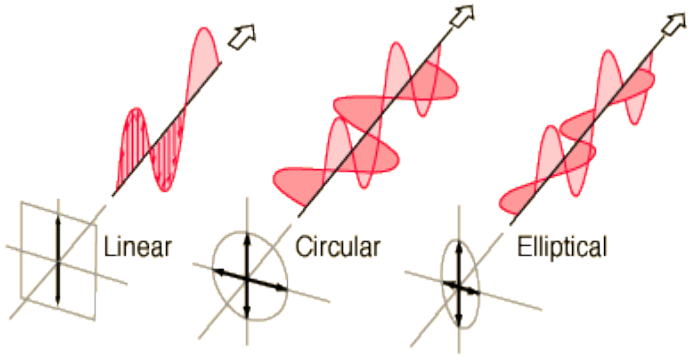

Figure 3.15: Linear, circular and elliptical polarization illustrations (Nave, 2017)

For the coaxial-fed design in Figure 3.9, the rectangular shape of the micro-strip is modified with angled cuts at the edges. These angled cuts act like reflecting walls for the flowing current, which change direction upon impact by approximately 90˚. The orthogonal change in direction makes the antenna radiate widthwise, as well as lengthwise, and the delay for the signal to reach the edge and reflect and reach another edge is designed to be just enough to cause an orthogonal phase shift improving the circular polarization of the antenna. One way to measure circular polarization is to determine the axial ratio, which takes a signal strength ratio of both axes and compares them for balance (Milligan, 2005). Unlike the ideal world, all circularly polarized antennas are actually elliptically polarized due to minor imperfections.

Figure 3.16 illustrates the axial ratio of one specific phase compared with others in the background. In simplistic terms, the peaks and troughs represent the dual-axis stability of the signals on the micro-strip antenna. Peaks represent imbalance between the signals propagating in the two axes. At key points, between 60˚ and 80˚ the axial ratio drops as low at 2–4 dB, which is a positive sign. A perfectly circular polarized signal would have an axial ratio of 1 dB, which would be considered an ideal scenario.

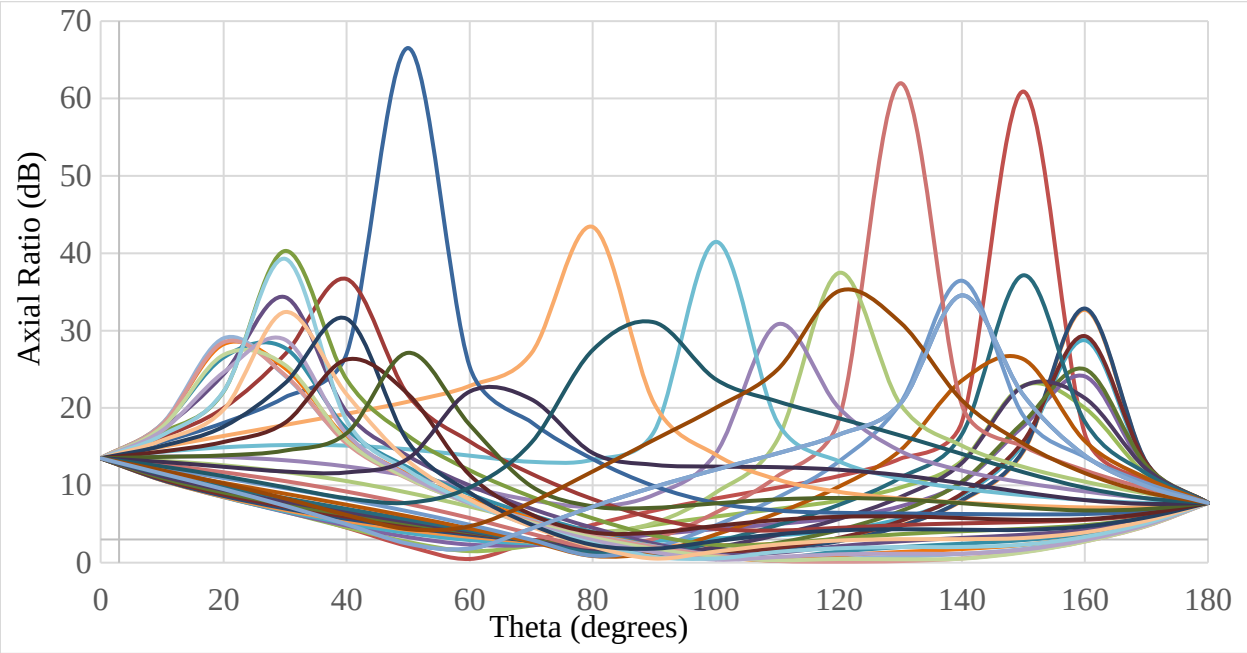

Figure 3.16: Axial ratio of a coaxially-feed circularly polarized micro-strip antenna

3.6 Phased-Array

As mentioned, phased-arrays have a form of directional control with regards to transmitting and receiving signals. This ability is achieved by controlling the phase difference between each radiating element (Hansen, 2009), adding several complications to the design. Much like a circularly polarized signal, the multiple element control with either a fixed or variable phase shift can be a daunting task as designs are computationally, financially and resource intensive. After having studied several different factors that affect antenna design, an approach to designing a planar phased array is demonstrated.

The designed array in Figure 3.17 is a 4x4 grid of identical eighth wavelength micro-strip antennas (linearly polarized) with a coaxial-feed input using Rogers RO 6002/duroid as the

substrate. In an ideal scenario, antennas should be placed a half wavelength away from each other in order to minimize any interference that may occur. At 2.4 GHz, the wavelength of a signal is 125 mm, which implies 62.5 mm spacing between antennas (Hansen, 2009). However, by reducing the antenna size to a one-eighth-wavelength design (Length = 14 mm, Width = 12 mm), enough spacing can be kept between antennas to reduce interference and have the entire design fit on an 18 cm by 18 cm PCB.

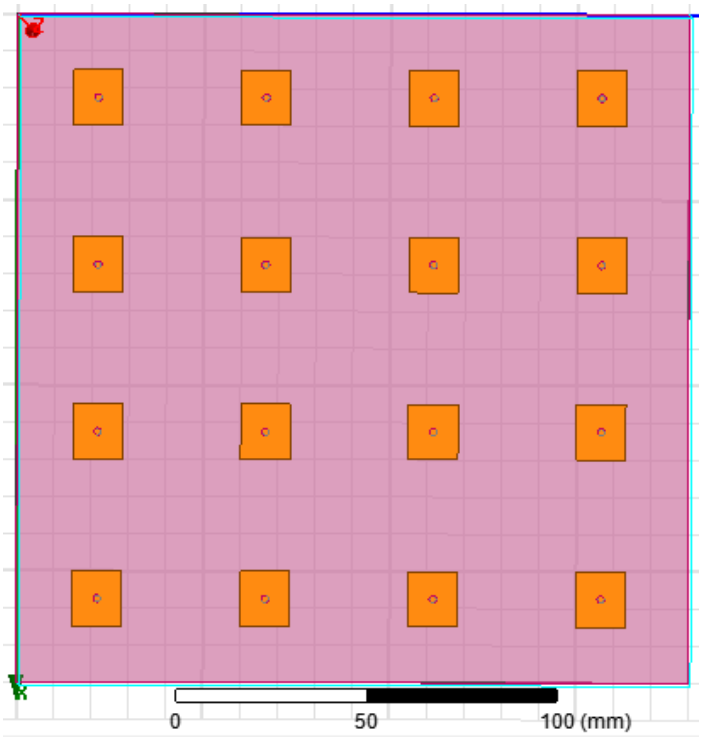

Figure 3.17: Coaxial-feed phased array antenna with eighth wavelength micro-strip antennas

The simulated 3-D radiation pattern of the design demonstrated in Figure 3.17 is shown in Figure 3.18. The red peak beside the theta axis illustrates the natural phase-centre of the designed antenna. As discussed in Chapter 1, the main lobe of the antenna, which is illustrated in this simulation by the red patch, can be steered by creating phase shift to the input signals provided for each antenna. The electronic control would ideally be performed by a front-end, which when

designed, would provide each antenna element with a phase shifted signal to steer the main lobe in 2 dimensions.

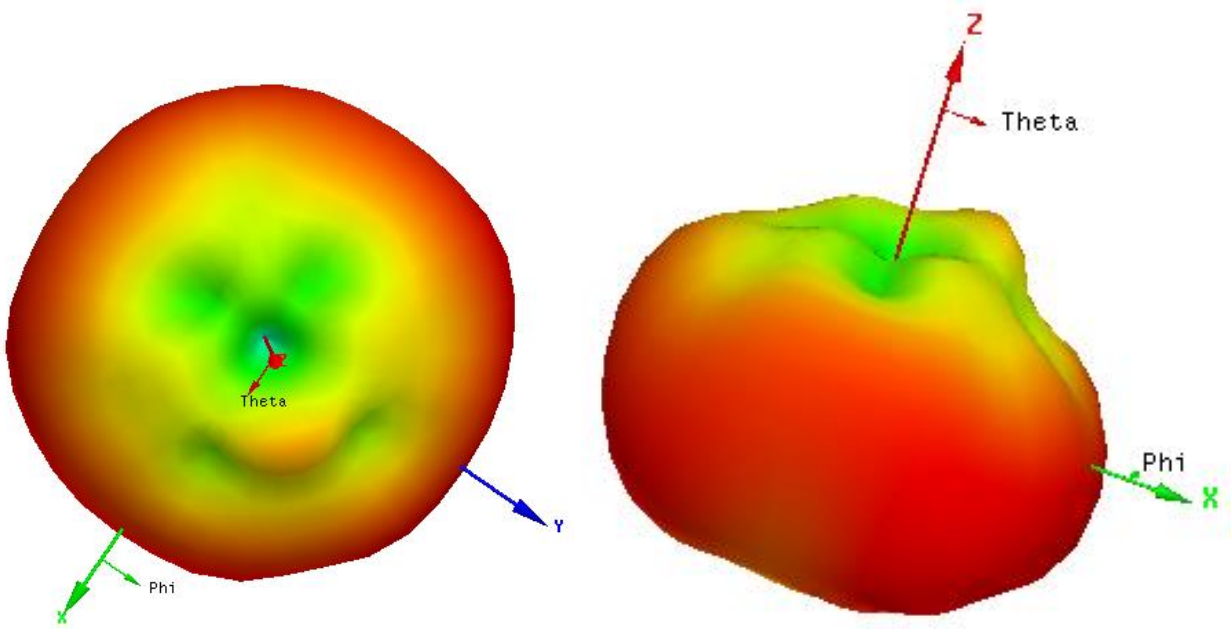

Figure 3.18: 3D radiation plots of a phased array antenna in Figure 3.19

There are disadvantages to reducing antenna size and spacing on the PCB, most notably the reduction in antenna gain as there simply is less surface area of antenna as compared to a larger half wavelength array. Any lack of symmetry would affect the phase centre stability of the design, which would magnify the error at long distances. An example of a non-centred phase centre is demonstrated using the 3D radiation plot of the antenna design in Figure 3.18. An unknown symmetrical error has caused a red bulge to miss the Z-axis, the orthogonal axis to the antenna, and angle away slightly. Additionally, the 3D plot in Figure 3.18 shows the radiation pattern having a low gain value along the Z-axis, where the antenna should ideally be transmitting, and high gain at the side lobes. The side lobe performance is due to unshielded coaxial inputs underneath the substrate and anything below the antenna (X-Y plane) can be

ignored for the simulation purposes. However, the top symmetrical depressions on the surface suggesting that the distance between the patches corresponds to the phase in such a pattern that crests and troughs develop on the surface. These crests and troughs can be matched to Figure 3.19, where a similar design of phased array antennas shows why the symmetrical pattern appears. As can also be understood from Figures 3.18 and 3.19 is that the number of radiating elements affects the shape of the radiation pattern.

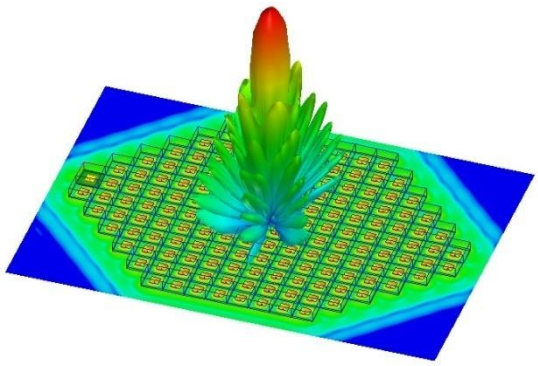

Figure 3.19: 3D radiation plot of a phased array antenna (ANSYS, 2018)

Fewer radiating elements offer a lower resolution peaks of the main beam such as the red bulge, and a larger number of radiating elements offer precise control of the direction of the main beam. The precision of the control also depends on the type of phase shifters and phase shift detectors used on the front-end. Depending on the precision of the phase shifting necessary for a particular application, the front-end design would incorporate as many phase shifting and phase shift detecting elements as antennas. However, no amount of precise phase control can compete with a major advantage in the number of radiating elements (Hansen, 2009).

In an example of a linear array of antennas that are equidistant from each other, the signal received at one end of the array, or the first element, will have to travel a fixed distance calculated by the product of the sine of the angle of the incident wave and the distance between

antenna elements in the array (Visser, 2005). This delay in signal reception between elements of the array introduces phase differences. In this example, when the signals received at each element are combined after removing the phase differences, the obtained signal is the overall response of the antenna array. The change in the incident angle directly affects the change in phase across each element by the same factor. Therefore, the number of elements do not affect the signal steering capabilities of an antenna array. The main beam of an antenna array gets smaller when spacing between elements increases and when the number of elements increases (Visser, 2005). This relationship is demonstrated when comparing Figures 3.18 and 3.19, where the number of elements determines the size of the main beam and the number of side lobes present. Therefore, the signal steering resolution is solely a function of the phase difference between the radiating elements.

The performance of an antenna array differs greatly from its individual elements. There is additional signal loss and error in synchronization between elements that cause signal deviations. The importance of symmetry and the design of an efficient feed network will improve the performance of the antenna array (Hansen, 2009). However, software-based solutions to synchronization errors between elements can also be solved in post-processing, where the phase shifters can perform minute corrections to account for losses. Therefore, the focus in the following chapter will be based on single element designs and how they cope to reconfigurability by analyzing their most optimized versions. In order to determine generic antenna characteristics such as antenna gain, frequency response and signal reflection response, the antenna array designs will consist of a merging feed network. This merging feed network will place each element equidistant from the source connection (coaxial input) in order to characterize the antenna before signal steering can be applied by a front-end.

By characterising the important attributes of what makes antennas function and how, the theory used behind the simulations aid in design optimization. However, the objective is not to design a high-gain antenna for space applications, rather to demonstrate the compatibility of two separate antenna operation modes for a nanosatellite based configuration. These two operation modes are reconfigurability and antenna array design for signal steering.

CHAPTER 4: ANTENNA DESIGN METHODOLOGY AND SIMULATION RESULTS

Based on the theoretical analysis done in Chapter 3, micro-strip antenna designs for nanosatellites are finalized in this chapter. Individual antenna parameters are optimized or tuned to achieve the results that meet the objectives of this thesis. All design parameter choices are explained using simulation results in the form of S11 plots, frequency response plots, and radiation plots, where necessary. The software tool used to simulate the antenna designs was HFSS by ANSYS (ANSYS, 2018).

4.1 Inset-, aperture- and coaxial-feed designs for a single patch

Beginning with the inset-feed design, there is noticeable difference between the theoretically calculated length and width values and the values obtained in Table 4.1 after tuning. The centre frequency for design is targeted at 2.4, GHz which has a wavelength of 125 mm. Figure 3.4 in Chapter 3 is considered a half wave patch antenna, since the length and width of the patch antenna (44.3 mm and 55.3 mm, respectively) are approximately half the wavelength of the centre frequency. A larger antenna patch surface area can prevent the implementation of an array within the CubeSat/nanosatellite size constraints and thus the design chosen in Figure 4.1 is a quarter wave inset-feed micro-strip antenna.

Table 4.1: Inset-feed design parameters

Antenna parameter	Calculated size (mm)	Optimized size (mm)
Length of patch antenna	11.1	13
Width of patch antenna	8.8	15
Substrate height	0.8	0.8

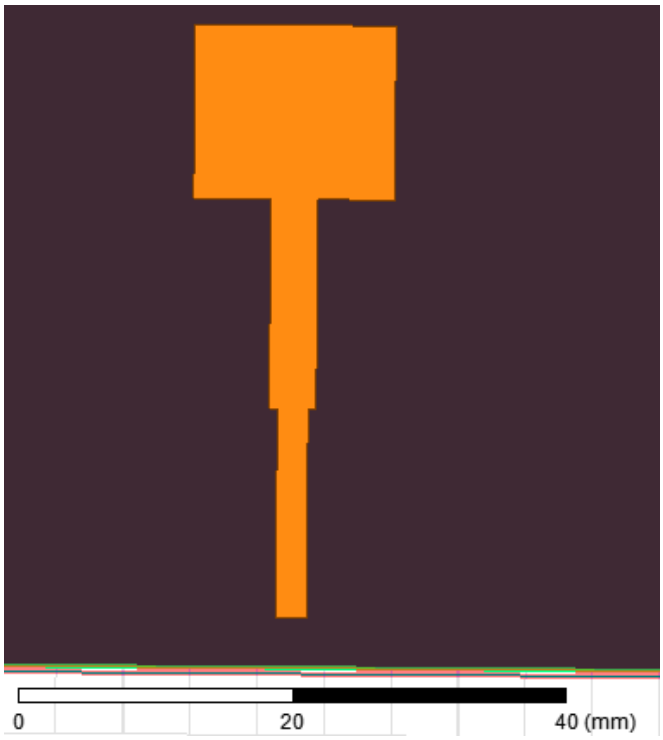

Figure 4.1: Inset-feed micro-strip of eighth wavelength

Figure 4.2 confirms that the size modification of the inset-feed micro-strip antenna is still centred at 2.4 GHz. The eighth wave antenna will have a lower peak gain value compared to the half wave antenna patch, due to its smaller surface area (Milligan, 2005. p. 313). The substrate used in this design was Rogers RO 6002/duroid as it yielded the highest peak gain, which is an important parameter to consider given the range of satellite radio operations.

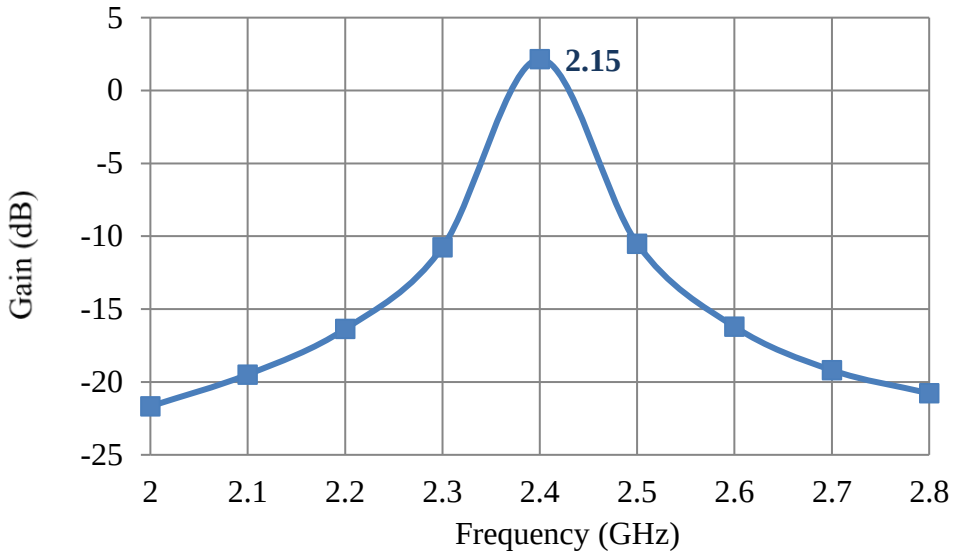

Figure 4.2: Frequency response of inset-feed antenna in Figure 4.1

The radiation pattern of this eighth wave patch antenna at 2.4 GHz in Figure 4.3 shows that the lobe of the main beam is centred towards the Z-axis (at 0 degrees), which is orthogonal to the micro-strip antenna. The radiation pattern is the sensitivity of the antenna to transmit and receive signals from a particular direction. The figure also displays the changing antenna gain towards the side lobes. As expected, the gain at the peak is approximately 2.15 dB and drops as one moves away from the Z-axis. However, in a functional test, the peak gain at the Z-axis is expected to be much lower due to errors and losses that may be introduced during testing.

The second design for an aperture-coupled system required several design iterations, which modify parameters such as the aperture size, aperture placement, transmission line extension, and main patch size and substrate heights as they affect antenna characteristics. Figure 4.4 shows the bottom view of the last aperture coupled iteration. Figure 4.5 shows the side view of the layered design of an aperture coupled antenna.

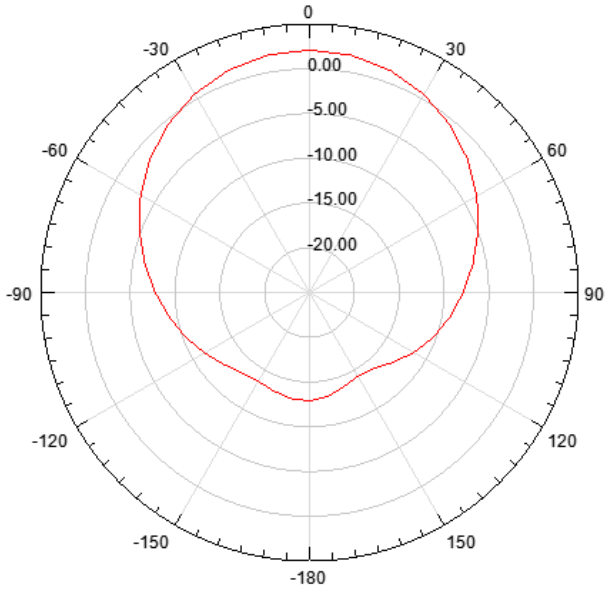

Figure 4.3: Radiation pattern of inset-feed antenna in Figure 3.21

The half wave aperture-coupled antenna was not reduced to a quarter wave antenna because of the way coupling works. For the inset and coaxial feed antennas, the input impedance and the signal reflection response can be controlled by supplying the input signal closer to the centre of the micro-strip. As discussed in Chapter 2, the impedance is controlled by distance from the position of maximum power (where the current is highest and voltage is lowest), which lies at the midpoint of the micro-strip's length. The aperture-coupled antenna, like the other two input types, is also inset closer to the centre. However, changing the half wave antenna to a quarter wave antenna does not change the power delivered to the inset and coaxial feed antennas, but it does affect the aperture-coupling. Since the aperture-coupling relies on the aperture slot to receive the signal from the transmission line, any loss of the maximum power required adversely affects the gain values on the frequency response plot (Milligan, 2005). Therefore, the aperture-coupled antenna design has as a half wavelength micro-strip.

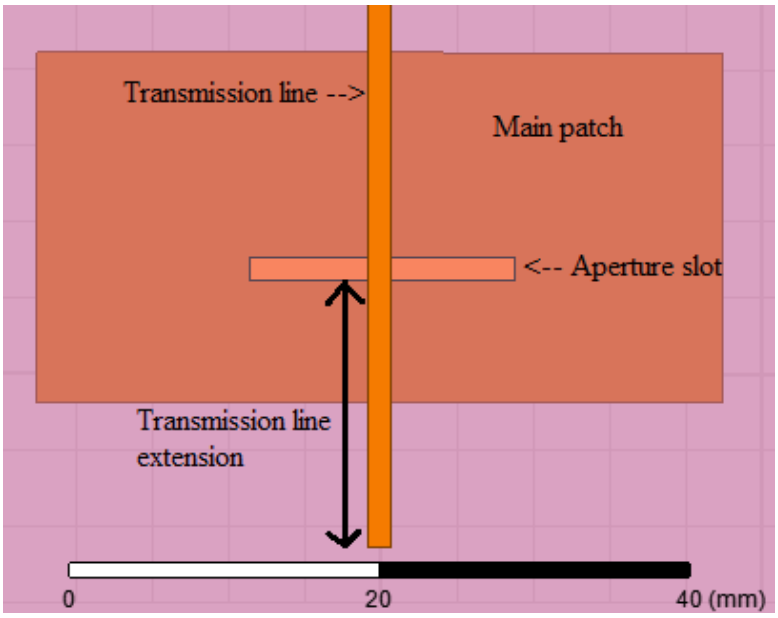

Figure 4.4: Aperture coupled antenna layout bottom view

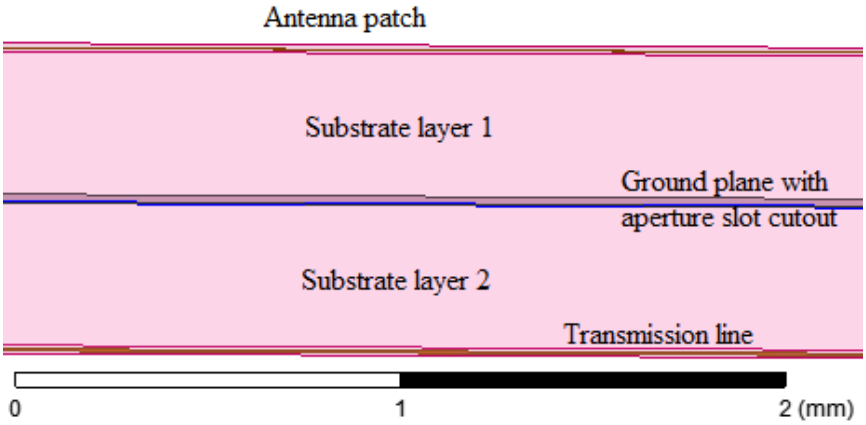

Figure 4.5: Aperture coupled antenna layout side view

Table 4.2 below highlights the specifications of key antenna parameters. Similar to inset-feed, the half wave patch can be too large for an array structure and therefore the illustrated design is a quarter wave patch since the length of the patch is close to a quarter of the 125 mm signal wavelength. The width of the patch and the length of the aperture slot help counteract the loss sustained by the antenna during the coupling between the patch and the transmission line. Figure

4.6 shows the wider nature of the aperture-feed quarter wave patch, which is due to the width and aperture slot length. Another factor contributing to the coupling performance of the patch and transmission line is the extension of transmission line. The extension of the transmission line beyond the aperture slot assists in coupling with the main patch based on the slot width and acts like a low pass filter. The effect is similar to a patch filter design which uses spacing between copper traces to pass signals below a certain frequency, and this effect is visible in Figure 4.6 as the gain sharply drops from and after 2.45 GHz. The width of the transmission line is determined based on the input impedance that the antenna is designed for, which is 50 ohms for the all antenna designs in this thesis.

Table 4.2: Aperture-feed antenna design parameters

Antenna parameter	Calculated size (mm)	Optimized size (mm)
Length of patch antenna	38.7	23
Width of patch antenna	30.4	45
Length of aperture slot	13.8	17.5
Width of aperture slot	1.5	1.5
Substrate 1 and 2 heights	0.4	0.4
Length of transmission line	35.8	86.4
Width of transmission line	1.5	1.5
Extension of transmission line	14.4	17.5

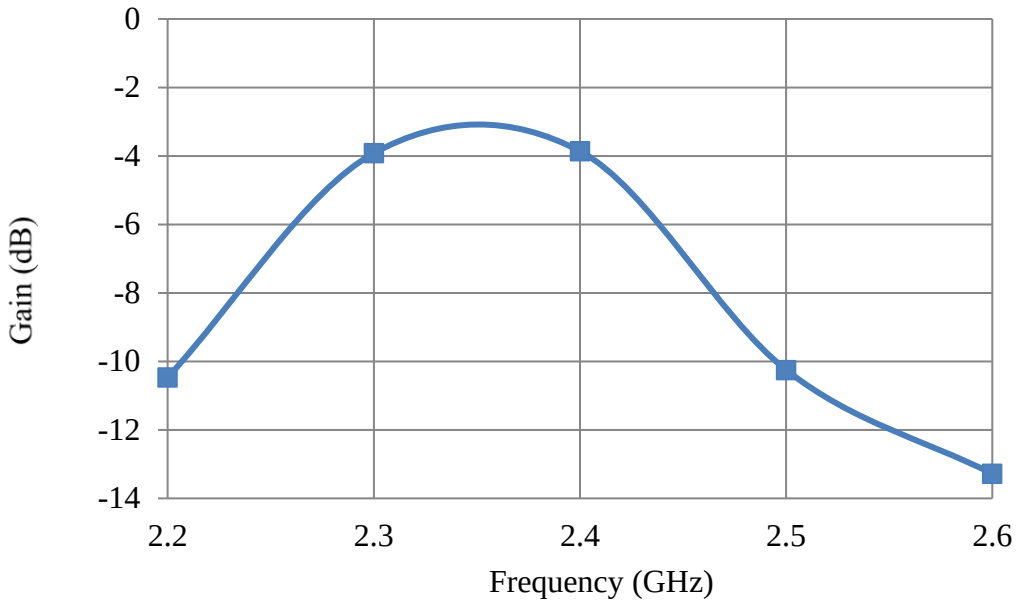

Figure 4.6: S21 frequency response of aperture-feed antenna in Figure 4.3

The radiation pattern of the aperture-feed patch has a very weak side lobe response, which is caused by the thin aperture slot in the ground plane preventing signals that have a smaller orthogonal component to the antenna patch from coupling with the transmission line (Pozar, 1996). The mentioned effect may give cause for concern when using aperture-feed antennas in an array; however, the weaker side lobe response can also inhibit a sharper beam steering capability with lower energy loss during transmission. Since the antenna is designed as a receiver, using an aperture-feed array may not be as beneficial as using the inset or coaxial-feed methods.

In order to further understand why the aperture-coupled antenna is not ideal for an array, we need to analyze the radiation patterns in two axes. Figure 4.7 is the second axis (phi or X-axis) orthogonal to theta or Z-axis. This figure shows the weaker main lobe further highlighting why an aperture-feed patch might be too small to couple well with the transmission line given the size

constraints. Figure 4.8 is the third axis (r or Y-axis) orthogonal to theta or Z-axis, which shows a similarly weak response as demonstrated by Pozar (1996).

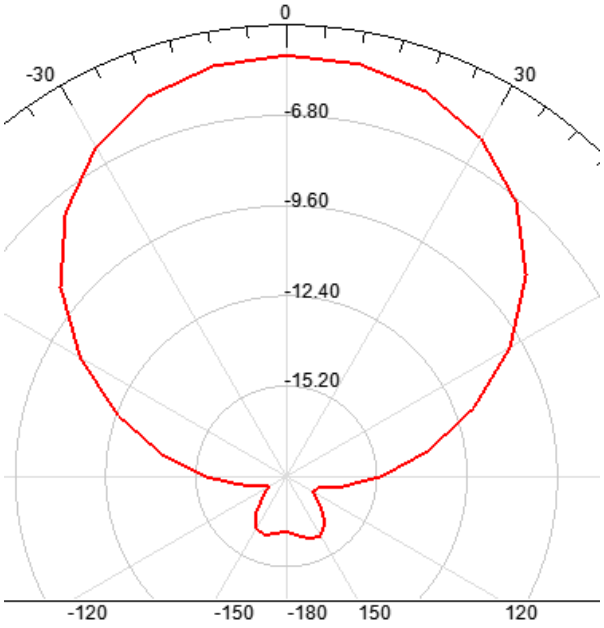

Figure 4.7: Radiation pattern of the aperture-feed antenna in horizontal direction

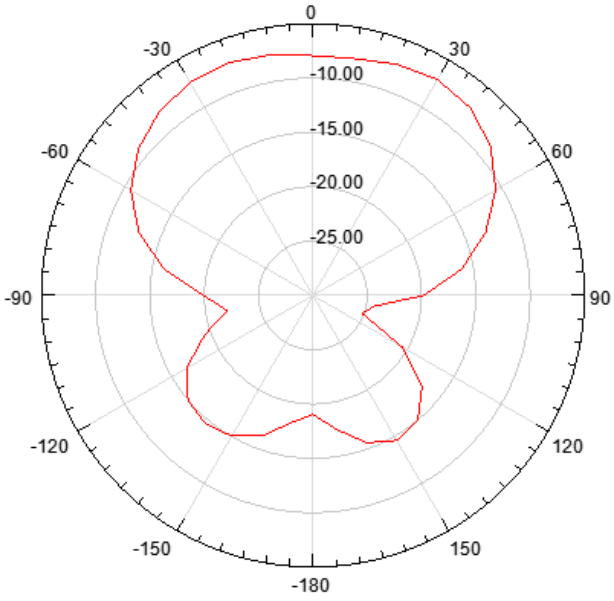

Figure 4.8: Radiation pattern of the aperture-feed antenna in azimuthal direction

The final input feed design in consideration is a coaxial feed design. Figure 4.9 shows a top down view and Figure 4.10 is a side view of the finalized coaxial design. Although not visible in Figure 4.10, there are two cylinders. The inner cylinder is the conductor, and the outer one is the dielectric shield.

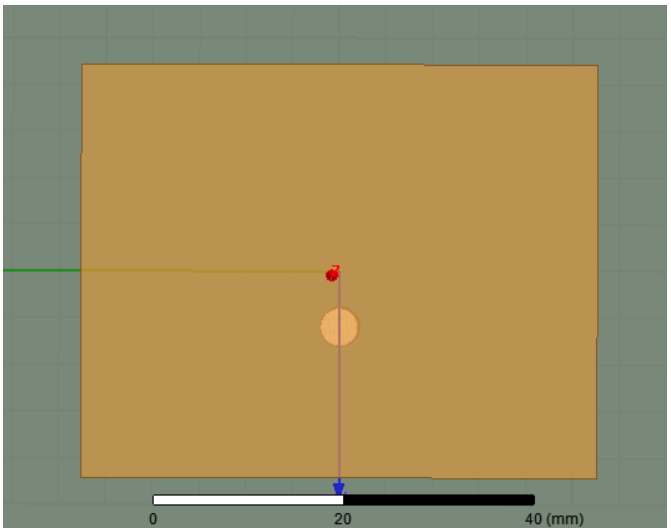

Figure 4.9: Coaxial-feed antenna design top view

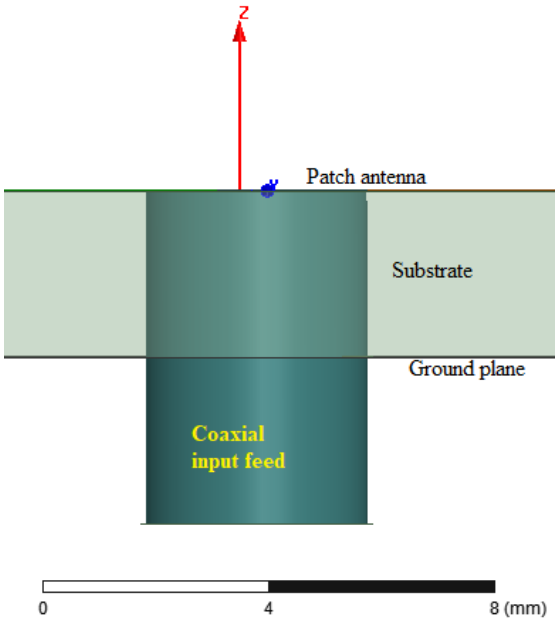

Figure 4.10: Coaxial-feed antenna design side view

After several attempts at micro-strip size reduction of the coaxial-feed antenna design, a half wavelength micro-strip antenna with linear polarization yielded a gain pattern as illustrated in Figure 4.11. The radiation pattern is a familiar symmetrical bulge that exhibits a low front-to-back ratio as seen by the lower semi-circle, but also demonstrates the phase variations that can occur in antenna designs. Although small variations in phase-relative radiation pattern plots occur, larger difference between the phase values can cause a drop in overall gain of the antenna (Hansen, 2009). Coaxial feed designs, like by Singh (2014), demonstrate their popularity in circularly polarized applications. A high-gain antenna, that retains a gain of 0.4 dB at 60˚, is why coaxial feed antennas are widely popular (Lo, 1979). Table 3 contains the important dimensions of the design. The antenna achieved a peak gain of approximately 4.6 dB centred at 1.6 GHz and a spherical dome shaped radiation pattern.

Table 4.3: Coaxial-feed antenna design parameters

Antenna parameter	Calculated size (mm)	Optimized size (mm)
Length of patch antenna	38.7	44.3
Width of patch antenna	29.5	55.3
Substrate height	3	3
Length of transmission line	6	4
Radius of transmission line (inner cylinder)	0.4	0.4

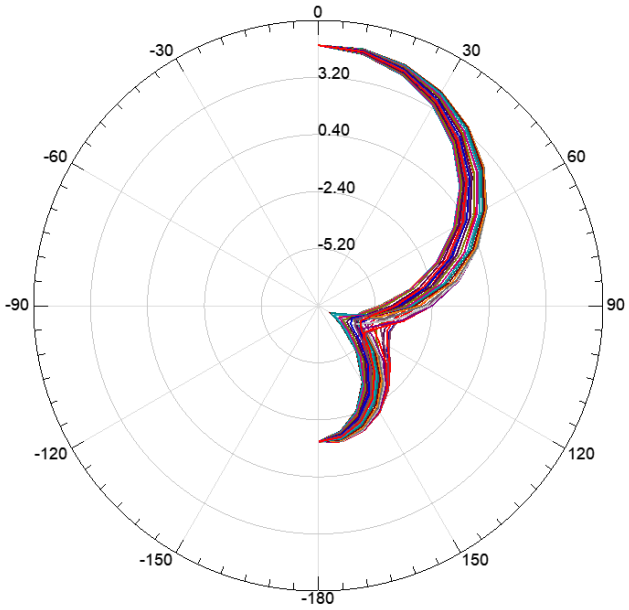

Figure 4.11: Radiation pattern of a coaxial-feed antenna with phase variations

However, when the micro-strip was reduced to quarter wavelength, it suffered a serious drop in gain as illustrated in Figure 4.13. This drop is attributed to the unchanged size of the coaxial input line, which may not correspond well with size and centre frequency change in the smaller antenna when compared to the larger one as in Figure 4.9. Although a lower gain is expected because of smaller surface area, Milligan (2005) suggests there is a need for a shorting wall. A

shorting wall takes advantage of the lowest mode of operation of a micro-strip antenna, when the voltage is 0, to short the ground plane and the micro-strip. The shorting wall momentarily acts as an extension to the micro-strip improving gain performance while keeping the bandwidth similar. However, the shorting wall requires that the micro-strip length reach the edge of the substrate and wrap around the PCB (Milligan, 2005), which cannot be achieved for all antennas in a 2-dimensional array.

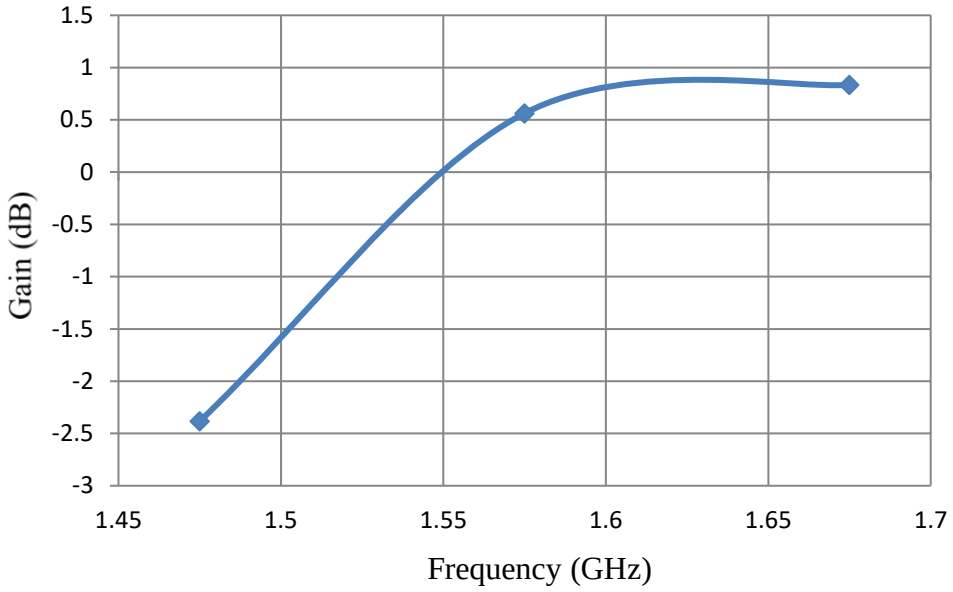

Figure 4.12: S21 frequency response of a quarter wavelength coaxial-feed antenna

Both aperture coupled and coaxial feed designs show lack of versatility with regards to switching frequencies or changing sizes of the micro-strip. Aperture-feed requires a coupling between the transmission line and the micro-strip, with the transmission line extension running off outside the main patch as can be seen clearly in Figure 4.4. If a secondary patch was attached to increase the length of the main patch, there would be additional interference with the main patch. Previously mentioned in Chapter 3, when two micro-strips are close to each other, they are bound to produce electromagnetic interference upon each other. The interference acts as a filter for some

frequencies, but allows some others through, therefore it is possible that the interference may cause issues with the transmission line coupling with the main patch. In the case of a coaxial-feed design, the change in length would affect the symmetrical placement of the coaxial input. As length is added, the coaxial feed is no longer symmetrical to main patch, and therefore antenna properties such as radiation pattern and frequency response may be affected. Figure 4.13 illustrates the disruption in the radiation pattern due to change in length, not by a secondary patch, but just by size reduction. The coaxial feed input can be relocated to a symmetrical point for a quarter wave micro-strip antenna; however, the disruption in the symmetry shows that the coaxial input method would not perform well in a reconfigurable setup, where the length is required to change.

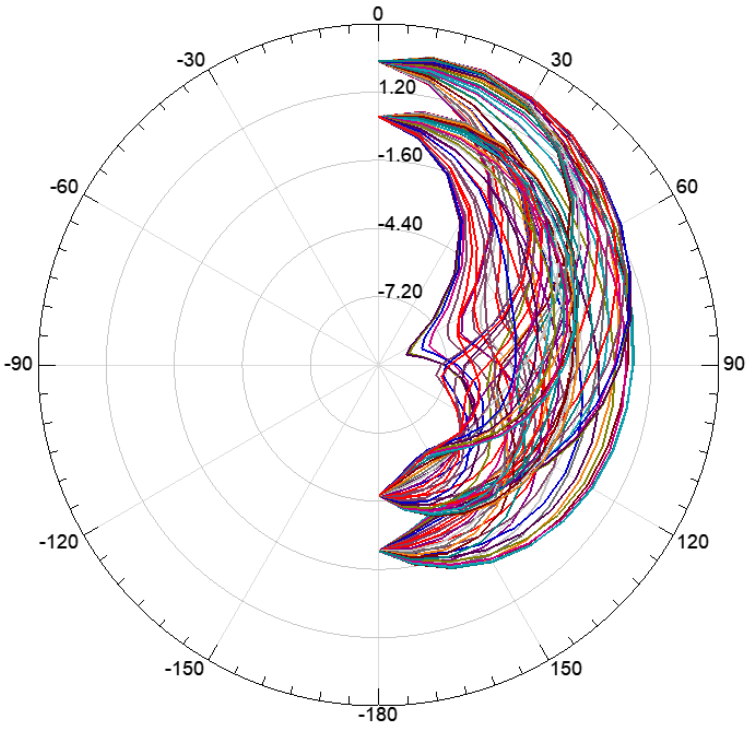

Figure 4.13: Radiation pattern with individual phase measurements

4.2 Inset- and aperture-feed designs for a reconfigurable patch

A top view of the inset-feed reconfigurable micro-strip antenna is shown in Figure 4.14. This design has been upgraded from the quarter wavelength inset-feed antenna to include a secondary patch that allows for a variable length configuration. During simulations, the two patches are connected via thin traces that are the same thickness as the pads on the RF IC switches. For inset-feed antennas, there is one clear direction of flow which allows for a linear expansion. Table 4 contains important size changes from the previous inset feed design, as both length and width have been increased. Following from Chapter 3, the phased array design was 18 cm by 18 cm and to continue using the same amount of space while maximizing on the available surface area for a micro-strip antenna, the size of the main patch was increased. Increment in size of the micro-strip allowed for a better gain response than the non-reconfigurable antenna as seen in Figure 4.2.

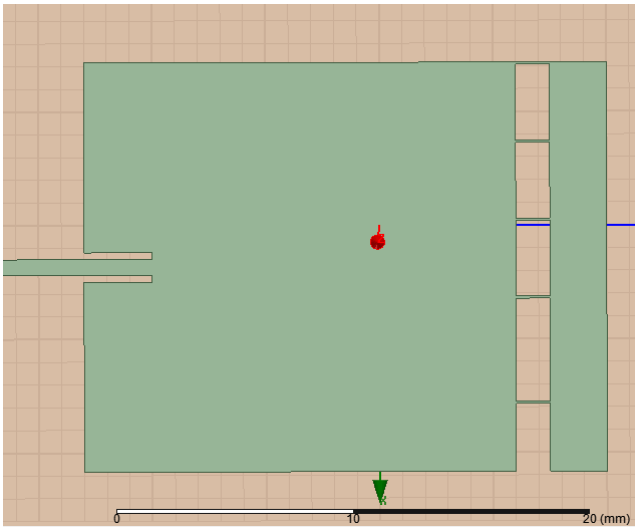

Figure 4.14: Inset-feed antenna design with secondary patch attached

Table 4.4: Inset-feed antenna design with secondary patch design parameters

Antenna parameter	Calculated size (mm)	Optimized size (mm)
Length of patch antenna	11.4	19
Width of patch antenna	14.8	18
Substrate height	0.8	0.8
Length of secondary patch	6	2.5
Width of RF switch lines	1.2	0.1

The frequency response of the reconfigurable aperture-feed antenna is shown in Figure 4.15, when the reconfigurability is added by turning on the switch, in simulation, to yield a peak gain of 6.81 dB centred at 1.5 GHz. Therefore, in simulation it is possible to see the switch in the frequency coverage of the micro-strip antenna when the secondary patch is activated.

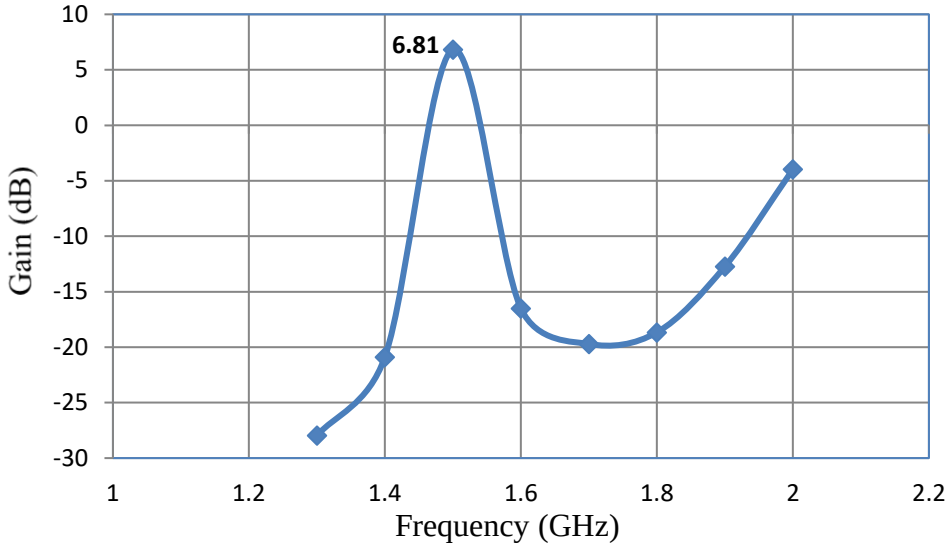

Figure 4.15: S21 frequency response of inset-feed design with secondary patch

The reconfigurable aperture-feed micro-strip antenna is illustrated in Figure 4.16 with Table 5 highlighting key antenna parameters. When compared to the inset-feed design above, the

aperture-coupled reconfigurable design is still quite large and would need a rectangular shape of approximately 22 cm by 33 cm. The size is calculated by adding the approximate length of four micro-strips and leaving a spacing margin on 3 cm from one edge to another and adding 1.5 cm on either edge of the PCB. Similarly, the width calculation is done with 3 cm spacing and 1.5 cm on either edge.

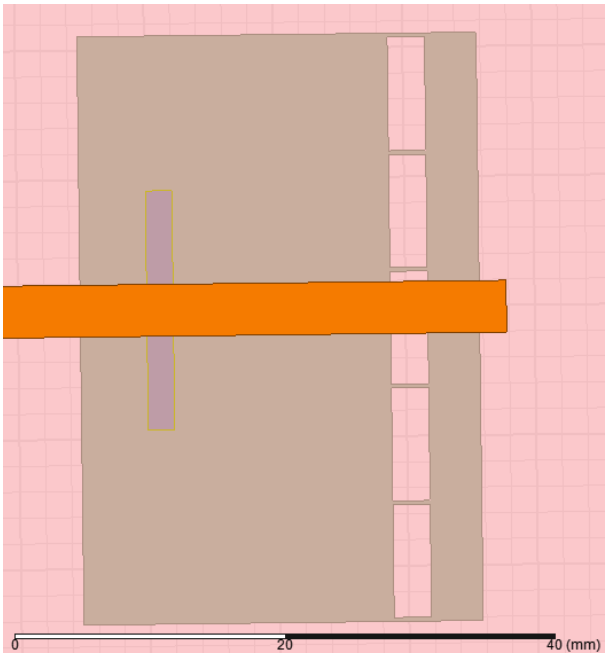

Figure 4.16: Aperture-feed antenna with secondary patch attached

Table 4.5: Aperture-feed antenna with secondary patch design parameters

Antenna parameter	Calculated size (mm)	Size (mm)
Length of patch antenna	30.4	24
Width of patch antenna	38.7	45.4
Substrate 1 and 2 height	0.4	0.4
Length of secondary patch	6	2.5
Width of RF switch lines	1.2	0.1

The frequency response of the reconfigurable aperture-feed micro-strip is shown in Figure 4.17 and highlights the main reason why it is not suitable for a reconfigurable approach. The overall antenna gain has dropped compared to the non-reconfigurable variant (Figure 4.6) and the reason is quite clear in Figure 4.18. The S11 response reveals that despite the antenna length increasing and causing a shift in the frequency response, the poor S11 shift to a lower frequency is hampered by the coupling between the transmission line and the micro-strip. As mentioned earlier, the secondary patch added for reconfigurability may cause interference, but more importantly, the micro-strips ability to accept a signal of a particular frequency has changed. In case of a coaxial feed or inset feed, the micro-strip is physically connected to the incoming signal and accepts all frequencies that are contained in the incoming signal. In this case, the S11 response of the micro-strip, designed for a specific bandwidth, reflects the unwanted signals back. For the aperture-feed design, the unwanted signals never reach the micro-strip and the coupling between the transmission line and the main patch filters them out. However, when the resonant frequency of the main patch is changed by adding a second patch, the S11 response of the micro-strip changes, but the coupling between the transmission line and main patch does not. The addition of the secondary patch causes more signals to be rejected since it is now operating outside the coupled bandwidth, hence why Figure 4.18 illustrates a very minor frequency shift. There is still a frequency shift in Figure 4.17 compared to the non-reconfigurable frequency response, however it comes at a significant loss of gain. The mismatch of the S11 trough at 2.2 GHz and the S21 peak at 2.5 GHz suggests that frequency reconfigurability is not a suitable option for the aperture-feed micro-strip on a PCB.

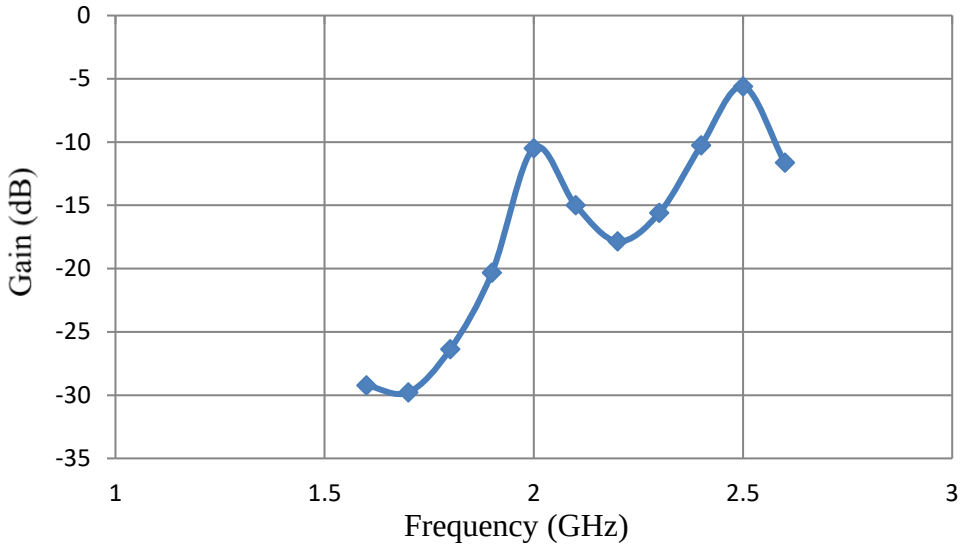

Figure 4.17: S21 frequency response of aperture-feed antenna with secondary patch

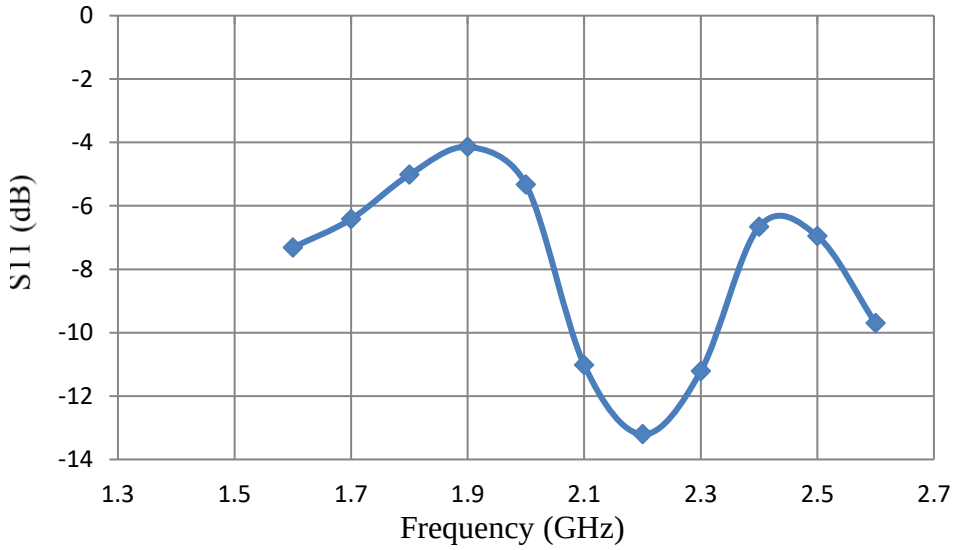

Figure 4.18: S11 signal reflection of aperture-feed antenna with secondary patch

4.3 Phased-Array Antenna

The inset feed design is chosen to be the basic phased array element. Figure 4.19 illustrates the design behind an array, one that is frequency reconfigurable. The base element is the reconfigurable inset-feed antenna designed in Chapter 4.2, each with its own RF IC solder pads

between the main and secondary patch. As shown in Figure 4.14, there are 5 RF IC connections between the two patches, and each one of them requires a 3 V DC supply of power and a ground pin to enable the switch. The RF switch was chosen based on the frequency response it obtained in the operational range of the frequency reconfigurable antenna design, and on the small PCB footprint of the switch which could fit in the gap between the main and secondary micro-strip. In Figure 4.19, the RF input is located where a coaxial connector was soldered on the PCB with a thickness of 0.8 mm. The substrate material used is Rogers RO3210. After minor modifications to the inset-fed reconfigurable antenna, the same performance was achieved as they are both very similar geometrically.

The next major task was creating the antenna feed network which would trace from the coaxial connector to each antenna while being of the same length. The symmetry of the antenna placements was vital, as small miscalculations would lead to out of phase signals reaching the antennas.

The DC pins that needed power were given access points in the shape of rectangular pads for easy soldering, and the ground plane beneath the substrate was also connected to the common ground. After a thorough check of all measurements, parts and components, the PCB was generated in Altium designer. The copper layer file is previewed in Figure 4.20.

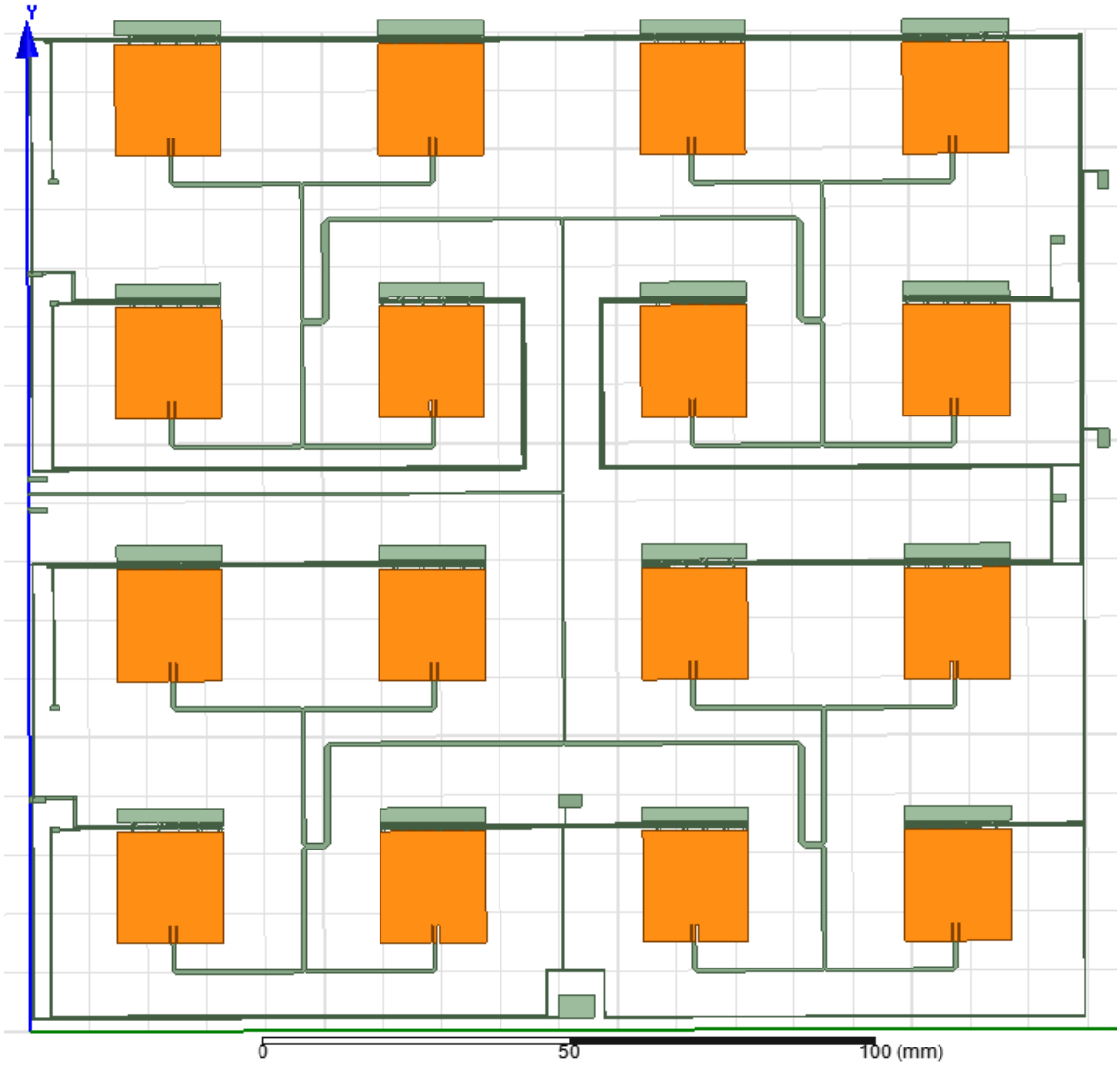

Figure 4.19: Reconfigurable inset-feed antenna array with 16 elements

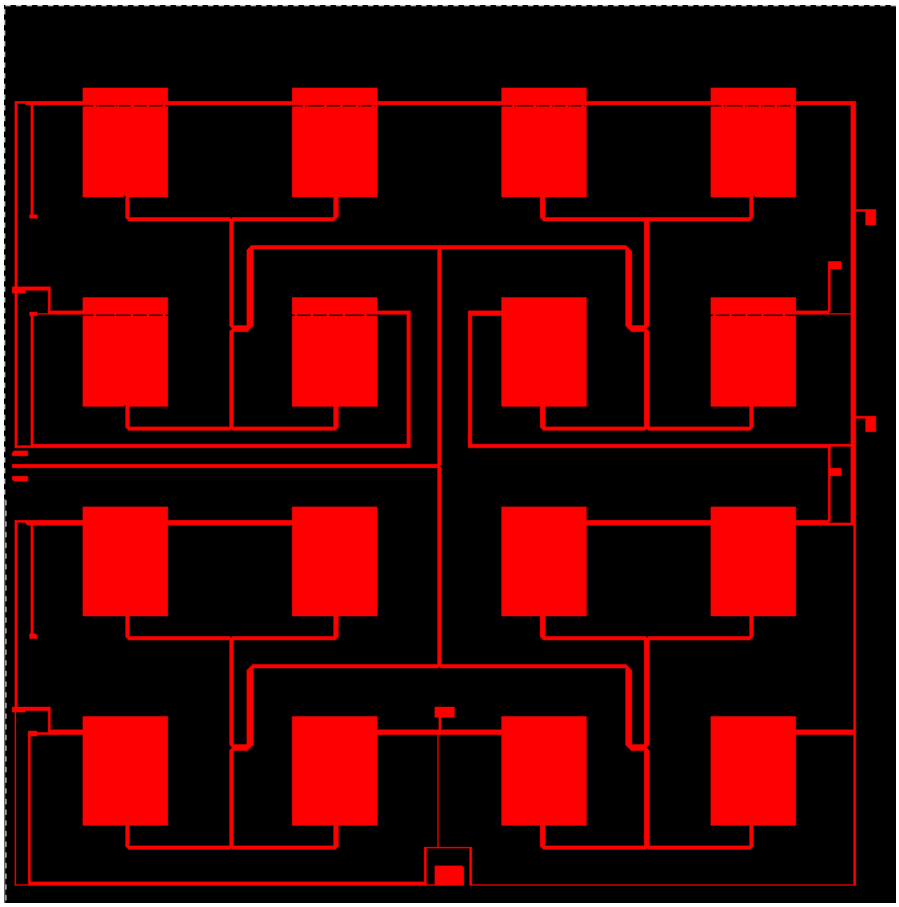

Figure 4.20: Top layer of PCB in Altium Designer for Figure 4.18

Table 4.6 summarizes the individual micro-strip sizes and the peak gain achieved in simulation for each design. The inset-feed designs demonstrate higher gain values than the aperture- and coaxial-feed designs, and continue to do so with the reconfigurable design and thus is chosen as the base element for the phased-array antenna. The antenna array simulation remains incomplete due to the complexity in design of the array. However, following the trend of gain increments for the inset-feed design due to increase in overall surface area of the micro-strip, the antenna array performance is expected to yield a theoretical gain of 6.8 dB

Table 4.6: Micro-strip design summary

Antenna type	Length (mm)	Width (mm)	Peak Gain (dB)
Inset-feed single micro-strip	13	15	2.2
Aperture-feed single micro-strip	23	45	-3.9
Coaxial-feed single micro-strip	44.3	55.3	0.8
Inset-feed reconfigurable micro-strip	19	18	6.8
Aperture-feed reconfigurable micro-strip	24	45.4	-5.6
One element of the Phased-array antenna	19	18	N/A

Simulated antennas in this chapter highlight the most optimized state of the design presented. As mentioned before, antenna designs require a tuning process of minor changes to its parameters for the antenna to perform as required. In the single step changes mentioned above, tens if not hundreds of single parameter modifications are performed to exhaust all possible configurations. These modifications are not based on estimation, but rather by applying the theory and knowledge from Chapter 3. After the final optimization steps, the simulated antennas were then fabricated and the results are discussed in Chapter 5.

CHAPTER 5: ANTENNA TESTS AND CHARACTERIZATION

The finalized antenna designs were simulated and then fabricated. The fabrication process requires individual layers from HFSS (antenna simulation software), which were then packaged together in Altium (PCB design software) to generate a gerber file. The gerber files were forwarded to the manufacturer, which was used to fabricate the top copper layer on the PCB. The rest of the layers, such as the ground plane and the substrate were then combined with the top layer to form the final PCB antenna.

This chapter contains the test procedure and the results using the fabricated antennas. The obtained results are then compared to their respective simulation counterparts. The antenna designs were tested in the same sequence as their design in Chapters 3 and 4: S-band micro-strip antenna, reconfigurable micro-strip antenna with switches on and off, and reconfigurable micro-strip antenna array (or phased array) with switches on and off.

5.1 Reference antenna and test setup

Antenna gain, like voltage, is a relative measurement. For example, when the antenna gain is specified in dBi, it is relative to an isotropic antenna. An isotropic antenna is one that radiates in all directions equally without any signal losses. However, when the antenna gain is specified in dB, it is relative to a particular antenna to which the measurements reference. In simulation, all antenna gain values are dBi, however they are generally referenced as dB for simplification. In Chapters 5 and 6 however, all dB references are measurements relative to a specific antenna (unless specified otherwise), which will be known as the reference antenna. The gain comparison requires 3 antennas: one is the antenna under test (AUT), second is the gain horn antenna (A-info P/N:LB-430-10-C-SF/reference antenna), and the third is an antenna (Wilson Electronics

314411/Wilson) capable of transmitting similar range of frequencies as the AUT (IEEE, 2008). Gain horn antennas are some of the most accurately modelled antennas commercially available, and one was used as the reference antenna for all tests in this thesis. Figure 5.1 shows the tripod mounted reference antenna and Figure 5.2 shows the third (Wilson) antenna.

Figure 5.1: A-info P/N:LB-430-10-C-SF gain horn antenna (A-info, 2017)

Figure 5.2: Wilson Electronics 314411 (Wilson Electronics, 2015)

In order to test these antennas together, a vector network analyzer (VNA) is used. A network analyzer, as seen in Figure 5.3, analyzes the characteristics of one or many signals and plots the data on a screen for visualization (Keysight Technologies, 2017). The Keysight Technologies' PNA-L N-5232 network analyzer is capable of operating between 300 kHz and 20 GHz and has 2 ports for signal comparisons.

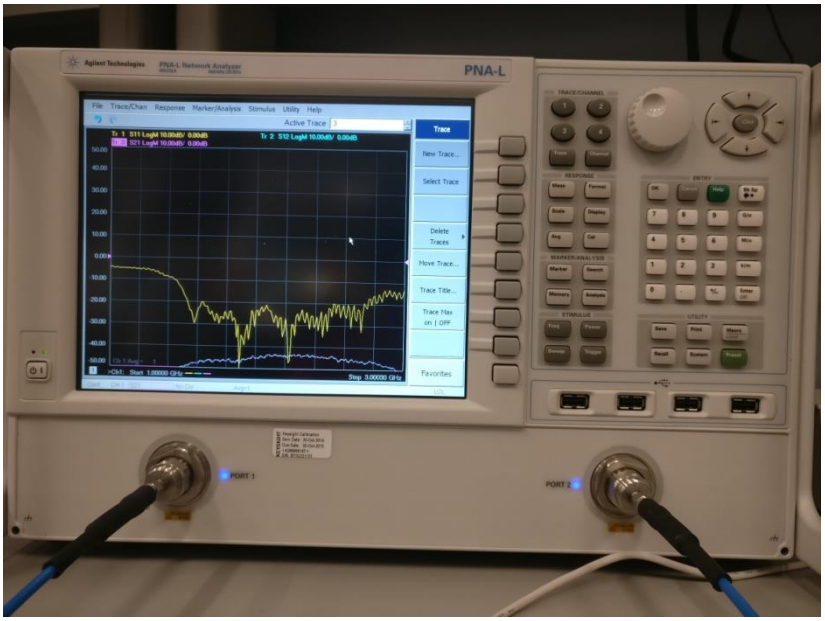

Figure 5.3: Front view of a 2-port PNA-L N-5232A network analyzer (Keysight Technologies, 2017)

Before any tests can be conducted, port calibration must be performed on the VNA. Generally, analyzers contain calibration kits and software to simplify port calibration. The ports in use are connected by a coaxial cable before the calibration begins, in order to ensure the loss due to the coaxial cable is accounted for. Antenna tests are best performed in anechoic chambers, where there is minimal external noise and the walls are designed to absorb most of the electromagnetic waves. However, the testing performed in this research is conducted in a laboratory, and

therefore error sources such as external noise and signal reflections must be accounted for during discussion.

5.2 Test Procedure

After calibration of the network analyzer was completed, the first step of the test procedure was to connect the reference antenna (REF) and the third antenna (Wilson) to either calibrated ports via the coaxial cable. The S11 (for the Wilson antenna connected to port 1) and S22 (for the reference antenna connected to port 2) values were recorded. Next, a far-field setup is established, which places the antennas 3-10 times the signal's wavelength apart: which was set at 1 metre (IEEE, 2008). Once the antennas were visually aligned at each other, the network analyzer recorded the necessary S21 measurements (gain comparison between ports 1 and 2) and then was calibrated to 0 dB to normalize it. Then the Wilson antenna was replaced with the AUT and another set of S21 measurements were recorded. Therefore, in order to calculate the AUT gain, the normalized AUT gain was added to the gain of the REF to yield the actual gain of the AUT (IEEE, 2008). In order to reduce the effects of any RF noise present in the surrounding area, the calibration and normalization procedure was performed before every recorded measurement. This step ensured that any noise or signals that fluctuated between measurements were calibrated out of the recordings.

5.3 Test results

The objective of this research is to demonstrate the feasibility of mounting a frequency reconfigurable, phased-array antenna on a nanosatellite. The design steps in Chapter 4 demonstrate, in simulation, that such an antenna design is possible. However, compared to the simulation results, the test results obtained are expected to be non-identical. There are many

sources of errors between simulation and testing: free-space errors such as, multipath (reflected copies of the original signal), external signal sources, antenna errors such as, fabrication imperfections, misalignment during testing, imperfect impedance matching, and equipment errors such as, inaccuracy of components and equipment (IEEE, 2008). Although not all errors can be mitigated, based on the results, predictions are made as to how much the errors contribute to a particular test. The tests conducted in this research comply with IEEE Standard Test Procedures for Antennas (IEEE, 2008).

5.3.1 Benchmark tests

Figure 5.4 represents the S11 response of the Wilson Electronics antenna that was used as the third antenna in this test setup. The Wilson is a Yagi antenna (a wire mesh antenna), with an SMA connector that is traditionally used for cellular networks. The antenna frequency range is from 1710-2700 MHz (Wilson Electronics, 2015) and the S11 plot confirms this. The signal reflection is almost consistently below -20 dB between 1.7 and 2.7 GHz, which shows that the antenna performs better at this frequency range than at other frequencies. Signal reflection measures how much of the signal provided to the antenna is reflected back, if the reflection is low, the signal is radiated well compared to other frequencies.

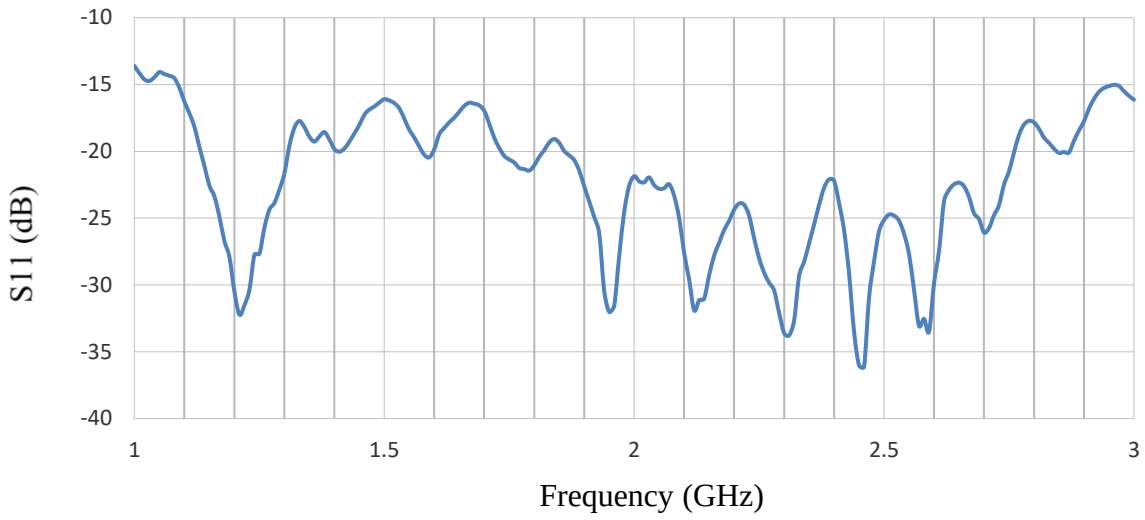

Figure 5.4: S11 signal reflection of Wilson Electronics antenna

Figure 5.5 represents the signal reflection response for the REF or gain horn antenna that was used in this experiment. The REF S-band gain horn antenna is certified from 1.7–2.6 GHz, as is proven by the signal reflection (S22). The signal reflection is almost consistently below -20 dB between 1.8 and 2.7 GHz. The known gain of this antenna is 10 dB.

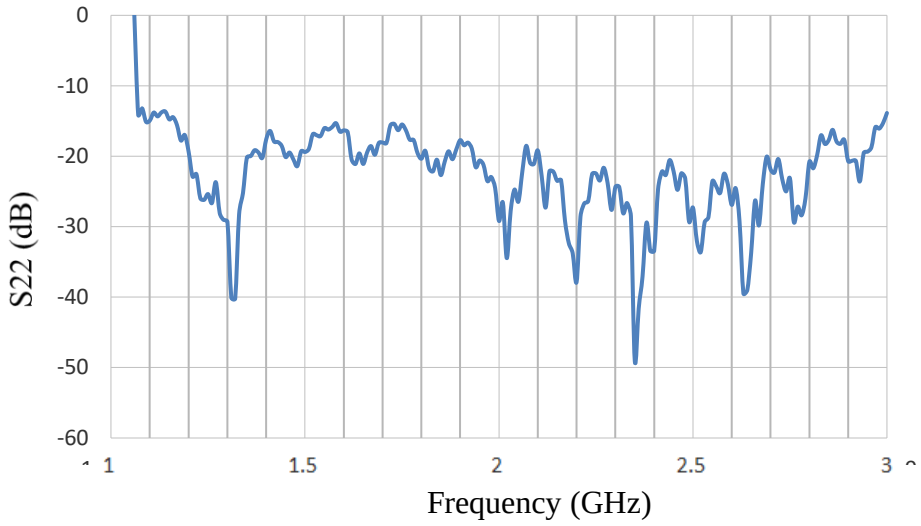

Figure 5.5: S22 signal reflection of the gain horn antenna

Figure 5.6 shows the S21 and S12 or the gain comparison plot between the reference and Wilson antennas. The Wilson antenna was connected to port 1 and the reference antenna to port 2, and the plot below represents the frequency response of the signal received at port 2 in comparison to port 1 and vice versa. S21 represents the losses incurred by the signal when travelling from the Wilson antenna to the reference antenna, while S12 represents the flow of signal in the opposite direction. The two plots, in an ideal scenario, are meant to look identical; however, small errors may occasionally occur due to the environment the test is conducted in. As visible, the two plots nearly overlap. The average difference between S21 and S12 across the 1 to 3 GHz spectrum was calculated to be 0.26 dB. The differences between the two plots may occur due to antenna orientation, as they are pointed at each other and can be sensitive to pick up other signals originating from behind the opposing antenna. Additional errors can be attributed to difference between the sensitivity of the two ports and their connections or any difference in electromagnetic noise affecting the two cables.

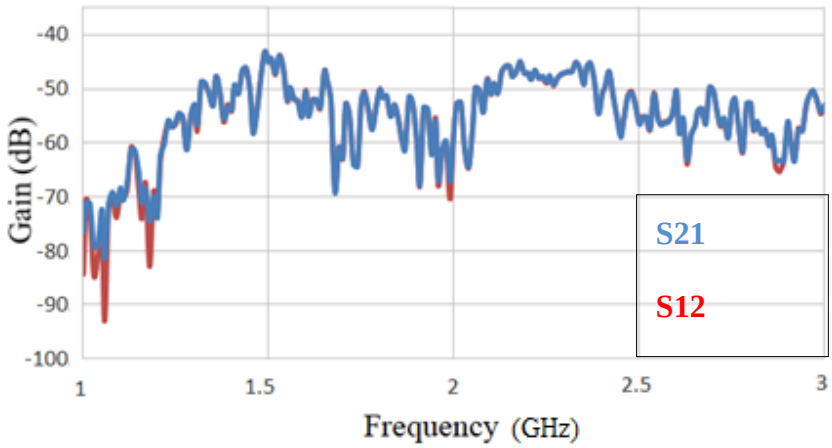

Figure 5.6: S21 and S12 gain comparison between Wilson-Gain horn

Figure 5.7 below represents the S21 frequency response of the inset feed antenna that was designed at 2.1 GHz in Chapter 2.1 (tuning of Figure 3.4 and 19) after reference calibration. Reference calibration is performed when the S21 plots between two antennas are used to normalize the frequency response of the network analyzer. Reference calibration ensures that the obtained S21 response of an AUT (antenna under test) is referenced or relative to the reference antenna. Figure 5.8 shows the frequency response plot when the network analyzer is reference calibrated. To retrieve the actual frequency response of the AUT from the reference calibrated plot in Figure 5.6, a minor calculation is required (IEEE, 2008). At each known point, the value of the reference calibrated plot is subtracted from the S21 plot in Figure 5.6, and then 10 dB is subtracted from the result of the subtraction in order to offset for the gain of the reference antenna. The reference calibration step is required in order to remove the common noise present in both the measurements. These benchmark tests illustrate how the S21 plots in the following sections are generated, and the benchmark tests are not intended for analysis.

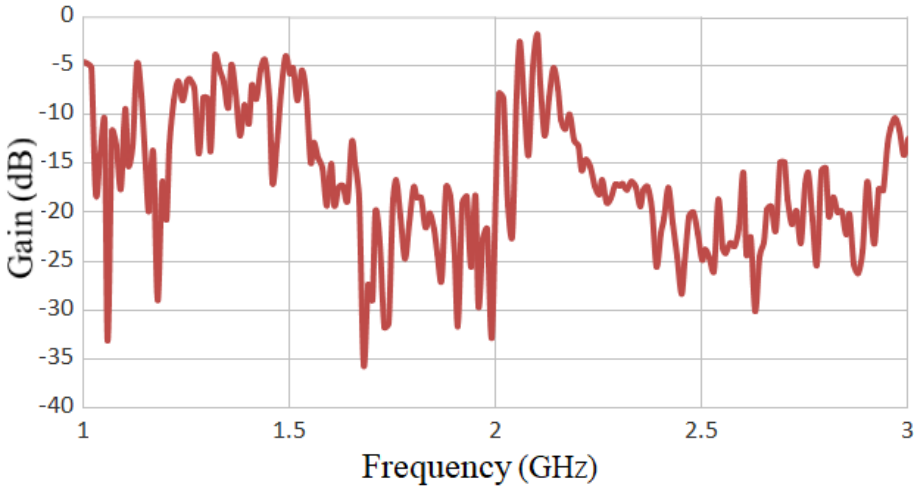

Figure 5.7: S21 response of an inset-feed micro-strip antenna and reference antenna

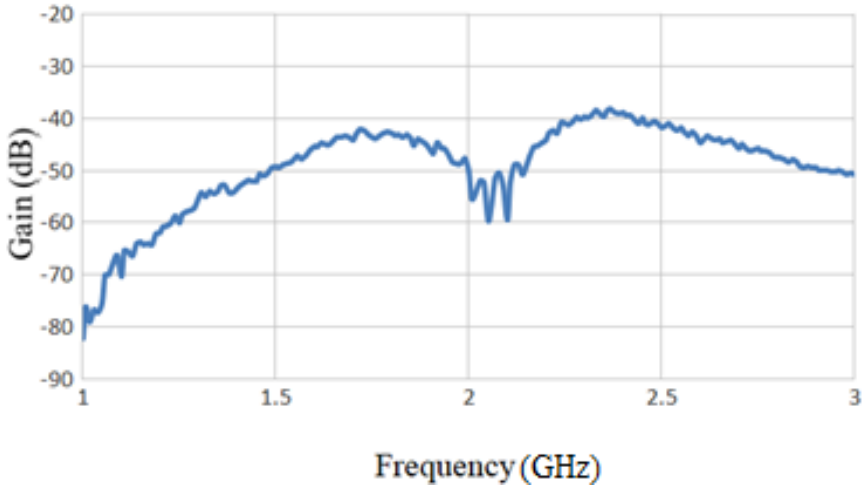

Figure 5.8: S21 response of an inset-feed micro-strip antenna with reference calibration

5.3.2 Inset feed antenna

Figure 5.11 is an image of the fabricated version of the quarter wavelength inset feed antenna design shown in Figure 4.1. Figure 5.9 illustrates the S21 frequency response plot of this antenna after reference calibration. Compared to its simulation counterpart in Figure 4.1, where the peak gain value of 2.15 dB is recorded at 2.4 GHz, the test results show a peak at 2.45 GHz with a gain of 1.57 dB. However, at 2.4 GHz, the gain obtained during testing was -6.96 dB. The half

power bandwidth (-3dB from peak power on either side of the centre frequency) of the S21 plot is very similar to the simulation: at approximately 70 MHz, which suggests that there is a frequency shift of approximately 50 MHz from simulation to fabrication. Errors in manufacturing, imperfect soldering of the coaxial connector and accuracy limitations of the simulation are potential reasons for this minor mismatch (IEEE, 2008). As discussed in Chapter 3, substrate height and dielectric constant are the main parameters that affect signal bandwidth, despite which, a minor difference in substrate height has a negligible effect on the bandwidth (Milligan, 2005). Therefore, by matching the bandwidth from simulation to fabrication, it is determined that the centre frequency offset is likely due to the mentioned errors.

Figure 5.9 illustrates the signal reflection plot, which demonstrates a similar shift in the centre frequency, as the trough reflected -22.7 dB at 2.44 GHz. The length of a micro-strip directly affects the frequency response of the antenna; however, a manufacturing error could not result in a 50 MHz frequency shift (IEEE, 2008). The most likely source of error is the accuracy of the simulation software, because after tuning the antenna to obtain the exact response required, the fabricated antenna exhibited the correct bandwidth at the wrong frequency. Although the centre frequency was shifted, the bandwidth was still within range of the original centre frequency making this antenna functional at the desired 2.4 GHz.

The objective of this design was to demonstrate a communications capable antenna in the S-band and 2.4 GHz was arbitrarily chosen as one of the communication capable frequencies, as it is also used for satellite-to-ground communication. Therefore, the antenna designed and tested is capable of Wi-Fi 802.11 based channels 5-13, which range from 2.432 to 2.472 MHz (Halperin, 2010). The objective of the single element inset-feed antenna design was not to achieve maximum gain, but to obtain a near positive gain value, while keeping the antenna size at a

minimum. This size restriction is what allows the antenna array to fit in the 18 cm by 18 cm PCB layout.

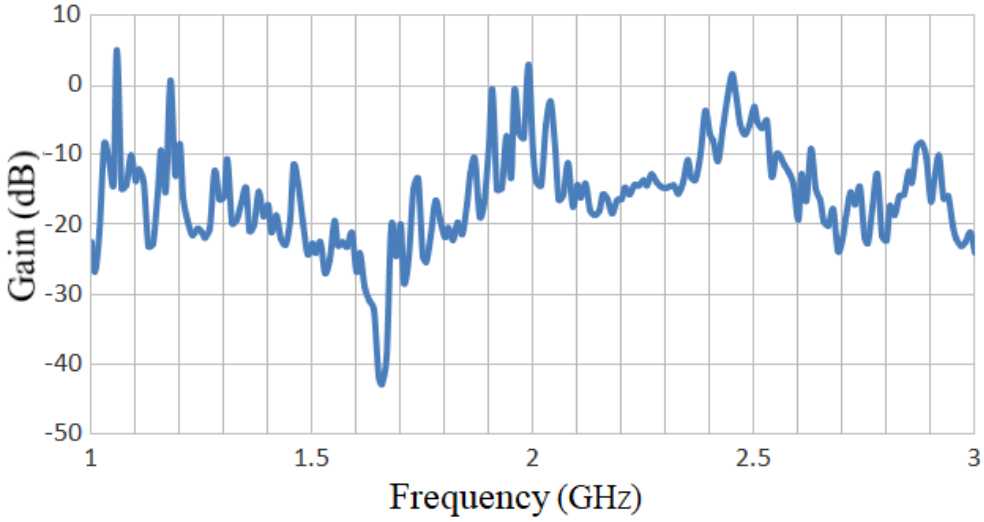

Figure 5.9: S21 frequency response of the inset feed antenna from simulation in Figure 3.21

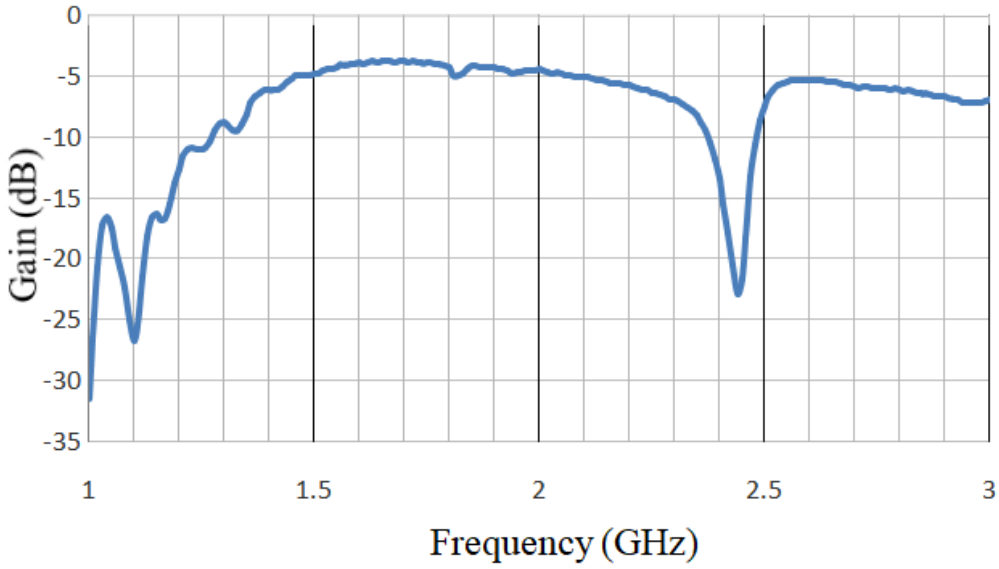

Figure 5.10: S11 of the inset-feed antenna design from simulation in Figure 3.21

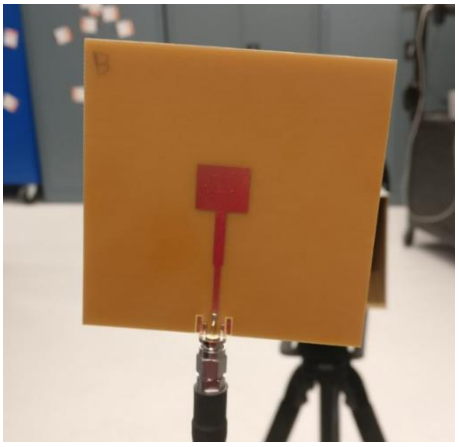

Figure 5.11: Inset-feed antenna mounted with a coaxial connector

5.3.3 Reconfigurable inset feed antenna without switches

The next step was to test the reconfigurable inset feed antenna without connecting the secondary patch in order to observe the effects of interference that might be caused by the secondary patch. Figure 5.12 is a close up of the single antenna with no switches connected. The S21 plot presented in Figure 5.13, illustrates a chaotic frequency response that shows the effects of the secondary patch. Without any connection to the secondary patch, the antenna loses some gain over the range of 2.3–2.4 GHz coverage likely due to the interference from the secondary patch. The interference caused by the secondary patch acts like the aperture design coupling, causing signals of some frequencies to be filtered out and others to pass through (Milligan, 2005). Since increasing the length decreases the centre frequency of the antenna (as per Equation 2), the unwanted coupling between the main and secondary patch produce a new harmonic, which shifts the centre frequency of the main patch.

The centre frequency of the antenna tested in Figure 5.10 is 2.45 GHz, which represents a wavelength of 122.4 mm. Figure 5.14 illustrates the relationship between wavelength and frequency, and shows that at the desired resonating frequency of 2.45 GHz or 122.4 mm, adding

2.5 mm to the resonating wavelength causes a frequency shift of almost 60 MHz (0.06 GHz). The reason why the 2.5 mm extension is added to the wavelength of the centre frequency and not the length of the patch is because the secondary patch is not connected to the main patch. Therefore, the response does not append to the length, and rather it causes interference at the new extended wavelength. With the additional interference, the new peak (in S-band) is -7.5 dB at 2.33 GHz as shown in Figure 5.13. Due to the 1.5 mm spacing between the secondary patch and the main patch, and the presence of two traces for DC voltage in between them, the gain at the new frequency drops. This reasoning would make sense if the peak measured with the switch on at 2.33 GHz remained with a similar gain value. Despite the switch connecting both the patches, the conductivity gap between the two patches remains. Therefore, the gain at 2.33 GHz is still caused by interference and the only solution to mitigate this interference is to connect both the patches with a switch as wide as the antenna. A switch this wide would remove the conductivity gap; however, it would accept more interference. Since the effect of the interference is known, the main patch would have to be designed to resonate 60 MHz higher than the design in Chapter 5.3.2. This design change would offset the effect of the secondary patch on the main patch, maintaining the functionality of the antenna with the switch off. Although the centre frequency was shifted, the interference caused by the secondary patch solidifies the frequency reconfigurability even before connecting the two patches. However, unlike the inset feed antenna in Figure 5.11, the bandwidth of the frequency shifted antenna does not cover the desired 2.4 GHz channel. In order to make this antenna cover the 2.4 GHz frequency range, a minor reduction in length, by approximately 1.5 mm would be necessary.

Figure 5.12: Reconfigurable micro-strip antenna without switches

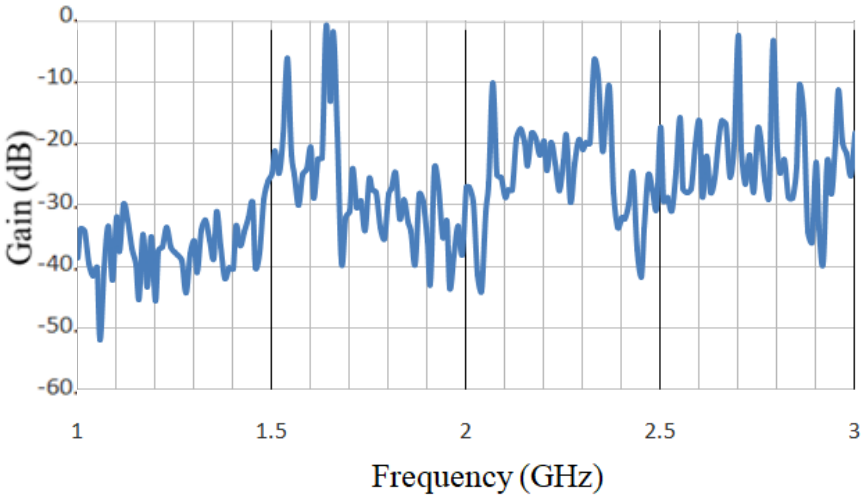

Figure 5.13: S21 response of the reconfigurable antenna without switches

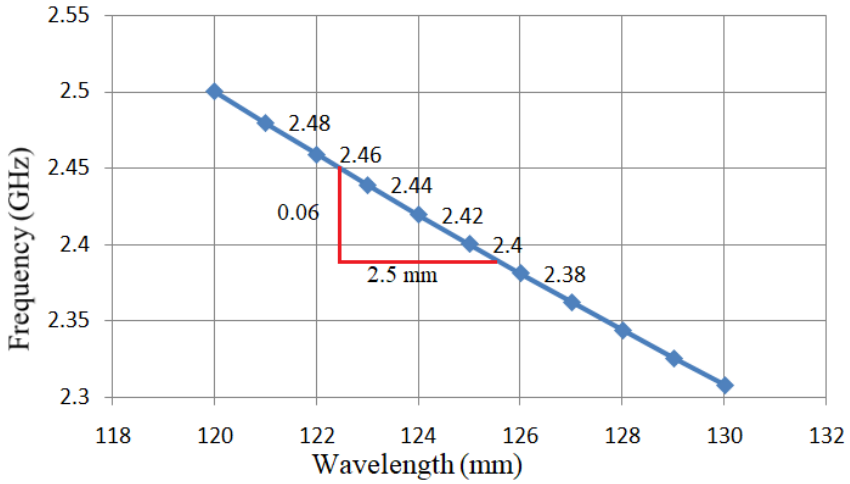

Figure 5.14: Frequency and wavelength comparison

5.3.4 Reconfigurable inset feed antenna with switches

Figure 5.15 represents the fabricated design of the reconfigurable antenna with the switches. With the secondary patch now enabled, Figure 5.16 illustrates how the frequency response transforms into a plot comparable to Figure 4.15. Comparing to Figure 5.13, the three major gain peaks at L-band have more bandwidth; -0.80 dB at 1.44 GHz, -3.95 dB at 1.58 GHz, and -3.31 dB at 1.82 GHz. As mentioned earlier, the conductivity gap between the main patch and secondary patch still causes interference at 2.33 GHz.

The objective of a frequency reconfigurable antenna was to demonstrate performance change based on the activation and deactivation of a switch. As GPS-based positioning is common for satellites, the intent was to show the L1 GPS signal at 1.575 GHz could be detected with the same antenna. Observing the peak at 1.58 GHz, with a bandwidth wide enough to cover the L1 signal, the designed antenna, as seen in Figure 5.15, is capable of receiving GPS L1 signals. However, with a gain of -3.95 dB, usage of this antenna design would require amplification

before any signals are processed. As mentioned earlier, the objective of this design is not to maximize gain, but to design an array that can fit on an 18 cm by 18 cm PCB for a nanosatellite application. In order to increase the gain of this antenna, further tuning is required to centre the reconfigured frequency (with switches on) closer to the GPS L1 signal. However, the reconfigurable inset feed antenna with switches enabled proves that frequency reconfigurability is achievable and is able to perform in existing applications.

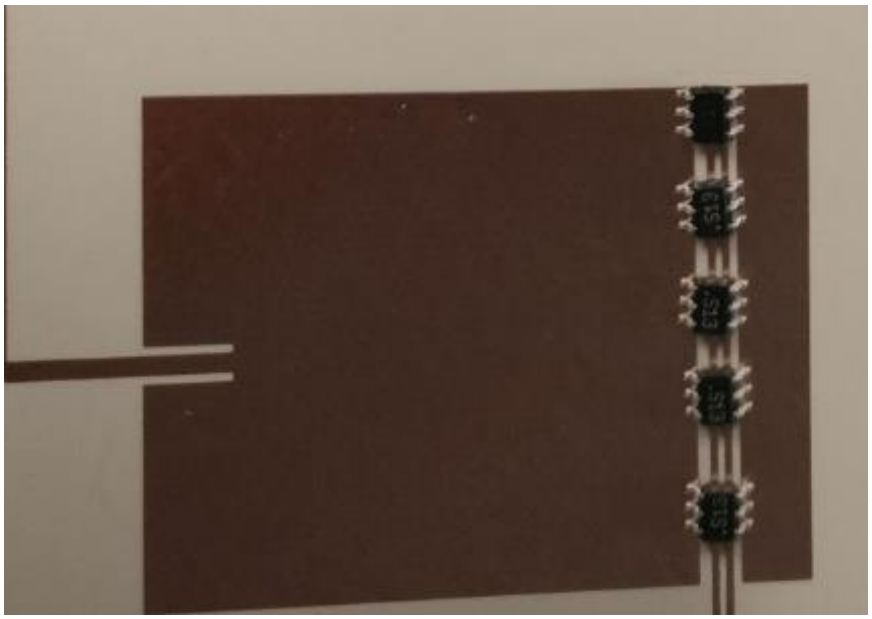

Figure 5.15: Reconfigurable micro-strip antenna with switches

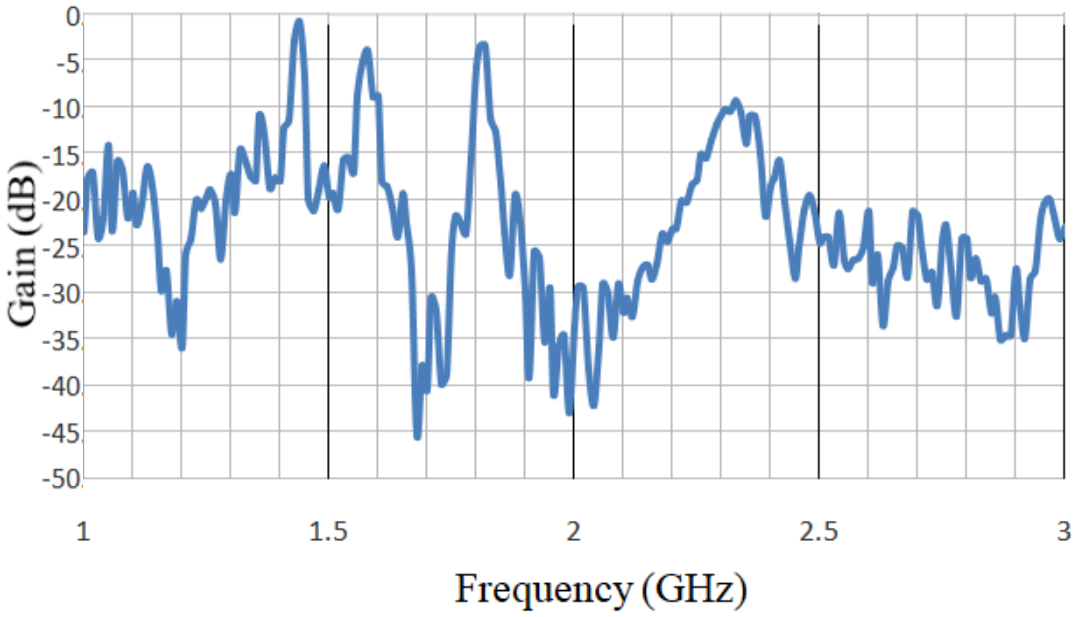

Figure 5.16: S21 response of the reconfigurable micro-strip antenna with switches in Figure 5.15

5.3.5 Reconfigurable antenna array without switches

Designing an array based on a single element with a reconfigurable patch requires a symmetrical layout that ensures all feed lines for the antennas are the exact same length. If the lengths of any two input feed lines differ, a phase shift is applied causing the array to have a fixed natural offset in its phase centre stability. As illustrated in Figure 3.20, the phase centre stability is the natural direction of the signal's transmission when no external phase shift is applied.

Figure 5.17 shows a fabricated antenna array with the feed network designed to distribute the power to each antenna. In order to ensure 50 ohms of impedance at the coaxial connection, the feed line is split into two, then four and all the way up to 16. As the line splits, the traces get wider in order to maintain the 50 ohms. Complex feed networks require excessive tuning, much like a micro-strip antenna in order to minimize signal loss and maintain antenna impedance.

Observing the frequency response in Figure 5.18, the same interference pattern that appeared in the previous two designs exists in the array. This interference is expected, because the interference effect is caused by the same individual antennas that are now part of an array. Due to 16 different elements collecting the same signal and adding up the power, the interference at 2.34 GHz has a higher gain than a single antenna. The interference peak at 2.34 GHz has a gain of -1.78 dB, which is considerably higher because of the accumulation of the signal present in all the antenna elements. The increase in gain demonstrates that the individual antennas are not out of phase and the feed network is performing the task of accumulating the signal from each element (Hansen, 2009). The difference between the interference peaks at 2.34 GHz for the reconfigurable design with switches off in Figure 5.13 and the array version of the design in Figure 5.18 is approximately 5.72 dB. The increase in gain and duplication of interference patterns demonstrate the antenna's ability to retain characteristics of individual elements, while amplifying the overall gain performance.

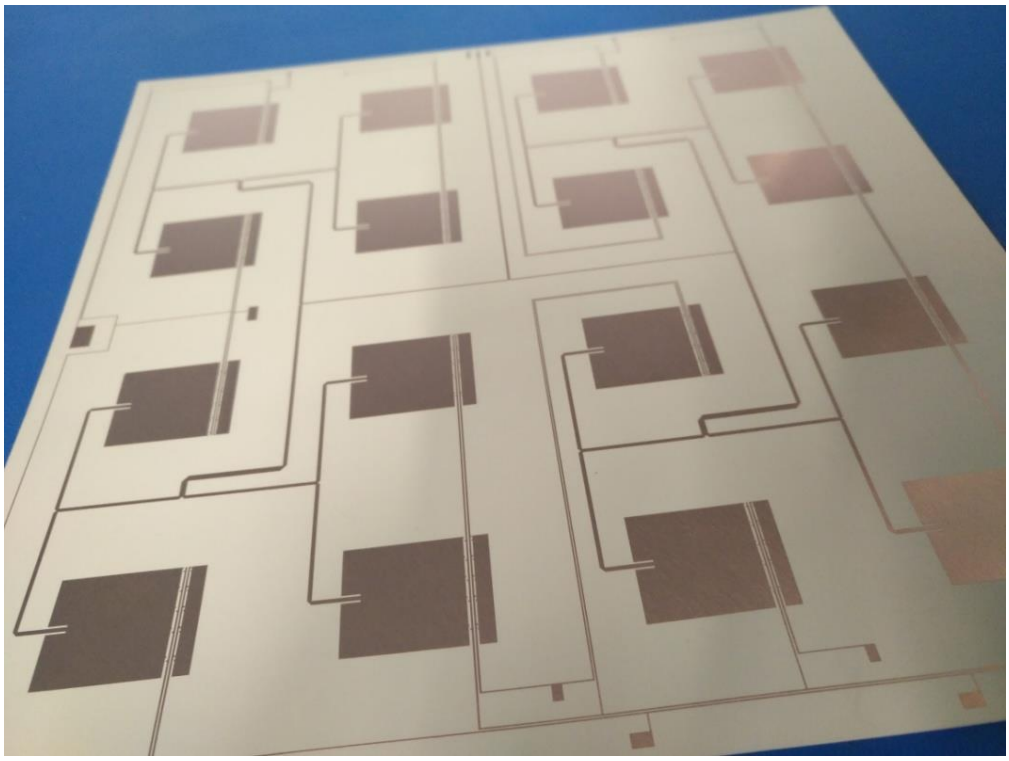

Figure 5.17: Inset-feed antenna array with feed network

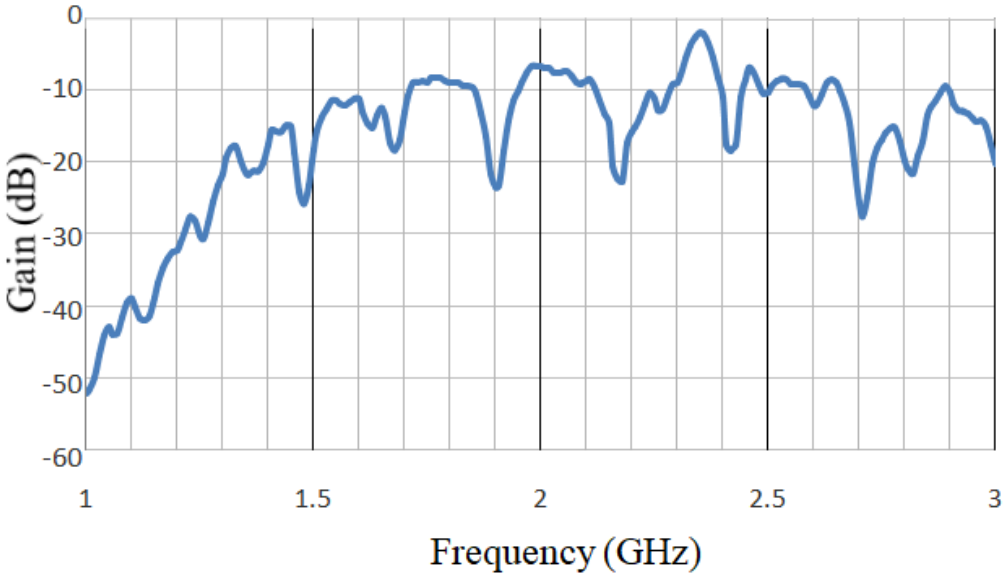

Figure 5.18: S21 frequency response of the antenna array without switches in Figure 5.17

5.3.6 Reconfigurable antenna array with switches

Similar to Figure 5.17, the antenna array is laid out in Figure 5.19 with switches that can enable reconfigurability with the antenna array. Observing from Figure 5.20, the frequency response shows a higher gain value when compared to the reconfigurable antenna in Figure 5.16, however another frequency shift takes place. The signal, intended to be at 1.575 GHz now peaks at 1.5 GHz with a gain of 0.3 dB. Also, the interference peak that was intended to be at 2.33/2.34 GHz has also shifted to 2.18 GHz. Based on this information, there is a shift of anywhere between 82.5 to 158 MHz. Since the shift is not constant for both the data points, the potential cause of error is antenna spacing. The layout of the traces and connectors is likely not a big factor for the frequency shift here because the layout remains unchanged for the antenna array without any switches. Since the layout remains unchanged, the interference/frequency shift with neighbouring antennas might be caused by turning the switches on. Since the shift is not constant for all frequencies, the likely cause is unwanted coupling between antennas.

In reference to Figure 5.19, the right edge of the secondary patch is exactly 21.7 mm away from the left edge of the main patch to its right. Without the secondary patch activated, the distance from the main patch's right most edge to the left most edge of the next antenna is 25.6 mm. By activating the secondary patch, the conduction gap between two antennas reduces by 3.9 mm. A spacing of half wavelength apart is a good rule of thumb for antenna array placement; however, this design is an eighth wavelength micro-strip. For a 2.4 GHz signal, the ideal spacing between edges would be 62.5 mm for half wavelength spacing and 31.3 mm for a quarter wavelength spacing and for a 1.575 GHz signal, the spacing would be 95.3 mm and 47.6 mm, respectively. Although interference was avoided for the S-band signals, when the secondary patch is turned on the spacing between antennas is inadequate. Counteracting this design would require smaller

antennas or preferably a larger PCB. Smaller antennas, perhaps eighth wavelength micro-strips, could reduce the interference effect between the many conductive components on the antenna, but it will adversely affect the gain as well. The gain lost by using eighth wavelength antennas would likely be due to the need for larger feed networks for more than 16 antennas. A larger PCB, and more spacing between antennas, would certainly help mitigate the interference effects; however, they would be hard to justify as nanosatellite compatible.

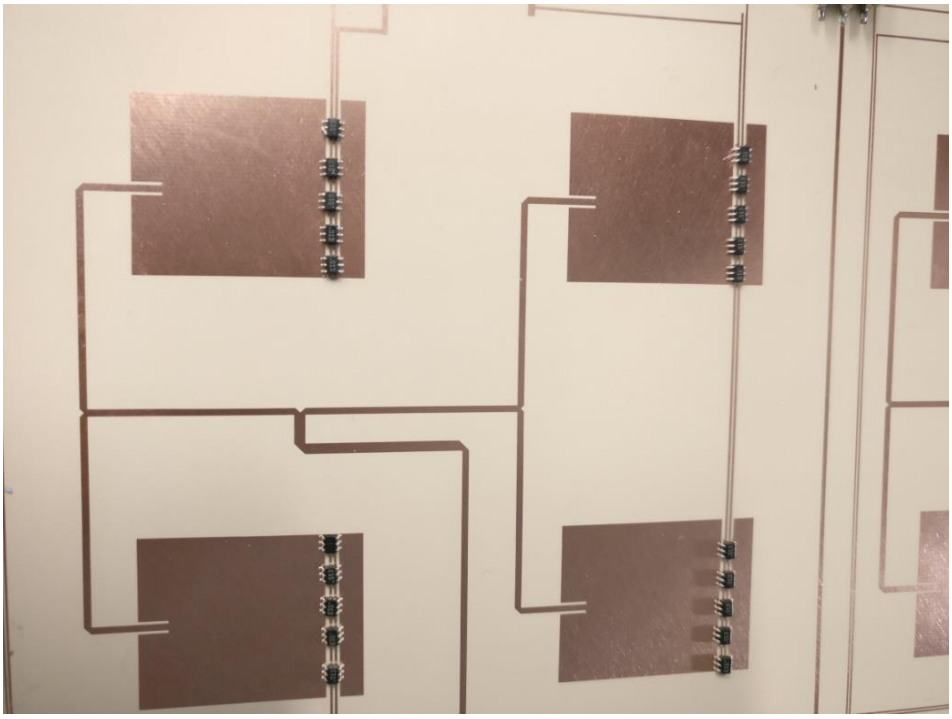

Figure 5.19: Reconfigured antenna array with switches

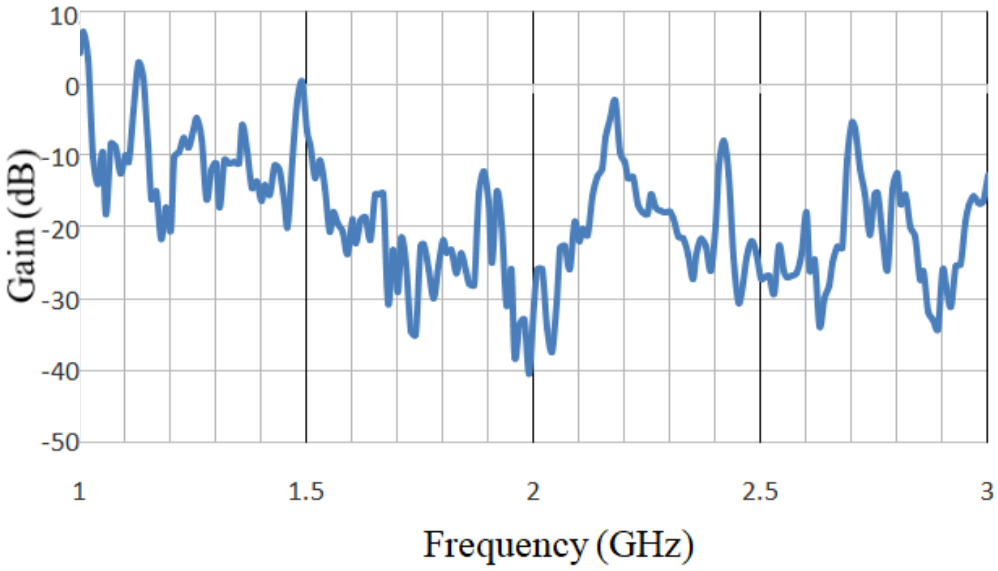

Figure 5.20: S21 frequency response of reconfigured antenna array

The results of testing the antenna designs demonstrate the inaccuracy of the simulation software to anticipate a real-world scenario. However, in most cases, the deviation from the desired response was minor and would only need minor corrections. In case of the single inset-feed micro-strip antenna, a deviation of 50 MHz from the desired frequency of 2.4 GHz was low enough to still be within a 70 MHz bandwidth of the incorrectly achieved 2.45 GHz. However, as the design complexity grew, so did the interference effects. With a deactivated secondary micro-strip, the interference caused a frequency shift of approximately 60 MHz. As discussed earlier, the shift was caused by coupling between the main micro-strip and the secondary micro-strip. The 2.5 mm micro-strip was placed 1.5 mm away; however, the interference coupling induced current onto the main micro-strip, changing the centre frequency. The test results illustrate the need to extend the length of the reconfigurable main micro-strip antenna in order to negate the 60 MHz frequency shift. The effect of interference was amplified as single antenna design was modified into an array. Although the interference and frequency shifts adversely

affect the desired frequency response from the antenna, SDR can still utilize the reconfigurable nature of the antenna designed in this thesis.

Additionally, with the design of a symmetrically feed 16 element antenna array, with a gain of -1.78 dB at 2.34 GHz and 0.3 dB at 1.49 GHz, the research demonstrates the ability to mount a phased array antenna on a nanosatellite by meeting the defined size requirement. However, in order to improve frequency response and reduce interference coupling, a larger PCB would be needed. The gain achieved by the antenna array is not an optimized version of the design, because there is an unknown amount of power is lost during interference coupling. On a satellite implementation, the antenna array would use the Space Fence (Gruss, 2014) transmitters as a signal source to track RSOs. Not taking into consideration the antenna gain of the Space Fence transmitter, 766 kW of transmit power is approximately 88.8 dBm (power measurement in dB) (Milligan, 2005). Free space path loss, for approximately 2000 km (upper edge of LEO) at 2.4 GHz for a -1.78 dB antenna would yield 166.8 dB (Milligan, 2005). The difference yields 78 dB of loss of transmission without taking into account the antenna gain at the transmitter. Although there is no specific cut-off point, the power emitted by the Space Fence transmitter is easily capable of being detected by a moderate antenna in LEO. Additional loss of signal strength would be incurred when the S-band signal from Space Fence would reflect off of RSOs before reaching the antenna designed in this thesis. The loss of signal strength here would be dependent on the type of material and distance from the antenna, and the sensitivity of a radio to detect faint signals, which depends on the gain of the antenna and the sensitivity of the front-end (Fararone, 2012). Thus, by further optimizing the gain of the reconfigurable phased array antenna, based on the results in this chapter, the antenna array designed in this thesis can be used as radar on a nanosatellite.

Therefore, with the analysis completed, a second iteration of antenna design and fabrication would certainly correct the errors and achieve the desired frequency response. By demonstrating frequency reconfigurability of the phased array antenna, this research succeeds in designing a reconfigurable antenna array that can be used by a SDR for multiple frequency bands. Additionally, this research successfully designed a phased array antenna that can be used as a beam steering radar. As mentioned earlier, beam steering is directly related to the phase difference of the signal across each element and would require a front-end to demonstrate complete beam steering. Additionally, a multi-port VNA would be necessary to determine the phase shift offset or phase centre stability of the antenna array. However, in order to determine the overall gain and frequency response of the antenna array, the antenna transmission lines are merged into a feed network that is symmetrical. By splitting the transmission lines of each antenna element to be fed separately into a front-end, beam steering can be achieved by this antenna design.

CHAPTER 6: CONCLUSIONS AND RECOMMENDATIONS

The objective of this thesis was to demonstrate a novel design of a reconfigurable phased array antenna that can be used as a communications or radar receiver in both the S and L bands. Additionally, the antenna design should also be mountable on a nanosatellite. Over the course of the last few chapters, antenna design and testing challenges have been presented. This thesis provides a novel antenna array design that incorporates reconfigurability on a hardware element, the conclusions of which are summarized in the following paragraphs.

6.1 Conclusions

In this research, reconfigurability of a micro-strip antenna was achieved that is capable of communication in the S-band and has the ability to reconfigure the frequency response to receive GPS L1 signals in the L-band. The design also demonstrates the capability of a reconfigurable antenna design to be configured as an array capable as a phased array antenna for signal steering. This thesis highlights the step-by-step design procedure that demonstrates not only frequency reconfigurability, but also highlights other key parameters that can become reconfigurable.

Issues highlighting the static nature of a hardware component brought to the fore other problems with debris tracking and signal steering. The antenna designs developed in this research illustrate how antennas work and how they can be modified and what the consequences of those modifications are.

During this research, the following was accomplished:

1) In Chapter 2, a literature review is performed on progress in design and application of varying types of antennas and their implementations. The study analyzed different methods of

debris tracking and concluded that no one method is capable of tracking all objects currently in orbit around the Earth. In addition, many shortcomings of the existing systems were identified and a proposal to improve antenna performance by implementing frequency reconfigurability and a phased array layout is pitched.

2) In Chapter 3, major antenna design characteristics such as input feed types, substrate materials, frequency reconfigurability, polarization and array designs were studied and simulated. The theory behind how antennas work and the effects of geometrical changes was explained. The chapter concluded that using Rogers RO6002/duroid and Rogers RO3210 would provide the best performance for high frequency antennas. A secondary patch in addition to the main patch with a switch configuration was proposed based on existing ideas to conclude that frequency reconfigurability would require a physical change in the geometry of the micro-strip. Finally, a phased array antenna was designed to demonstrate the concept of phase centre stability in antenna arrays.

3) In Chapter 4, various antenna designs and simulations concluded that the inset feed antenna would obtain the best response for a frequency reconfigurable setup, while using either of the Rogers substrate materials. It was concluded that the coaxial-feed antenna design was most suitable for circular polarization. Upon further simulations and testing, the inset feed antenna array was designed to mount on 18 cm by 18 cm PCB board with Rogers RO3210 as the chosen substrate. Additionally, two designs for a single inset feed reconfigurable antenna were fabricated, as seen in Figures 5.11 and 5.12, to demonstrate the increase in antenna gain and confirm that reconfigurability would still function as an array.

4) As discussed in Chapter 5, antenna simulations from Chapter 4 concluded that the linear feed system of the inset-feed antenna was able to outperform the aperture and coaxial-feed networks in the reconfigurable rectangular micro-strip. A test benchmark was established in order to demonstrate how the antenna gain calculations are made based on a reference calibrated response, and how port calibration and reference calibration can mitigate errors. In the first set of tests for the static inset-feed antenna, a 60 MHz offset in the centre frequency from the simulation was determined to be caused by soldering imperfections and/or manufacturing errors because of which the S11 (signal reflection) response of the antenna was also offset.

When the first reconfigurable antenna was tested without connecting switches, a frequency offset was caused by the secondary patch interfering with the main patch due to a conductivity gap. The magnitude of the frequency offset was determined to be based on the length of the secondary patch, as per Equation 2, and it was concluded that an ideal design would have a switch as wide as the main micro-strip.

When the second reconfigurable antenna is tested with enabled switches, the frequency offset remains, but only at the S-band region. In the L-band, the S21 frequency response plot shows the antenna's ability to pick up GPS L1 signals. It was concluded that the same offset effects would be apparent in the antenna array designs, and offset effect was confirmed with S21 plots.

For the switch off position, the peak S-band gain for the antenna array reached -1.78 dB at 2.34 GHz whereas the single antenna peak at S-band reached -7.5 dB at 2.33 GHz showing a large improvement. Similarly, for the switch on position, the L-band peak gain (near the GPS L1 signal) for the antenna array reached 0.3 dB at 1.49 GHz, while the single antenna reached -3.95 dB at 1.58 GHz. The research also was able to conclude that an adequate spacing of a quarter of

the wavelength of the lowest frequency of interest would help mitigate any interference between antennas when dealing with eighth wavelength antenna elements.

As stated in the objectives, the antenna array designed is intended for passive radar use based on signals that reflect off the debris and are received by this antenna. In this configuration, the symmetrical array design is capable of detecting the direction of the signal source with post processing capabilities. When each radiating element is configured with its very own source/transmit connection, processing and performing phase detection on each antenna signal is a simplified task due to the symmetry of the design. With a better understanding of the interference on board due to spacing and trace lines, a future design would address these issues and improve performance.

In conclusion, the objectives to design a frequency reconfigurable phased array antenna that can be mounted on a nanosatellite were met. The unique antenna array in Figure 4.19 is able to switch between the S and L bands, while mountable on a nanosatellite and demonstrates the ability to passively determine signal source with assistance from a capable front end.

6.2 Recommendations

This research has demonstrated the unique method in which reconfigurability can be intertwined with arrays, while keeping size in consideration. As manufacturing techniques improve, software simulations get more accurate and testing becomes easier, improvements on current and past designs are inevitable. Despite the unique results obtained during this research, there is always room for improvement. This thesis provides the base understanding of how antennas radiate and understands where demands may appear in the future. In preparation of future applications, a few

recommendations to make improvements to this thesis and other aspects of this research are presented below.

Simulation software advances

Antenna design and simulation comes with many challenges that were not discussed in this research. Lengthy simulation times, complicated component design procedure for simple tasks, lack of training courses in Canada and not regarded as highly user friendly, are some of the reasons why simulation tools need an upgrade. In this research, ANSYS – HFSS is used to create and simulate all antenna designs and then Altium Designer Suite is used to produce fabrication models of the PCB and antenna designs. Simple antenna layouts take hours, and simulation times are between 30 minutes to 8 hours depending on the design. However, HFSS electronics suite remains one of the most popular industrial software for electronics and electromagnetic simulation and is known to be very accurate.

A simple recommendation is the addition of machine learning algorithms to assist in designing and managing the software. This addition would make complicated tasks easier by suggesting better methods as adapted by more experienced users. A collection of data for a project would ease the learning curve by analyzing the results obtained for each simulation to determine which parameter changes affect what characteristic of the design in question. By implementing machine learning to ANSYS server and client application, lessons and modifications learnt from others can be shared with new learners to develop a community of experienced antenna/RF component designers.

PAA beam steering

In order to demonstrate signal beam steering of the PAA designed in this research, the antenna feed network that merges the transmission lines from all of the individual radiation elements, can be replaced by separating the transmission lines of each antenna. The antenna output can then be fed into a front-end that is capable of performing in parallel to determine the phase difference across each antenna. Using a post-processing element such as an FPGA and the known phase differences between the antennas, the direction of arrival can be determined. Alternatively, the post-processing unit can provide phase variation values for each antenna to a phase shifter in order to steer the beam of the PAA in the desired direction. The individual phase control also allows the radiation pattern of the PAA to be moulded as per mission requirements.

Passive debris tracking

Taking the phased array antenna to the next step would be the design of a high frequency radar (preferably in X-band). The higher frequency would reduce the antenna size and allow more elements to be placed on a smaller board. The higher frequency would also enable the tracking of smaller objects that lower frequency signals would miss. A phased array X-band radar design that can be mounted on a nanosatellite would revolutionize not only debris tracking, but also be implemented in satellite to satellite communications. However, higher frequency signals and system design would consume more power and force certain front-end components to be analog. Additional elements on the phased array would also add complications to the front-end design, limiting use on large satellites only.

GPS multipath mitigation

Phased array antennas are applicable in many industrial sectors, however their design size and complexity prevent them from being commercialized. A dedicated phased array antenna for detecting and mitigating reflected GPS signals is one potential application. Such an antenna could filter out signals from a known multipath source electronically, improving the response of the receiver. The receiver, in certain conditions, would receive less multipath signals, which would improve signal acquisition and tracking. By improving the phase steering of the antenna and orienting antenna designs to be frequency reconfigurable, specific to GPS signals, a nanosatellite mountable phased array antenna could be added to automobiles for improved accuracy in areas with high multipath signals, such as urban centres.

Additionally, antenna designs, such as the one presented in this research, can be modified to only work at the GPS L1 frequency (1.575 GHz) with a specific radiation pattern. Since the radiation pattern is reconfigurable due to digital phase control, the main lobe of the radiation pattern and multiple side lobes can be directed to acquire maximum number of satellites while mitigating multipath. As described in this research, the number of antenna elements in an array determine how narrow the radiation pattern of the main beam can be. This concept is similar to the design demonstrated in Brown (2000) using a high gain GPS antenna array to reject multipath signals and act as protection against interference and jamming. However, this design is aimed for ground applications that may not necessarily have the power, weight, size and cost restriction as the antenna design presented in this research. With certain modifications, the design presented in this research demonstrates its versatile nature.

REFERENCES

Abidi, A. A. (2006). Evolution of a Software-Defined Radio Receiver's RF Front-End. IEEE Radio Frequency Integrated Circuits (RFIC) Symposium, 2006, 17–20. http://doi.org/10.1109/RFIC.2006.1651080

A-info. 2017 A-info P/N:LB-430-10-C-SF gain horn antenna, 9, 475–493. Retrieved from http://www.ainfoinc.com/en/pro_pdf/new_products/antenna/Standard Gain Horn Antenna/tr_LB-430-10.pdf

Ali, Z., Singh, V. K., Singh, A. K., and Ayub, S. (2011). *E-shaped microstrip antenna on rogers substrate for WLAN applications*. Proceedings - 2011 International Conference on Computational Intelligence and Communication Systems, CICN 2011, (3), 342–345. http://doi.org/10.1109/CICN.2011.72

Arndt, G. D., Fink, P., and Warren, W. B. (1993). *A space station-based orbital debris tracking system.* Advances in Space Research, 13(8), 65–68. http://doi.org/10.1016/0273-1177(93)90569-W

Arora, A., Khemchandani, A., Rawat, Y., Singhai, S., and Chaitanya, G. (2015). *Comparative study of different feeding techniques for rectangular microstrip patch antenna.* International Journal of Innovative Research in Electrical, Electronics, Instrumentation and Control Engineering, 3(5), 32–35. http://doi.org/10.17148/IJIREEICE.2015.3509

Astronautics Vocabulary. (2003, August 01). http://www.asc-csa.gc.ca/eng/resources/vocabulary/view.asp?id=512

Azarmanesh, M., Boudaghi, H., and Mehranpour, M. (2012). *A frequency-reconfigurable monopole antenna using switchable slotted ground structure*. IEEE Antennas and Wireless Propagation Letters, 11, 655–658. http://doi.org/10.1109/LAWP.2012.2204030

Bouwmeester, J., and Guo, J. (2010). *Survey of worldwide pico- and nanosatellite missions, distributions and subsystem technology*. Acta Astronautica, 67(7–8), 854–862. http://doi.org/10.1016/j.actaastro.2010.06.004

Brown, A., and Silva, R. (2000). *A GPS Digital Phased Array Antenna and Receiver.* Proceedings 2000 IEEE International Conference on Phased Array Systems and Technology, 153-156. https://ieeexplore.ieee.org/stamp/stamp.jsp?tp=&arnumber=858930

Buchen, E. (2014). SpaceWorks 2014 Nano / Microsatellite Market Assessment. AIAA/USU Conference on Small Satellites, 1–5.

Buske, I., Kirchner, G., Koidl, F., Friederich, F., Völker, U., and Riede, W. (2013). *Laser measurements to space debris from Graz SLR station*. Advances in Space Research, 51(1), 21–24. http://doi.org/10.1016/j.asr.2012.08.009

Campbell, W. S., Spencer, D. B., Hogge, C. B., Sorge, M. E., andMcwaters, S. R. (2000). *Some Technical Issues of an Optically Focused Small Space Debris Tracking and Cataloging System*. Space Debris, 2(3), 137–160. http://doi.org/10.1023/A:1022990214830

Carter, D., Riot, V., Vries, W. De, Simms, L., Bauman, B., Phillion, D., and Olivier, S. (2013). *SSC13-XI-11 The Space-based Telescopes for Actionable Refinement of Ephemeris (STARE) mission*. 27th Annual AIAA/USU Conference on Small Satellites.

Cristea, O., Dascal, V., Dolea, P., and Palade, T. (2013). *Low-cost SDR-based ground receiving station for LEO satellite operations*. 2013 11th International Conference on Telecommunications in Modern Satellite, Cable and Broadcasting Services, TELSIKS 2013, 2, 627–630. http://doi.org/10.1109/TELSKS.2013.6704456

Douglas, M., and Segundo, E. (2010). Space Based Space Surveillance. Revolutionizing Space Awarness, 100–114.

Drysdale, T., & Vourch, C. (2014). *V-band "Bull's Eye" Antenna for CubeSat Applications*. IEEE Antennas and Wireless Propagation Letters, 13, 1092-1095. https://ieeexplore.ieee.org/stamp/stamp.jsp?arnumber=6824803

Dunbar, B. (2011). NASA's Cubesat Launch Initiative. https://www.nasa.gov/directorates/somd/home/CubeSats_initiative.html

Electronic Products. (2013). Microwave radio front-end block diagram. Digital Image http://www.electronicproducts.com/RF_and_Microwave_Components/RF_and_Microwave/Microwave_radio_front-end_block_diagram.aspx

ESA. (2017). Scanning and observing. http://www.esa.int/Our_Activities/Operations/Space_Debris/Scanning_and_observing2

Faraone, A., Gardner, P., and Hall, P. S. (2012). *Antenna Requirements for Software Defined and Cognitive Radios*. Proceedings of the IEEE, 100(7), 2262–2270. http://doi.org/10.1109/JPROC.2012.2182969

Gaposchkin, E. M., von Braun, C., and Sharma, J. (2000). *Space-based space surveillance with the space-based visible*. Journal of Guidance Control and Dynamics, 23(1), 148–152. http://doi.org/Doi 10.2514/2.4502

Gavigan, P., and McKenzie-Picot, S. DRDC. (2013). *Communication Link Analysis for a Nanosatellite Constellation in Low Earth Orbit.*

Gruss, M. (2014, December 10). Haney: U.S. Partners To Have Indirect Access to Space Fence Data. Retrieved from http://spacenews.com/42619haney-us-partners-to-have-indirect-access-to-space-fence-data/

Guo, Y. J., Qin, P. Y., Weily, A. R., and Liang, C. H. (2010). *Polarization reconfigurable U-slot patch antenna*. IEEE Transactions on Antennas and Propagation, 58(10), 3383–3388. http://doi.org/10.1109/TAP.2010.2055808

Haines, L., Phu, P. (2011). Space Fence PDR Concept Development Phase.

Hall, P. S., Gardner, P., and Faraone, a. (2012). *Antenna Requirements for Software Defined and Cognitive Radios*. Proceedings of the IEEE, 100(7), 2262–2270. http://doi.org/10.1109/JPROC.2012.2182969

Hansen, R. *Phased Array Antennas*, *2nd Ed*. John Wiley and Sons Inc, 2009.

Heidt, H., Puig-Suari, J., Moore, A. S., Nakasuka, S., andTwiggs, R. J. (2000). *CubeSat: A new Generation of Picosatellite for Education and Industry Low-Cost Space Experimentation*. AIAA/USU Conference on Small Satellites, 1–19.

Hertzfeld, H., Woellert, K., Ehrenfreund, P., and Ricco, A. J., (2011). *Cubesats: Cost-effective science and technology platforms for emerging and developing nations*. Advances in Space Research, 47(4), 663–684. http://doi.org/10.1016/j.asr.2010.10.009

Hosain, M., Paul, L., Sarker, S., Prio, M., Morshed, M., Sarkar, A. (2015). *The Effect of Changing Substrate Material and Thickness on the Performance of Inset Feed Microstrip Patch Antenna*. American Journal of Networks and Communications. 4(3), 54-58. http://article.sciencepublishinggroup.com/html/10.11648.j.ajnc.20150403.16.html

IEEE. (2008). IEEE Standard Test Procedures for Antennas (Vol. 1979).

IERS. (2013). Satellite Laser Ranging. https://www.iers.org/IERS/EN/Science/Techniques/slr.html

Jondral, F. K. (2005). Software-defined radio - Basics and evolution to cognitive radio. Eurasip Journal on Wireless Communications and Networking, 2005(3), 275–283. http://doi.org/10.1155/WCN.2005.275

Keysight Technologies. 2017. Keysight 2-Port and 4-Port PNA-L Network Analyzer. Retrieved from https://literature.cdn.keysight.com/litweb/pdf/N5235-90004.pdf?id=2755232

Khan, A., and Nema, R. (2012). *Analysis of Five Different Dielectric Substrates on Microstrip Patch Antenna.* International Journal of Computer Applications, 55(18), 6–12. http://doi.org/10.5120/8826-2905

Kovitz, J. M., and Rajagopalan, H. (2014). *MEMS Reconfigurable Optimized E-Shaped Patch Antenna Design for Cognitive Radio*, 62(3), 1056–1064.

Lo, Y. T., Solomon, D., and Richards, W. (1979). *Theory and experiment on microstrip antennas.* IEEE Transactions on Antennas and Propagation, 27(2), 137–145. http://doi.org/10.1109/TAP.1979.1142057

Lockheed Martin. (2013). FPS-117 Long-Range Radar System.

Malik, B. I. (2009). U.S. Satellite Destroyed in Space Collision. Retrieved December 13, 2017, from https://www.space.com/5542-satellite-destroyed-space-collision.html

Milligan, T. (2005). *Modern Antenna Design*, 2nd Ed. http://doi.org/10.1002/0471720615

Moernaut , G J.K., and Orban, D. "Basics Of GPS Antennas." Basics Of GPS Antennas (2008): 12-18. Web. http://orbanmicrowave.com/wp-content/uploads/2014/12/Orban-BasicsofGPSAntennas-article-RF-2008-final.pdf

NASA International Laser Ranging Service. (1999). Satellite Laser Ranging and Earth Science, 11.

Nave, R. (2017) Linear, circular and elliptical polarization. Digital Image. http://hyperphysics.phy-astr.gsu.edu/hbase/phyopt/polclas.html

Orbital Sciences. (2013). "Antares Test Launch "A-ONE Mission" Overview Briefing"

O'Sullivan, C. T. (1980). Ohm's law and the definition of resistance. Physics Education, 15(4), 237–239. http://doi.org/10.1088/0031-9120/15/4/009

Peixeiro, C. (2011). *Microstrip Patch Antennas An Historical Perspetive of the Development*. Microwave and Optoelectronics Conference, 684–688.

Pozar, D. M. (1996). A review of aperture coupled microstrip antennas: History, operation, development, and applications. University of Massachusetts at Amherst, (May), 1–9.

Puvaneswari, M., and Sidek, O. (2004). *Wideband analog front-end for multistandard software defined radio receiver*. 2004 IEEE 15th International Symposium on Personal, Indoor and Mobile Radio Communications (IEEE Cat. No.04TH8754), 3(I), 1937–1941. http://doi.org/10.1109/PIMRC.2004.1368336

Rueters. (2017). "India launches record 104 satellites at one go".

Simms, L. M. (2012). Space-based telescopes for actionable refinement of ephemeris pathfinder mission. Optical Engineering, 51(1), 11004. http://doi.org/10.1117/1.OE.51.1.011004

Singh, H., Kanwar, R., and Singh, M. (2014). *Steering Wheel Shaped Frequency Reconfigurable Antenna for Cognitive Radio*. International Journal of Engineering Research and Applications, 4(5), 138–142.

Smith, Craig H., and Ben Greene. "Future Space Debris Tracking Requirements." 33rd AIAA International Communications Satellite Systems Conference and Exhibition (2015). Print.

Tang, T. K. (1999). MEMS for space applications. 1999 IEEE International SOI Conference. Proceedings (Cat. No.99CH36345), 3680(April), 1–13. http://doi.org/10.1109/SOI.1999.819857

Tutorials Point. (2018) Antenna lobes and half-power point. Digital Image. https://www.tutorialspoint.com/antenna_theory/antenna_theory_beam_width.htm

Visser, H. J. (2006). *Array and phased array antenna basics*. Chichester: Wiley.

Werner, D. (2014). "Planet Labs CubeSats Deployed from ISS with Many More To Follow". SpaceNews, Inc.

Wikimedia. (2016). Davidjessop - Own work, CC BY-SA 4.0, https://commons.wikimedia.org/w/index.php?curid=48304978

Wilson Electronics. 2015. Log Periodic Antenna. Retrieved from https://wilsonamplifiers.ca/content/pdfs/Yagi-Antenna-Spec-Sheet.pdf